CERTIFICATO DI **FIRMA DIGITALE**

Si certifica che questo documento informatico

phd_unisi_085964.pdf

composto da n° 105 pagine

È stato firmato digitalmente in data odierna con Firma Elettronica Qualificata (FEQ), avente l'efficacia e gli effetti giuridici equivalenti a quelli di una firma autografa, ai sensi dell'art. 2702 del Codice Civile e dell'art. 25 del Regolamento UE n. 910/2014 eIDAS (electronic IDentification Authentication and Signature).

PROCESSI INFORMATICI COMPLETATI

- **Apposizione di Firma Elettronica Qualificata Remota** emessa da Intesi Group S.p.A. in qualità di prestatore di servizi fiduciari qualificati autorizzato da AgID, per garantire con certezza l'autenticità, l'integrità, il non ripudio e l'immodificabilità del documento informatico e la sua riconducibilità in maniera manifesta e inequivoca all'autore, ai sensi dell'art. 20 comma 2 del CAD - D.lgs 82/2005.
- **Apposizione di Marca Temporale Qualificata** emessa da Intesi Group S.p.A. in qualità di prestatore di servizi fiduciari qualificati autorizzato da AgID, per attribuire una data e un orario opponibile a terzi, ai sensi dell'art. 20 comma 3 del CAD - D.lgs 82/2005 e per far sì che la Firma Elettronica Qualificata apposta su questo documento informatico, risulti comunque valida per i prossimi 20 anni a partire dalla data odierna, anche nel caso in cui il relativo certificato risultasse scaduto, sospeso o revocato.
- **Apposizione di Contrassegno Elettronico**, l'unica soluzione tecnologica che permette di prorogare la validità giuridica di un documento informatico sottoscritto con firma digitale e/o marcato temporalmente, rendendolo inalterabile, certo e non falsificabile, una volta stampato su supporto cartaceo, ai sensi dell'art. 23 del CAD - D.lgs 82/2005.

Per risalire all'originale informatico è necessario scansionare il Contrassegno Elettronico, utilizzando l'applicazione HONOS, disponibile per dispositivi Android e iOS.

UNIVERSITÀ DI SIENA
1240

University of Siena – Department of Medical Biotechnology

Doctorate in Genetics, Oncology and Clinical Medicine

(GenOMeC)

XXXIV Cycle (2018-2021)

Coordinator: Prof. Francesca Ariani

Zebrafish models in melanoma research: analysis of coding and non-coding BRAFV600E

Scientific disciplinary sector: BIO/11-Molecular Biology

Tutor:

Dr. Laura Poliseno

PhD Candidate:

Raffaella De Paolo

Table of contents

List of figures

List of Tables

List of Abbreviation

µm: micrometer

p3E: 3’ entry clone

3’UTR: 3’ untranslated region

p5E: 5’ entry clone

aa: aminoacid

Ab: antibody

ABC: avidin biotin complex

ABCDE: asymmetry, border, color, diameter, evolving

Actb-1: actin beta 1

AKT: v-akt murine thymoma viral oncogene homolog 1

ALK1: activin receptor-like kinase 1

ALM: acral lentiginous melanoma

ANOVA: analysis of variance

ATP: adenosine triphosphate

BAP1: BRCA1 associated protein 1

BCL2: B-cell lymphoma 2

BCL2A1: BCL2-related protein A1

BMP: bone morphogenetic protein

bp: base pair

BRAF: v-raf murine sarcoma viral oncogene homolog B1

BRAFi: BRAF inhibitor

cAMP: cyclic adenosine monophosphate

CBP: cAMP-regulated-enhancer binding protein (CREB)-binding protein

CCDS: consensus coding sequence

CCNB1: cyclin B1

CCND1: cyclin D1

CCNF: cyclin F

CD40L: cluster of differentiation 40 ligand

CDK: cyclin dependent kinase

CDKN2A: cyclin dependent kinase inhibitor 2A

cDNA: complementary DNA

CDS: coding sequence

cm: centimeter

c-MET: mesenchymal-epithelial transition factor

COB: cobimetinib

CR: conserved region

CRISPR/Cas9: clustered regularly interspaced short palindromic repeat/associated protein 9

CSD: cumulative solar damage

CT: computed tomography

Dabra: dabrafenib

DAPI: 4′,6-diamidino-2-phenylindole

DCT: dopachrome tautomerase

DHI: 5,6-dihydroxyindole

DHICA: 5,6-dihydroxyindole-2-carboxylic acid

DHODH: dihydroorotate dehydrogenase

DMEM: Dulbecco's modified eagle medium

DMSO: dimethyl sulfoxide

DNA: deoxyribonucleic acid

DNP: 2,4-dinitrophenol

DOPA: 3,4-dihydroxyphenylalanine

dpf: day post fertilization

dre: *danio rerio*

dsDNA: double strand DNA

E2F1: E2F transcription factor 1

E3: embryo medium

ECL: enhanced chemiluminescence

Ef1a: elongation factor 1-alpha

eGFP: enhanced green fluorescent protein

EGFR: epidermal growth factor receptor

ERK: extracellular signal-regulated kinase

Ex: exon

F: filial

FATP1: fatty acid transport protein 1

FBS: fetal bovine serum

FDA: food and drug administration

FGF: fibroblast growth factor

FOXD3: forkhead box D3

Fw: forward

GADD45: growth arrest and DNA damage-inducible gene 45

gDNA: genomic DNA

GEF: guanine exchange factor

GEM: genetically engineered mouse

GEZ: genetically engineered zebrafish

GF: growth factor

GFR: GF receptor

gp100: glycoprotein 100

GPCR: guanine nucleotide-binding protein-coupled receptor

Grb2: growth factor receptor-bound protein 2

GRCh38.p13: human genome assembly from genome reference consortium [GCA_000001405.29 GCF_000001405.40]

GTP: guanosine triphosphate

HEK293: Human embryonic kidney cell line 293

H&E: hematoxylin and eosin

HMB-45: human melanoma black

hpf: hours post fertilization

Hsa: *Homo sapiens*

ICB: immune checkpoint blocker

ID: identifier

IFNg: interferon gamma

IHC: immunohistochemistry

IL-8/10: interleukin 8/10

Jmjd6: histone demethylase Jumonji C domain-containing protein 6

JNK-1/2/3: c-Jun N-terminal kinases-1/2/3

Ki-67: Kiel clone 67

Kita: receptor tyrosine kinase a

L: ladder

LDH: lactate dehydrogenase

L-DOPA: L-3,4-dihydroxyphenylalanine

Leflu: leflunomide

LIG1: DNA ligase 1

LMM: lentigo maligna melanoma

LTR: long terminal repeat

Luc2: Luciferase 2

MAB: maleic acid buffer

MBT: maleic buffer tween-20

MAPK: mitogen-activated protein kinase

MAPKi: MAPK inhibitor

MAPKKK: mitogen-activated protein kinase kinase kinase

MART-1: melanoma antigen recognized by T cells-1

MC1R: melanocortin 1 receptor

MCS: multi cloning site

MDM2: mouse double minute homolog 2

MEK: mitogen-activated protein kinase

MEKi: MEK inhibitor

MeOH: methanol

mg: milligram

MIA: melanoma inhibitory activity

pME: middle entry clone

miRNA: microRNA

MITF: microphthalmia-associated transcription factor

MLANA: melanoma antigen recognized by T cells 1 – see MART-1

MM: metastatic melanoma

mM: millimolar

mm: millimeter

mpv17: mitochondrial inner membrane protein 17

MRI: magnetic resonance imaging

mRNA: messenger ribonucleic acid

MS222: tricaine methanesulfonate

MSX1: msh homeobox 1

mTOR: mammalian target of rapamycin

myl7: myosin light chain

NC: neural crest

nCATs: nanopore Cas9-targeted sequencing

NCP: neural crest program

NF1: neurofibromatosis type I

NF-κB: nuclear factor kappa B

ng: nanogram

nivo: nivolumab

NM: nodular melanoma

nt: nucleotide

NTES: NaCl/Tris-HCl/EDTA/SDS

OMY: oligomycin

ON: over night

ONT: Oxford nanopore technology

PAX3: paired box 3

PBS: phosphate buffered saline

PBST: phosphate-buffered saline/tween.

PCR: polymerase chain reaction

PD-L1: programmed death-ligand 1

PD-L1i: PD-L1 inhibitor

PET: positron emission tomography

PFA: paraformaldehyde

PFS: progression-free survival

pg: picogram

PI3K: phosphoinositide-3-kinase

PIGMi: pigmentation inhibitor

PLIN2: perilipin-2

PMEL: premelanosome protein

PNK: polynucleotide kinase

PPARGC1A: peroxisome proliferator-activated receptor gamma coactivator 1-alpha

PRAME: preferentially expressed antigen in melanoma

PTEN: phosphatase and tensin homolog deleted on chromosome 10

PTU: phenyl-thiourea

qRT-PCR: quantitative reverse transcription polymerase chain reaction

RAS: rat sarcoma virus

RB: retinoblastoma

RBD: ras binding domain

Rev/Rw: Reverse

RFP: red fluorescent protein

RGP: radial growth phase

RNA: ribonucleic acid

ROS1: proto-oncogene tyrosine-protein kinase ROS/ ROS (reactive oxygen species) proto-oncogene 1, receptor tyrosine kinase

RTK: receptor tyrosine kinase

rUMP: pyrimidine ribonucleotide uridine monophosphate

SEM: standard error of the mean

SETDB1: SET (Su(var)3-9, Enhancer-of-zeste and Trithorax) domain bifurcated 1

sgRNA: single guide RNA

Shc: src homology 2 domain-containing

Sos: son of sevenless

SOX10: SRY (sex-determining region Y)-related high mobility group box-containing

SSC: saline-sodium citrate

SSM: superficial spreading melanoma

NTMT: NaCl/Tris-HCl/$MgCl_2$/Tween20

TBST: tris-buffered saline with 0.1% Tween® 20 detergent

TERT: telomerase reverse transcriptase

TF: transcription factor

Ct: threshold cycle

TNM: tumor, nodes, and metastases

TP53: tumor protein 53

Tram: trametinib

TRP1/2: tyrosinase-related protein 1- see TYRP1

TYR: tyrosinase

TYRP1: tyrosinase-related protein 1- see TRP

UV: ultraviolet

VEGF: vascular endothelial growth factor

VEM: vemurafenib

VGP: vertical growth phase

WHO: world health organization

WISH: whole mount in situ hybrization

WNT: wingless

WT: wild type

Abstract

Malignant melanoma is one of the most aggressive types of cancer. While early-stage melanoma can be cured by surgical excision, late-stage melanoma remains a highly lethal disease. Current therapeutic strategies, including single agents or combined therapies, are hampered by low response rates and by diverse resistance mechanisms.

The most frequent mutation in malignant melanoma is the V600E substitution in the *BRAF* oncogene. This mutation constitutively activates the MAPK pathway, promoting cell survival, proliferation, and motility. Among the impacting therapies, BRAFV600E inhibitors (BRAFi) are initially very effective, but, due to quick development of acquired resistance, they can be used for short periods of time (4-6 months). The development of current drug combinations just postpones the acquired resistance.

With the final aim to identify new molecular factors involved in BRAFV600E-driven malignant transformation, hence, to improve the response to BRAFi, we are developing and characterizing new melanoma models in zebrafish. In this 3-year PhD project, using the Tol2 system, I generated melanoma-prone transgenic lines in which tumors are driven by BRAFV600E in its reference and X1 isoforms (BRAFV600E-ref and BRAFV600E-X1). While BRAFV600E-ref is the isoform commonly used for similar models, BRAFV600E-X1 is a poorly characterized isoform that, as we discovered in our laboratory, always coexists with the ref.

The novelty of this project also lies in the study of the 3'UTR (three prime untranslated region) regulatory regions. These lines express either *BRAFV600E* ref/X1 coding sequence only or *BRAFV600E* ref/X1 coding sequence plus their respective 3'UTR. Our data in a mosaic condition show alterations in the pigmentation patterns and in the development of nevi, from which tumors originate, as well as a higher melanoma incidence in presence of BRAFV600E-ref compared to BRAFV600E-X1. Moreover, tumor development resulted to be faster in fish expressing each coding sequence with respect to the coding sequence + 3'UTR. Likewise, we are also generating stable lines. The determination of the location of the transgene is done through an innovative genotyping technique that combines CRISPR/Cas9-mediated DNA editing and Oxford Nanopore Technology (ONT) based sequencing. Stable lines will be studied for *BRAFV600E* variant-specific coding-(in)dependent activities and drug sensitivity.

With respect to drug screening, we will exploit the neural crest signature, which is present in progenitor cells during the early stages of embryonic development and is aberrantly reactivated in melanoma cells. We will use *crestin*, a common marker in zebrafish, to generate a dual reporter

zebrafish line expressing mCherry and Luciferase reporter genes under the control of the *crestin* promoter.

Crossed with the *BRAFV600E* variant-specific melanoma prone lines, this *crestin* line can be used as a tool for high-throughput quantitative screening of novel BRAFi-focused drug combinations in zebrafish embryos. Preliminarily, our data confirm a higher expression of *crestin* in the embryos of the *BRAFV600E* transgenic line compared to the wild type line. Furthermore, we observed reduced expression of this marker when treating *BRAFV600E* embryos with anticancer drugs, including BRAFi.

1. Introduction

1.1 Melanoma

Melanoma is an aggressive tumor resulting from the malignant transformation of melanocytes, cells determining the color of the skin and its protection from sun damage caused by UV rays. The skin is the largest organ in the body and is composed of three layers: the epidermis, the dermis and the subcutaneous or fatty tissue. The epidermis, the most external and photo-protective layer, is predominantly formed by melanocytes and keratinocytes that specifically establish a structural and functional unit (one melanocyte for almost 36 keratocytes) (Hoath and Leahy, 2003).

Global annual incidence of melanoma is increasing and has doubled over the last 15 years resulting in approximately 100,000 new cases arising annually worldwide. About 85% of cutaneous melanomas affect populations in North America, Europe, and Oceania (http://globocan.iarc.fr) (Fig.1). The incidence is higher in Caucasians and women are more affected than men. The age most at risk for melanoma is between 25 and 50 years, highlighting the need for primary prevention campaigns for this cancer. In Italy, more than 14,000 melanoma cases occurred in 2020 (AIRTUM 2020 data). In this country, it is the second most common cancer in males and the third most frequent in females under 50 years of age.

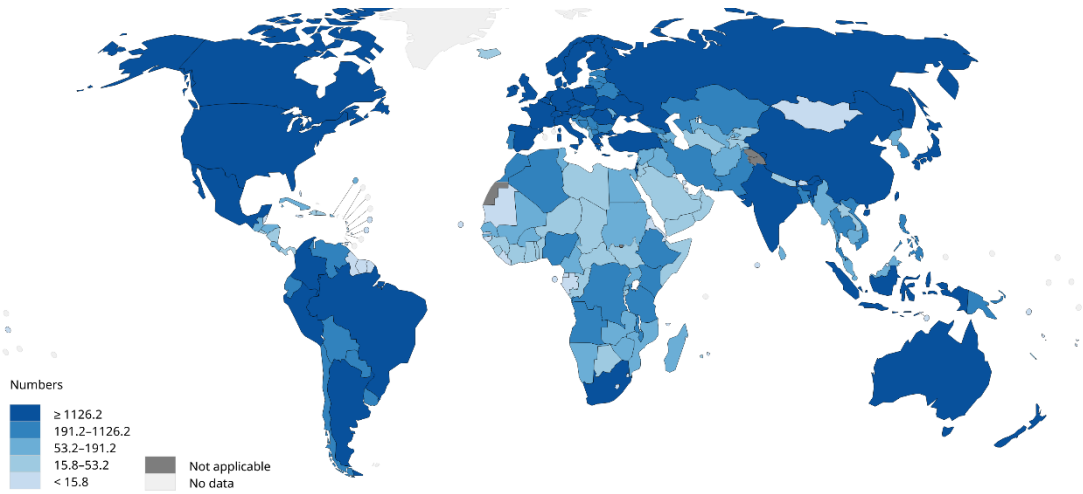

Figure 1 - Incidence of cutaneous melanoma in both men and women in 2020. Picture from © International Agency for Research on Cancer 2022. Data source: GLOBOCAN 2020 Graph production: IARC (http://gco.iarc.fr/today) World Health

The onset risk of cutaneous melanoma is associated to genetic, phenotypic, environmental factors and to the combinations between these. The most important environmental risk factor has

been identified in the exposure to UV rays associated to the absorbed doses, the type of exposure (intermittent rather than chronic) and the age (childhood and adolescence being at greater risk) (Rastrelli et al., 2014).

The net survival 5 years after diagnosis is 88% in men and 91% in women in the early stages of the disease (aiom.it). In these conditions, surgery is the treatment of choice for melanoma. Lymph node dissection is also indicated in cases of patients with a positive sentinel lymph node, mainly in cases of clinically evident nodal lymph node metastases (Tropea et al., 2022). Whereas in metastatic melanoma (MM) cases the mortality rate increases dramatically for its high potential of dissemination. Patient prognosis with MM is poor, with the net survival at 5 years dropping down to 5-19%, depending on the location and number of metastases. (Sandru et al., 2014)

Melanoma can arise on apparently healthy skin or from the modification of a pre-existing mole. Early diagnosis serves primarily to distinguish melanoma from common nevi. Usually, the moles are harmless spots of regular round or oval shape, flat or raised, of a uniform brown or blackish color, dimensions of a few millimeters (<6 mm) in diameter and show slow and gradual growth or fade away (Oliveira et al., 2015). Nevi are termed congenital when present from birth or acquired when developed later, and most of them (98%) develop in the first 30 years of age (Banky et al., 2005).

1.1.1 Melanoma diagnosis

Melanoma diagnosis is based on clinic, instrumental and histology techniques.

Clinic, observing a lesion with fresh alterations using the ABCDE rule (Thomas et al., 1998):

- Asymmetry, the melanoma moles are irregular and one half of it does not match the other;
- Border, the melanoma moles appear with irregular, jagged, hazy edges;
- Color, the moles have several colours and different shades that may include black, red-brown, pink, white or blue;
- Diameter, usually the melanoma size is larger than 6 millimeters;
- Evolving, the lesion tends to grow and widen rapidly, and changes in color.

Instrumental, observing the parameters used for clinical evaluation but acquiring and visualizing the surface's microscopic images. This comes with all the advantages of using variable

magnifications, comparing numerous lesions, and recording the images to follow their evolution over time (mole mapping). Tools used include the dermatoscope, videomicroscope, stereomicroscope and confocal microscopy (Akasu et al., 1994). Furthermore, imaging tests such as chest X-rays, CT scans, PET scans, and MRIs are helpful in determining the disease spreading (Garbe et al, 2022).

Histology, studying tissue sections using both optical microscopy (to assess thickness, regression, infiltration) and Immunohistochemistry with Ab that recognize specific surface markers (S-100, HMB-45, Vimentin, SOX10, MART-1, MITF, TYR, P16, Ki-67, BRAFV600E, ALK1, ROS1, BAP1, PRAME) (Lezcano et al., 2020; Dinehart et al., 2020; Zubovits et al., 2004).

1.1.2 Melanoma classification

The archival classification of melanoma (Arrington et al., 1977; McGovern et al., 1973; Clark et al., 1969) classified it into:

- Cutaneous melanoma subdivided into
    - Lentigo maligna melanoma (LMM), it is the least common form of melanoma (4-15%) and affects the exposed areas of the head/neck region (McKenna et al. 2006);
    - Superficial spreading melanoma (SSM), it is the most common form (70%), often with a slow (1-5 years) evolution by a precursor and affects any location (Jemal et al., 2008);
    - Nodular melanoma (NM), accounts for 15-30% of all melanoma forms. It is the most aggressive form with invasiveness and rapid metastasis, and affects the limbs less frequently (Kalkhoran et al., 2010);
    - Acral lentiginous melanoma (ALM), which affects the planes of the feet, palms of the hands and the hoof region. It is very rare in Caucasian people (Csányi et al., 2020);
- Uveal melanoma, which affects the iris, ciliary body, or choroid of the eye. In most cases arises from scratches and in rare cases from a nevus (Singh et al., 2018).
- Mucosal melanoma, which rarely affects mucosal surfaces, including the oral, nasal, anorectal, genitourinary, and vulvovaginal region (Ma et al., 2021).

Additional subtypes of melanoma were recognized by the World Health Organization (WHO) 2018 classification in nine pathways. They integrate the etiopathogenetic role of exposure to ultraviolet radiation (cumulative solar damage), the cell of origin (melanocyte associated or not with the epithelium), and the most characteristic genetic-molecular alterations (Elder et al., 2020):

A. Melanomas typically associated with cumulative solar damage (CSD)

Pathway I. Superficial spreading melanoma/low-CSD melanoma

Pathway II. Lentigo maligna melanoma/high-CSD melanoma

Pathway III. Desmoplastic and desmoplastic neurotropic melanoma

B. Melanomas not consistently associated with cumulative solar damage (no CSD)

Pathway IV. Spitz melanomas

Pathway V. Acral lentiginous melanoma

Pathway VI. Mucosal melanomas

Pathway VII. Melanomas arising in congenital nevi

Pathway VIII. Melanomas arising in blue nevi

Pathway IX. Uveal melanoma

C. Nodular melanoma (any or most of the pathways)

1.1.3 Melanoma staging

Concerning cutaneous melanomas, they evolve through two main stages of progression. In the first phase, early lesions (usually pigmented) expand horizontally on the skin surface. This is termed the radial growth phase (RGP). In the second phase, the expansion becomes vertical, and the cells acquire the ability to infiltrate the dermis or form a nodule and is termed the vertical growth phase (VGP) (Clark et al., 1969).

The Clark scale (Fig.2) determines the stage of melanoma, describing the layers of the skin that the tumor has reached. It is therefore divided into five levels: intraepidermal, papillary dermis, complete filling of the dermis, reticular dermis, and infiltration of subcutaneous fat (Clark, 1967).

Level I – Involving only the epidermis, in situ

Level II – Invasion of the papillary dermis

Level III – Invasion of the junction of the papillary dermis and reticulus dermis

Level IV – Invasion of the reticular dermis

Level V - Invasion of the subcutaneous tissue

These five stages correspond to progressively more aggressive forms of melanoma with worsening prognosis.

Subsequently, it has been introduced the Breslow microstaging (Fig.2) that measures the depth of infiltration of melanoma (Breslow, 1978):

Stage I - <0,76mm;

Stage II – 0,76-1,49mm;

Stage III – 1,5-3mm;

Stage IV - >4mm.

Also in this case, the greater the depth, the more aggressive the melanoma will be defined and the worse the prognosis will be (Breslow, 1970).

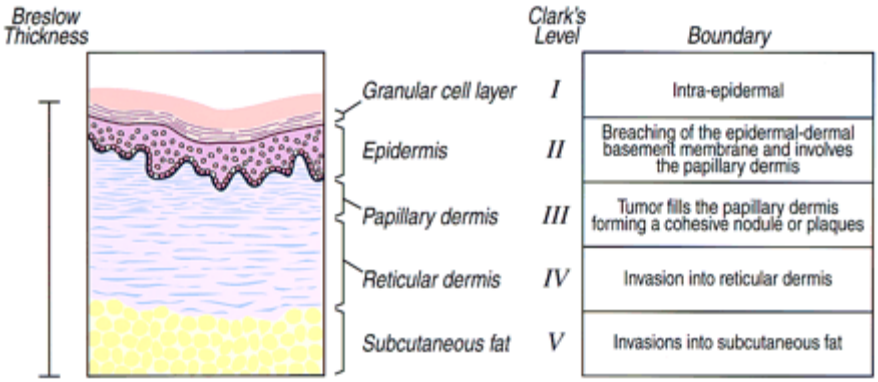

Figure 2 - Clark and Breslow Staging Systems (Chin et al., 1998).

1.1.4 Melanoma evolution

To follow their development, cutaneous melanomas are generally classified into five stages, from 0 to IV, based on the TNM system. This system considers tumour characteristics such as the lesion thickness, the replication rate of the tumor cells, the presence of ulcerations (T), the lymph nodes involvement (N) and the presence of any metastases (M) (Keung and Gershenwald, 2018; Imai, 1976).

Stage 0 - Also referred to as melanoma in situ, the tumor is confined to the superficial layers of the epidermis. The treatment is surgical. Virtually all these cases are cured.

Stage I - the tumor reaches up to 2 mm in thickness. With or without tissue tearing (ulcerations). Includes subclasses IA and IB, based on Breslow thickness. Treatment is surgical.

Stage II - the tumor reaches up to 4 mm in thickness and more, can have lacerations, satellite tumors. Includes subclasses IIA, IIB and IIC, based on Breslow thickness. Treatment is surgical.

Stage III - The tumor metastasizes to nearby lymph nodes and may have lacerations and satellite tumors. It includes subclasses IIIA, IIIB and IIIC, based on the number of involved lymph nodes. The treatment is surgical. Adjacent lymph nodes are often removed. Adjuvant drug therapy (dabra + tram or nivo - BRAFi + MEKi or PD-L1i) may be associated.

Stage IV - Melanoma has metastasized beyond regional lymph nodes to other organs such as the lung, liver, brain, or other lymph node stations. Lactate dehydrogenase (LDH) levels can be elevated. It includes subclasses M1a, M1b, and M1c, based on the organs affected by the metastases, the number and size of tumors, and serum LDH levels. The treatment is surgical and with chemotherapy (Gershenwald et al., 2008; Balch et al., 2001).

1.1.5 Genetic alterations

1.1.5.1 MAPK

Often the histological features are characterized by specific molecular lesions in oncogenes and tumor suppressors. According to The Cancer Genome Atlas Network, the genomic classification of cutaneous melanoma is divided into 4 subtypes based on the most frequently mutated genes: 1. BRAF; 2. RAS; 3. NF1; 4. Triple-WT (characterized by mutations and amplifications in KIT, a receptor tyrosine kinase, and the absence of mutations in the BRAF, RAS and NF1 genes). (Hayward et al., 2017; Menzies et al., 2012; Cancer Genome Atlas Network, 2015). These specific mutations involve, directly or not, the MAPK (Mitogen-activated protein kinase) pathway regulating cell growth, survival, and proliferation.

The MAPK pathway is physiologically activated by growth factors (GF) which, interacting with the respective receptors (GFR), usually a receptor tyrosine kinase (RTK), activate a signal transduction cascade that, through cytosolic intermediates, concludes in the activation and regulation of effector genes (Cuevas et al., 2007). The extracellular GF binding activates the RTK (EGFR, c-MET, c-KIT) inducing its dimerization. This conformation allows the receptor

trans autophosphorylation in tyrosine residues in the cytoplasmic side (Aramini et al., 2012). The phosphorylated tyrosines become anchoring sites for ATP molecules or substrate proteins, such as Grb2. In turn, this forms a protein complex with the adaptor protein Shc and guanine exchange factor (GEF) Sos, which activates small GTP-binding protein RAS (H/K/N-RAS). The active form of RAS, RAS-GTP, interacts with the inhibitor N-term RBD domain of RAF, activating its catalytic serine/threonine kinase domain. The active RAF form, translocating on the membrane, phosphorylates MEK in serine and threonine. The active MEK form phosphorylates ERK in tyrosine and threonine. The active ERK form translocates to the nucleus and phosphorylates several substrates (Park et al., 1996) (Fig.3).

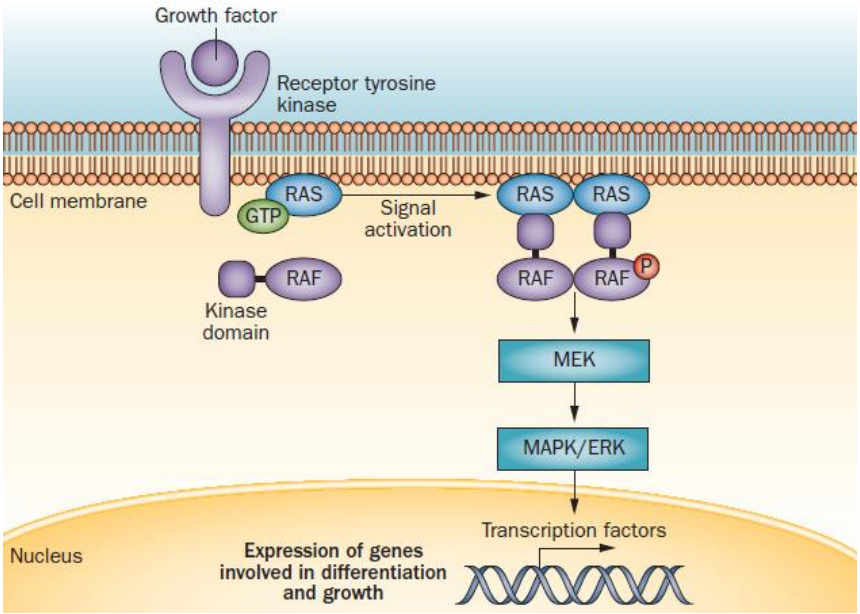

Figure 3 - The MAPK pathway (Gibney et al., 2013).

Each level of the cascade is controlled by a distinct family of proteins. The MAPKKKs (Mitogen-activated protein kinase kinase kinases) are represented by the RAF family, including A/B/C-RAF variants. The MAPKKs are represented by the MEK family, that includes MEK-1/2/3/4/5/6/7 isoforms. Finally, the MAPKs are represented by ERK-1/2 isoforms, JNK-1/2/3 (c-Jun N-terminal kinases) isoforms and p38-α/β/γ/δ isoforms.

Among the factors activated by the MAPK signaling pathway, there are transcription factors encoding proteins involved in cell replication, survival, proliferation, and differentiation. An example of an activated transcription factor is Fos, forming a heterodimer with the

transcription factor Jun (AP-1), allowing the cell to enter the S-phase of the cell cycle by activating a series of genes including those coding for cyclins D (Hess et al., 2004). Also, CREB (cAMP response element-binding protein), c-Myc (transcriptional regulator Myc-like) and NF-κB (nuclear factor kappa B) are well-known players in these dynamics (Kamran et al., 2013; Sang et al., 2003).

Furthermore, other signaling pathways interact, regulate, or cumulatively transduce together with the MAPK signaling pathway, such as P13k/AKT/mTOR (phosphoinositide-3-kinase/v-akt murine thymoma viral oncogene homolog 1/mechanistic target of rapamycin kinase) and TGFβ (transforming growth factor beta) (Braicu et al., 2019; Murugan et al., 2019; Silva et al., 2017; Fleming et al., 2009). Due to the role and the multiple interconnections of the MAPK signaling pathway, its constitutive upregulation and that of its components are involved in oncogenesis, tumor progression, and resistance to target therapy. Mutations in the *RAS / RAF / MEK / ERK* genes are very common in melanoma as well as in other cancers. Specifically, *NRAS* is found in 20% of melanoma cases, *BRAF* in 60% of cases. (Burotto et al., 2014)

1.1.5.2 BRAF

The RAF protein family, to which BRAF belongs, is characterized by 3 "Conserved Region" or CR domains (CR1, CR2, CR3) (Fig.4). In particular:

- CR1 is a RAS GTP-binding domain;
- CR2 is a serine-rich hinge region, that allows RAF membrane docking;
- CR3 is a serine/threonine protein kinase domain, in which most of the mutations are located.

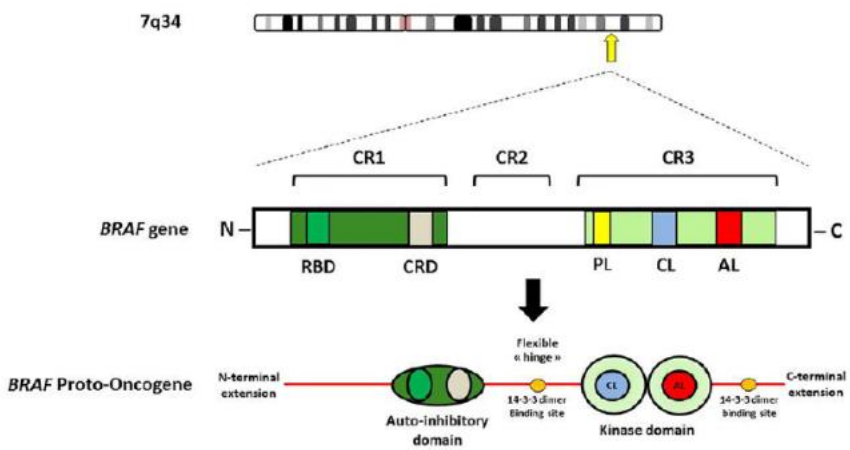

Figure 4 - Schematic representation of BRAF structure (Ducreux et al., 2019).

One way to aberrantly activate BRAF is represented by point mutations that activate the kinase activity in a constitutive way, for example because they are responsible for a conformational change of the activation loop that makes it more accessible to ATP and the substrate. In its active form BRAF forms a homo or heterodimer, further stabilized by the 14-3-3 proteins, activating ERK signaling independent of RAS (Cotto-Rios et al., 2020; Vido et al. 2018).

In BRAF mutated melanoma the most frequent mutation is V600E (approximately 85% of cases, in which valine (V) is substituted by glutamic acid (E) at amino acid 600), followed by V600K (approximately 10%, lysine (K) for V substitution) and V600R (2%, V to arginine (R)), and is anti-correlated with NRAS mutations (Cancer Genome Atlas Network). There is an inverse relationship between the presence of a BRAF mutation and age. BRAF mutations cover almost all patients under 30 years of age, compared with only 25% of those over 70 (Bauer et al., 2011).

1.1.5.2.1 BRAF splicing variants

Alternative splicing is a conserved physiological mechanism that allows the production of multiple coding and non-coding transcripts from a single gene. The different transcripts' expression follows tissue- and time-specific organism needs (Ampe et al., 2017; Stamm et al., 2004).

On the other hand, alternative splicing is involved in numerous pathologies, from Frausier syndrome to Parkinson's disease and cancer (Brosseau, 2018; Ampe and Van Troys, 2017; Garcia-Blanco et al., 2004; Venables, 2004), as it can promote the selective expression of pathological variants that are absent in healthy tissues. These variants are usually generated by genomic splice site point mutations, as observed for p53 and NRAS (Rásó, 2020; Holmila et al., 2003). The protein isoforms created this way often possess several novel biological properties including protein interaction, subcellular localization, or catalytic capacity. Similarly, non-coding variants can have different binding sites for miRNAs, pseudogenes, and RNA-binding proteins (RBPs) (Hu et al., 2022; Ilouz et al., 2017; Stamm et al., 2005). Basically, what varies is the interactions capability of the gene in its coding and non-coding nodes, potentially affecting malignant progression or resulting in mechanisms of escape from antineoplastic therapies or directly affecting malignant progression (Kahraman et al., 2020; Venables, 2004).

For example, in lung cancer transcripts 1 and 2 of *ehm2* gene have an opposite function. While variant 1 acts as tumor suppressor, variant 2 promotes growth, invasion, and migration in

vitro. Accordingly, variant 2 protein levels are higher in tumors, while variant 1 protein levels are higher in healthy tissues (Li et al., 2019).

When it comes to the *BRAF* gene, its alternative splicing variants are usually translated into smaller proteins that lack the Ras Binding Domain (RBD), hence are constitutively active (Poulikakos et al., 2011). Crucially, BRAFV600E splicing variants with this feature can dimerize in the absence of RAS, reducing the effectiveness of BRAF inhibitors (BRAFi): in this setting, their binding results in allosteric activation, rather than inhibition, with a consequent re-activation of MAPK signaling (Pupo et al., 2017; Samatar and Poulikakos, 2014).

While the splice variants involved in constitutive activation or drug resistance mechanisms are extensively studied, less is currently known about physiological splice variants of the BRAF gene, and about their individual contribution to disease initiation and progression. This is indeed one of the main fields of investigation in the lab where I have performed my PhD thesis and has already produced the experimental evidence summarized below.

To date, in the Ensembl database (GRCh38.p13 assembly) twenty transcript variants are reported for human *BRAF* gene, of which five encode proteins (BRAF-201/202/204/215/220). Of these, only two are reported in the CCDS database (BRAF-204/220). The Consensus CDS (CCDS) database is a collaborative effort by multiple public members: European Bioinformatics Institute (EBI), Ensembl Annotation Pipeline, HAVANA Curation Group, HUGO Gene Nomenclature Committee (HGNC), Mouse Genome Informatics (MGI), National Center for Biotechnology Information (NCBI), Eukaryotic Genome Annotation Pipeline and RefSeq Curation Group. CCDS is acting to identify a core set of human and mouse protein coding regions that are consistently annotated and of high quality (Pujar et al., 2018; Harte et al., 2012; Pruitt et al., 2009).

As previously reported (Marranci et al., 2017), we have established that the most expressed variants are three. *BRAF*-220 (NM_004333.6) transcript, which we named *BRAF*-reference transcript (BRAF-ref) (I), *BRAF*-204 (NM_001354609.2) transcript, which we named *BRAF*-X1 transcript (II), and NM_001378468.1 transcript reported only in NCBI, which we named *BRAF*-X2 transcript (III) (Table 1).

	Transcript	Length (nt)	Transcript name	CDS coordinates	Ensembl Transcript IDs	CCDS
BRAF-ref	NM_004333.6	6459	1	NM_004333.6:227-2527	ENST00000646891.1 (220)	CCDS5863
BRAF-X1	NM_001354609.2	9687	2	NM_001354609.2:227-2530	ENST00000496384.7 (204)	CCDS87555
BRAF-X2	NM_001378468.1	9533	7	NM_001378468.1:227-2503		

Table 1. *BRAF* transcript variant annotation

The three variants are identical from exon 1 to exon 17. ref variant is composed of 18 total exons, and, in this work, we divide exon 18 into 18.2 and 18b (Ex1-17 + Ex18.2/18b). X1 variant is made of 19 exons: exon 18.2 is spliced with a downstream exon 19, so that this variant is composed of Ex1-17 + Ex18.2 + Ex19. X2 variant consists of 18 exons, but exon 17 is spliced directly with exon 19 and exon 18 is missing (Ex1-17 + Ex19) (Fig. 5).

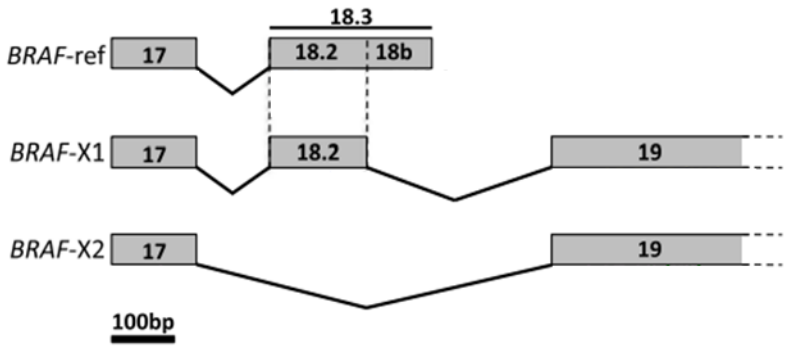

Figure 5 - Schematic representation of *BRAF* variants (Marranci et al., 2017).

Interestingly, the 3'UTR also differs between the variants, in terms of length and sequence. Although current annotation for ref 3'UTR is 3932nt, empirically we found a 3'UTR of 121nt long, while we confirmed that X1 and X2 3'UTRs are 7 kb long as reported in the database. Being transcribed from exon 18b and exon 19 respectively, ref and X1 3'UTR differ not only in length but also in sequence.

At the protein level, the isoforms differ in their C-terminal sequences (Table 2):

- BRAF-ref protein (NP_004324.2) matches the amino acid sequence **GAFPVH** for Ex18b;
- BRAF-X1 protein (NP_001341538.1) matches the amino acid sequence **GEFAAFK** for Ex19;
- BRAF-X2 (NP_001365397.1) matches the amino acid sequence **ENLQPSSSHHH GSICSYFLSL VFVQFVNIKT QFCSSNLFLK IQNFQCIS** for Ex19 (alternative ORF).

	Protein	Length (aa)	Isoform	Transcript type	UniProt ID	Ensembl Protein IDs
BRAF-ref	NP_004324.2	766	1	PROTEIN_CODING	P15056	ENSP00000493543.1
BRAF-X1	NP_001341538.1	767	2	PROTEIN_CODING	P15056	ENSP00000419060.2
BRAF-X2	NP_001365397.1	758	6	PROTEIN_CODING	P15056	

Table 2. BRAF isoform variant annotation

From the evolutionary point of view, BRAF is conserved across vertebrates in the X1 variant, as already demonstrated for mouse, rat and pig (Marranci et al., 2017), and here shown for zebrafish as well (Fig. 6).

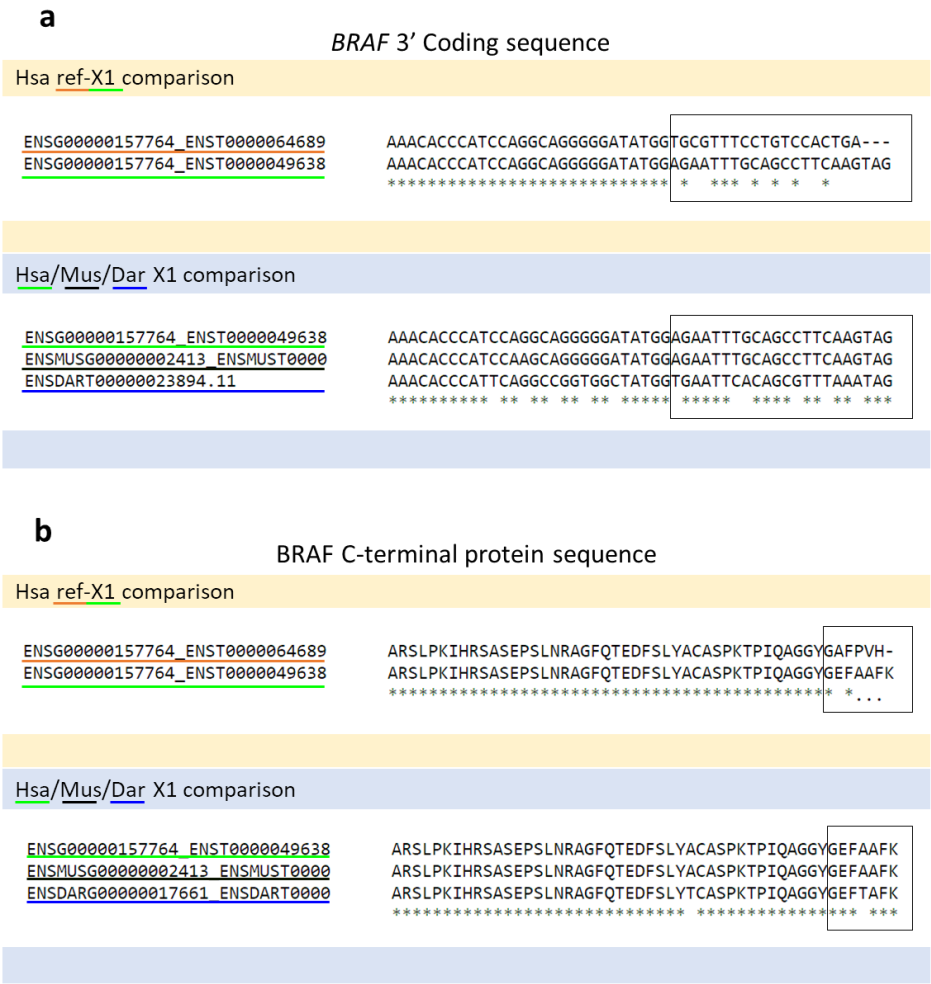

Figure 6 – BRAF 3' sequence comparison. (a) Alignment of last nucleotides of the cds. *Upper:* Alignment of ref (orange underline) and X1 (green underline) sequence of human *BRAF*. *Lower*: Alignment of human *BRAF*-X1 (green underline) with mouse *Braf* (black underline) and zebrafish *braf* (blue underline). (b) Alignment of C-terminal amino acids. *Upper:* Alignment of ref (orange underline) and X1 (green underline) sequence of human BRAF. *Lower:* Alignment of human BRAF-X1 (green underline) with mouse BRAF

(black underline) and zebrafish Braf (blue underline). The boxes on the right highlight the differences in sequence between ref and X1 variants in human and the conservation of X1 variant across zebrafish, mouse and human.

Accordingly, *BRAF*-X1 is also the most expressed variant among the 3. This was demonstrated by us in melanoma cell lines, as well as in TCGA melanoma samples, and its predominance persists also in lines that become resistant to BRAFi. However, while *BRAF*-X1 mRNA displays greater stability, *BRAF*-ref mRNA has greater translation efficiency, so that the protein levels of the two isoforms are similar in A375 cells. Together, they account for all BRAFV600E oncogenic functions.

Conversely, the X2 protein isoform is very unstable, as it gets rapidly degraded through the ubiquitin-proteasome pathway (Marranci et al., 2017) (Fig.7).

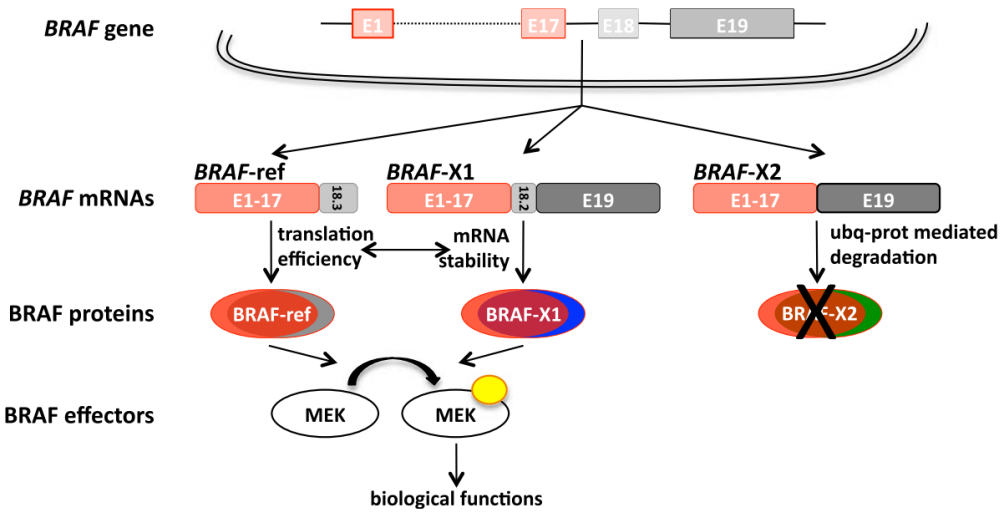

Figure 7 - Schematic representation of BRAF variants features (Marranci et al., 2017).

Due to the pivotal importance of BRAF as cancer driver and therapeutic target, ref and X1 variants deserve to be studied for their specificities. A different C terminal domain (ref: **GAFPVH** vs X1: **GEFAAFK**) can in fact result in different protein-protein interactions and/or different post-translational regulatory circuits. On the other hand, a different 3'UTR can result in different post-transcriptional regulation by RBPs, miRNAs and, therefore, competing endogenous RNAS (ceRNAs) (Kakumani et al., 2022; Kim et al., 2021; Qin et al., 2020). For example, YTHDF1, an RBP that recognizes the m^6A mark, most often located in the 3'UTR and near the stop codon, is a marker of worse prognosis for melanoma (Li et al., 2020). Furthermore, the Pandolfi group has

shown that the expression of mouse *Braf* is sustained by that of its pseudogene *Braf-rs1*, which acts as ceRNA for *Braf*-targeting microRNAs (Karreth et al., 2015; Poliseno et al., 2010).

1.1.5.3 TP53

Although the *BRAF* oncogene is one of the first genetic lesions found in dysplastic moles, alone it is not sufficient for the neoplastic transformation of the melanocyte. Consistently, genetic models in mice and zebrafish (GEM/GEZ) with the sole presence of BRAFV600E show only the development of moles, without the development of tumors (Patton et al., 2021; Goel et al., 2009; Patton et al., 2005). Loss of one or more tumor suppressors is generally a necessary condition, and in melanoma they are represented by CDKN2A (encoding p16), PTEN (involved in the PI3K pathway), and TP53 (encoding p53) (Daniotti et al., 2004).

Regulated by MDM2, TP53 maintains genome integrity by inducing arrest of the cell cycle (p21) to repair the damage or promoting apoptosis or senescence if the damage is not repairable (Fig.8). TP53 induces transcription of DNA repair genes (GADD45) and transcription and activation of cell cycle inhibitors (p21). Moreover, it induces apoptosis by transcription of the Bcl2 family (Noxa). The loss of p53 therefore causes an accumulation of uncorrected mutations, supporting the activity of the oncogene (Hertog et al., 2016).

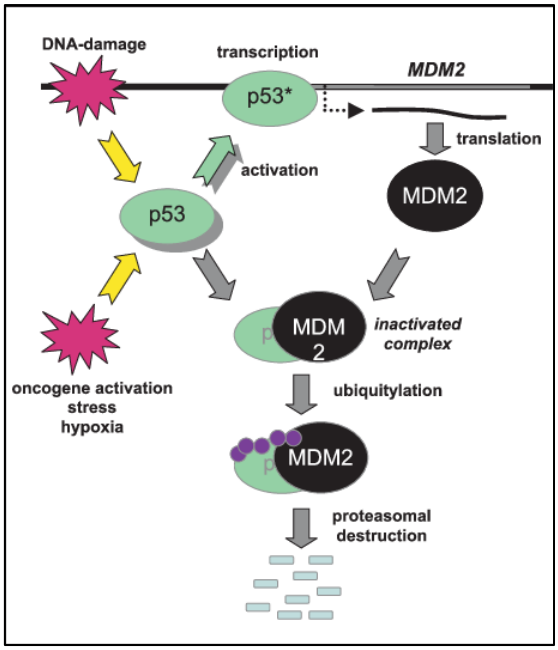

Figure 8 - Regulation of p53 activity through MDM2 protein (Hardcastle et al., 2006).

Although p53 mutations are found rarely in melanoma (<10%) (Box et al., 2008), melanoma genetic models with this mutation have been developed for mouse and zebrafish. The p53 knock out/loss of function model is compatible with life even in null zygosity in both mice and zebrafish. Since spontaneous tumors develop within 6 months in nullizygous p53-deficient mice, they are used in the heterozygous conditions (Donehower et al, 1996). Zebrafish instead requires the homozygous p53 mutant (loss of function (lf)) condition to increase tumor susceptibility, while tumors are spontaneously developed only late, at an average age of 14 months (Storer et al., 2010; Berghmans et al, 2005).

1.1.6 Targeted therapy

While in the early stages of melanoma progression the first choice of treatment is surgery excision, in the latest stages it is necessary to use radiotherapy and/or chemotherapy to remove any metastases, with molecular therapy being preferred for an increasingly personalized scenario for the patient (Domingues et al., 2018).

In patients with BRAF-mutated metastatic melanoma, overall survival rates are in fact higher in melanoma treated with target therapy against BRAFV600E, compared with conventional chemotherapy (Sosman et al., 2012, Chapman et al. 2011). The food and drug administration (FDA) approved Vemurafenib, Dabrafenib and Encorafenib, in 2011, 2013 and 2018 respectively as BRAF mutated inhibitors. Vemurafenib is a competitive kinase inhibitor binding to the ATP-binding domain of the mutant BRAF (Luke et al., 2012) Dabrafenib is a reversible ATP-competitive kinase inhibitor (Bowyer et al., 2015).

Unfortunately, in most patients the inhibition of BRAFV600E encounters resistance within 6-7 months, with most of them reactivating the MAPK signaling pathway. (Shi et al., 2014). The combination of BRAFV600E inhibitors (BRAFi) and MEK inhibitors (MEKi, allosteric inibitors) were then approved by the FDA. In detail, vemurafenib and cobimetinib (2015), dabrafenib and trametinib (2018), encorafenib and binimetinib (2018). Despite the rapid and strong pharmacological response, administration of BRAFi and MEKi reports the occurrence of serious adverse events (pyrexia, chills, fatigue, diarrhea, anemia, and rash) and a progression-free survival (PFS) of only 11-15 months with 5-year survival rate of approximately 30% (Long et al., 2018).

The combination of BRAFi, MEKi and checkpoint blockers of the immune system (ICB) was therefore approved by the FDA in 2020 for patients with BRAF V600 mutation-positive unresectable or metastatic melanoma. Specifically, atezolizumab (Ab anti-PD-L1) in combination

with cobimetinib and vemurafenib (Fig.9). ICBs exhibit a weak but prolonged response, in contrast to MAPK inhibitors (Kreft et al., 2019). Furthermore, MAPKi, particularly BRAFi, improve immunostimulatory signaling by increasing the activation of the immune system (CD40L, IFNg) and reducing tumor-induced immune escape mechanisms (IL-8, IL-10, VEGF). Among the activations of the immune system dictated by MAPKi, there is also a better response of T lymphocytes, due to an increase in tumor infiltration by CD8+ T cells, hence an improvement in tumor recognition. This in turn is due to an increase in the expression of antigens associated with melanoma differentiation (MART-1, gp100, TYRP1, DCT) (Kuske et al., 2018; Cebollero et al., 2016).

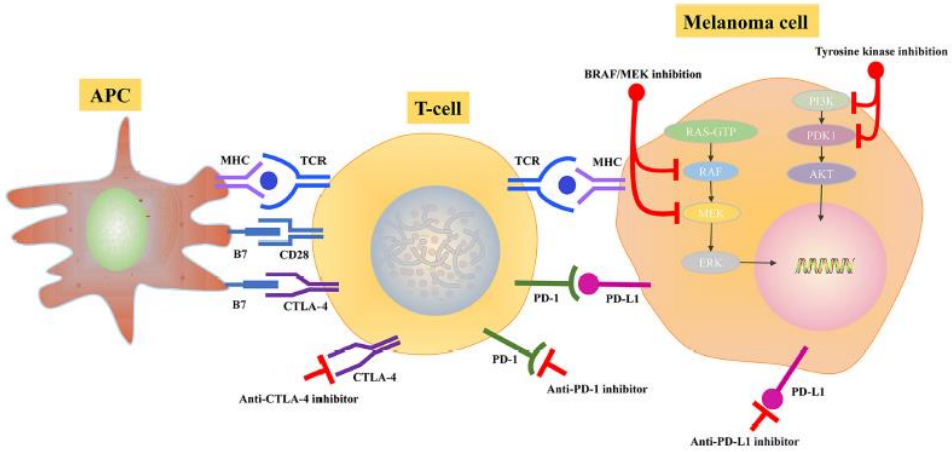

Figure 9 - Targeted therapy and immune checkpoint inhibitors in melanoma (Zeng et al., 2021).

Trials to date demonstrate some therapeutic benefit after 6-8 months of therapy by comparing triplet therapy with dual BRAFi and MEKi, but this is not clinically significant. The use of triplet therapy is not yet widespread because, in addition to a complicated dosage regimen, it presents an increase in toxicity rates with a toxic overlapping profile of individual drugs (Cebollero et al., 2016).

1.1.7 Pigmentation

Melanocytes, the cells from which melanoma arises, have the task of body protection from the harmful actions of the sun's rays, by producing melanin in specialized vesicles (melanosomes). In physiological conditions they give rise to dark clusters visible on the surface of the skin, known as moles (nevi) (Sardana et al., 2014).

Melanin absorbs solar radiation at various wavelengths and it comprises various pigments: eumelanin (dark pigments) and pheomelanin (red pigments). Pigmentation increases with sun exposure, causing tanning, in part through the melanotropin hormone and the MC1R receptor. The latter is a GPCR which, through cAMP, Calcium and Protein kinase A and C, induces MITF (Microphthalmia-associated transcription factor), a basic helix-loop-helix/leucine zipper transcription factor that in turn induces the expression of the enzymes that produce melanin. MC1R is polymorphic and the different allelic variants determine the color of the skin. Individuals with polymorphisms that make MC1R hypofunctional mainly produce pheomelanin, typical of individuals with light skin and red hair (Nasti and Timares, 2015; Shibahara et al., 2001). Eumelanin and pheomelanin derive from the common precursor tyrosine which is transformed into DOPA and Dopaquinone by the enzyme tyrosinase. In the presence of cysteine, cysteinyl DOPA is formed, through spontaneous oxidation becomes pheomelanin (Varga et al., 2016). In the absence of cysteine, TRP2/DCT and TRP1 use dopachrome to produce eumelanin (Fig.10).

Despite of the physiological protective role, in the pathological context of metastatic melanoma, melanotic tumors show worse prognosis and greater aggressiveness. The reasons are the following. The synthesis of pheomelanin generates highly reactive compounds, such as quinones or oxygen radicals, which can contribute to DNA damage and increase the risk of melanoma regardless of sun exposure (Napolitano et al., 2014). Melanin has indeed been defined a "photocarcinogen for cutaneous malignant melanoma", indicating that it is necessary to induce melanosomes and that its presence, although an index of melanocyte differentiation, does not exclude malignant transformation (Moan et al., 1999). Free radicals and reactive intermediates of melanogenesis can in fact generate a pro-oxidative and mutational environment at the genetic level. Adding to this type of endogenous damage there is also the exogenous damage due to exposure to UV rays, as pheomelanin does not absorb solar radiation as efficiently as eumelanin. This explains why subjects with fair skin are more predisposed to melanoma onset and progression.

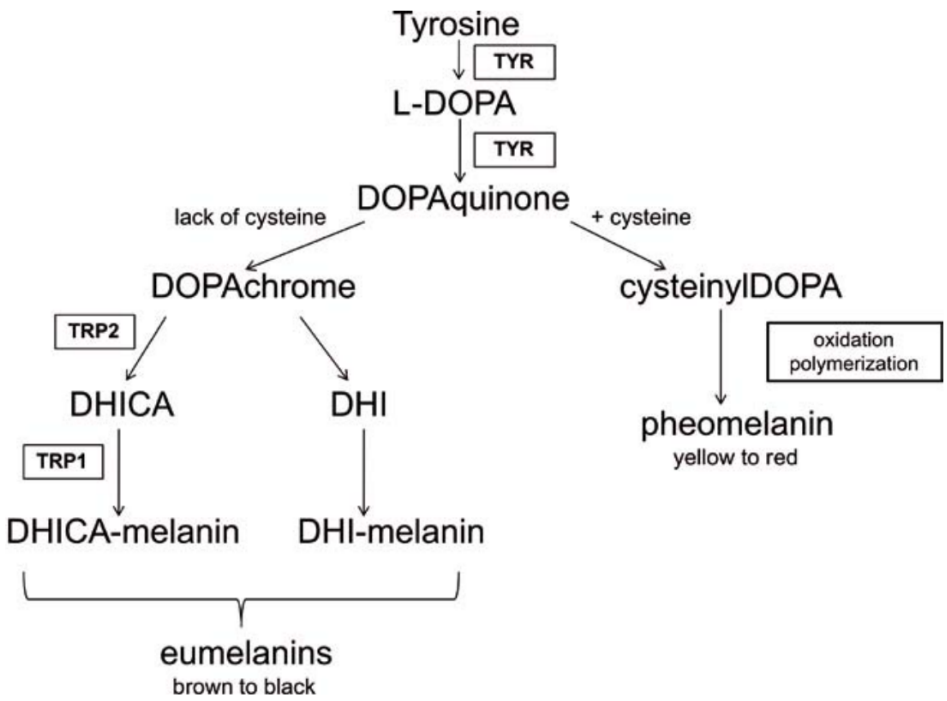

Figure 10 - Schematic eumelanin and pheomelanin synthesis (Cichorek et al, 2013).

Furthermore, eumelanin can attenuate chemotherapy and radiotherapy by acting as ROS quencher, metal chelator, and drug sequester. In addition, although the proteins involved in melanogenesis (TYR, TRP-1/2, gp100 and MART-1) are recognized as antigens by the immune system, the intermediates of melanogenesis inhibit immune activity (Slominski et al., 2022).

Also, we have shown that targeted therapy is compromised by pigmentation, with melanotic tumors being more resistant than amelanotic ones. (Vitiello et al., 2017). In turn, we have demonstrated that, by depressing MITF, BRAFi induce miR-211 which acts via EDEM1 inhibition, protecting TYR from degradation in melanotic melanoma cells (Mazar et al., 2010). In other words, BRAFi/MEKi induce the expression of miR-211, which in turn triggers a tolerance mechanism by exploiting the potential of melanin. Conversely, pigmentation inhibition by PTU sensitizes melanoma cells to BRAFi (Vitiello et al., 2017).

1.1.8 MITF

The activities exerted by MITF in melanoma go well beyond melanin synthesis. They are actually very pleiotropic, as mirrored on one side by the complex regulation of its expression, and on the other by its ability to dictate melanoma phenotype.

Just to make one representative example, the link between ERK signaling pathway and MITF expression is multifaceted. ERK acts by degrading MITF via the proteasome, but also by

increasing its activity recruiting the transcription cofactor p300 / CBP (Graf et al., 2014). RAFs, on the other hand, stabilize the nuclear localization of MITF and consequently its transcriptional activity (Estrada et al., 2022).

Through its activity as TF, MITF regulates genes involved in: DNA replication and cell cycle progression (CDK2, TERT, LIG1, CCNB1, CCNF and CCND1), cell cycle arrest (CDKN1A and CDKN2A), survival (BCL2 and BCL2A1), metabolism (PPARGC1A), and, as mentioned above, pigmentation (TYR, TYRP1, DCT, PMEL and MLANA) (Kawakami and Fisher, 2017; Strub et al., 2011). As a consequence, in melanoma cells two different states are dictated by MITF levels: a proliferative state when MITF levels are high, an invasive state when MITF levels are low (Tudrej et al., 2017).

Human *MITF* gene has its ortholog *Mitf* in mouse (86), and *mitfa/b* in zebrafish. Here, *mitfa* is mainly expressed in the eye and the neural crest, while *mitfb* is found in the eye, epiphysis, and olfactory organs (Lister et al., 1999). Therefore, the *nacre* line (*mitfa*-/-) without pigmentation (Dorsky et al., 2000), as well as the *mitfa* promoter dependent transgenic lines (e.g., *mitfa:*BRAFV600E (Patton et al., 2005), NRASQ61R (Dovey et al., 2009), and the MiniCoopR system (Iyengar et al., 2012) are widely used in the study of melanoma in zebrafish.

1.1.9 Neural crest

In recent years, a new subject of clinical trials has been the combination of vemurafenib (BRAFi) and leflunomide (leflu). The latter is an immunomodulatory drug that exerts its effects by inhibiting the mitochondrial enzyme dihydroorotate dehydrogenase (DHODH), which participates in the de novo synthesis of the pyrimidine ribonucleotide uridine monophosphate (rUMP) (White et al., 2011). The reduction in the levels of pyrimidine nucleotides, by inhibition of DHODH, is perceived as cell stress, thus activating p53. In turn, p53 can interrupt the cell cycle in G1 phase by inhibiting cyclin D activation or detect genetic damage in phase S and consequently interrupt the cell cycle (Fox et al., 1999). In melanoma, leflu has been highlighted for its detrimental effect on neural crest program (NCP), a phenotype shared with embryonic development. Although clinical trials have terminated due to adverse events, the results of effectiveness of leflu on melanoma cells has drawn attention on the NC phenotype as read out for drug screenings (ClinicalTrials.gov).

This similarity between the characteristics of melanoma and NC cells is a consequence of the embryonic origin of melanocytes, from which melanoma originates, as they are in fact the differentiation product of a cellular subpopulation of the neural crest. The neural crest is an

embryonic transient structure that develops during the neurulation phase, after the formation of the three germ layers (ectoderm, mesoderm, and endoderm) and the generation of the neural tube. At this stage, a specific cell population, that derives from the lateral margins of the neural folds, delaminates from the neural plate, and undergoes an epithelial-mesenchymal transition. Then, it migrates to specific positions of the body. Among the many cell lines that it contributes to, there are the cells of the peripheral nervous system and melanocytes (Bronner, 1993).

Most of the melanocytes that populate the epidermis are completely differentiated and, like neurons, have a long life and a low proliferative capacity (Cichorek et al., 2013. Specific markers characterize the melanocyte lineage line at different moments in time. Following stimulation with BMP and WNT by non-neural ectoderm and FGFs by the mesoderm, neural crest cells (NCCs) express MSX1, PAX3, FOXD3, and SOX10. In the delamination process, and therefore in epithelial-mesenchymal transition, the cells are characterized by the expression of SNAIL, SLUG, and a reduction of cadherin (Heppt et al., 2018, Tribulo et al., 2003).

In the precursor stage of the melanocyte, the melanoblast, SOX10 and PAX3 activate the expression of MITF that serves as master regulator of melanocyte development (Fig. 11). Upon reaching the epidermis, melanoblasts differentiate into pigmented melanocytes which, under the control of MITF, express specific enzymes including tyrosinase, dopachrome tautomerase and others (Wessely et al., 2021).

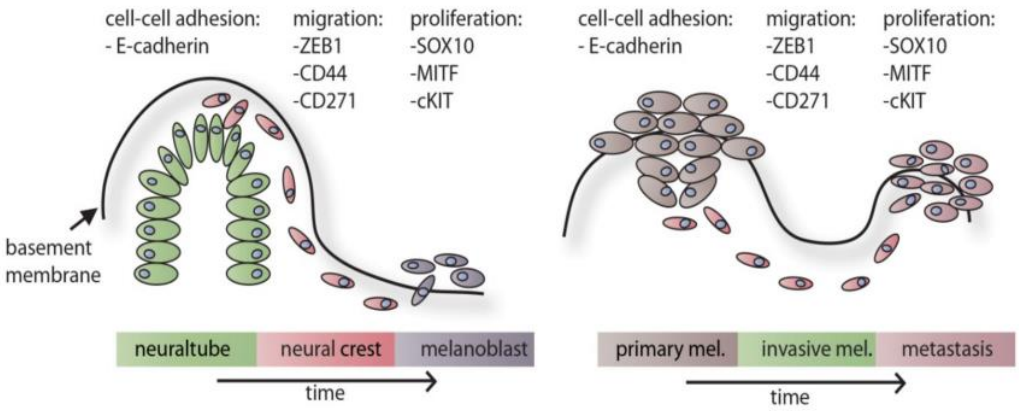

Figure 11 - Similarity between neural crest cells and advanced melanoma (Mirea et al., 2020).

1.1.9.1 SOX10

Malignant melanocytic cells invariably reacquire the potential of NCCs by developing advantages in growth, metastasis formation, and therapeutic resistance. The re-expression of NCCs markers such as SOX10, also used as a diagnostic histopathological marker, was highlighted both in primary and metastatic melanoma (Graf et al., 2014).

In melanoma SOX10 positively regulates the expression of CD271 (neurotrophy receptor belonging to the tumor necrosis receptor family), regulates the cell cycle via RB protein (RB-E2F1 complex), and increases the expression of MIA (melanoma inhibitory activity) and nestin (intermediate filament) (Gambichler et al., 2016).

1.1.9.2 Crestin

Using a melanoma model in zebrafish, reactivation of the neural crest program (NCP) has been highlighted from the early stages of melanoma initiation (Kaufman et al., 2016). The main actors of the neural crest process are highly and evolutionarily conserved. Zebrafish Sox10 is widely exploited for the study of melanoma, in screening models as well as in tumor onset and characterization models (Cunningham et al., 2021). In zebrafish, both embryonic and tumor Sox10 positive cells also express another marker, Crestin. Although unique to zebrafish and of unknown function, *crestin* is found expressed at much higher levels than *sox10* thus aiding the detection of NCP in melanoma cells (Kaufman et al., 2016).

1.2 Danio rerio

Danio rerio, more commonly known as zebrafish, first introduced by George Streisinger in 1960, is one of the most important non-mammalian vertebrate models in development and disease, including cancer.

Danio rerio is a freshwater teleost belonging to the Cyprinidae family of the Actinopterygii class, particularly advantageous for scientific research in vertebrates as it presents:

(I) simplicity of breeding in limited spaces due to its small size, its easy to satisfy nutritional requirements and the short intervals between generations;

(II) fast embryonic development, so that in just 24 hours it is possible to observe the formation of all primordial organs; furthermore, it is possible to see the internal development from the earliest stages thanks to the optical transparency of the embryo (Fig.12);

(III) rapid sexual maturation (about three months) and high prolificacy (a single female can lay about 100-200 eggs per reproductive event), allowing to obtain numerous offspring throughout the year to conduct large-scale genetic analyzes;

(IV) easy manipulation of cells and embryos, due to the external fertilization, allowing both transplantation and gene silencing experiments by microinjection of nucleic acids and oligonucleotides or by knock-out techniques;

(V) almost completely sequenced genome (diploid, about 1.7 gigabases with 25 pairs of chromosomes) (http://www.sanger.ac.uk/Projects/D_rerio) and extensive syntenic regions to the human genome (Howe et al., 2013).

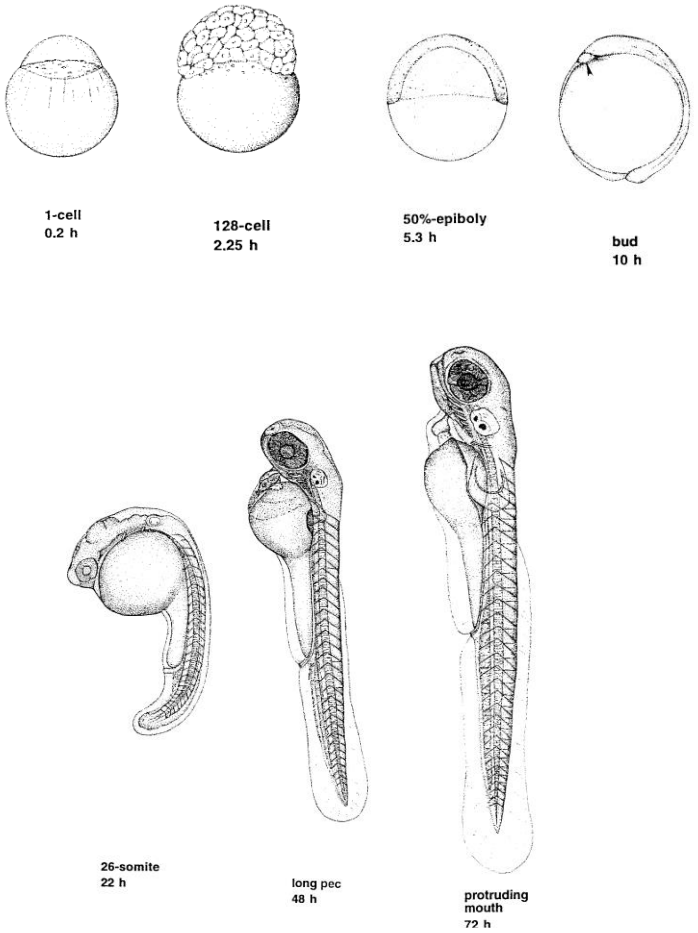

Figure 12 - Representative development stages in Zebrafish. Picture modified from Kimmel et al., 1995.

Furthermore, the transparency of the embryo facilitates the analysis of stable transgenic lines where fluorescent proteins (such as green fluorescent proteins eGFP or red RFP) can be expressed under the spatial and temporal control of the promoter of a gene of interest. Of note, this can be artificially prolonged by adding phenyl-thiourea (PTU), an inhibitor of melanin synthesis, to the culture water. Along the same line, stable genetic strains of zebrafish which retain much of their transparency throughout adulthood, known as nacre and casper (White et al., 2008), have been developed to exploit this advantage. The first one is lacking in the *mitfa* gene only (specific for pigmentation), the second one is lacking in *mitfa* and *mpv17* (specific for reflective iridophores). Due to conserved drug metabolism, preserved disease-associated genes, and genome similarity that provides reliable results (Bootorabi et al., 2017), zebrafish represents a useful tool for drug screening. In particular, it is perfect for high-throughput screenings in which drugs are absorbed directly thorough the culture water and large numbers of embryos can be studied in a 96-well plate, allowing a wide range of drugs to be tested in the same experiment.

Due to these advantages, zebrafish has allowed the identification of new genes by chemical mutagenesis. Hundreds of mutations have been identified and described (Driever et al., 1996; Kimmel, 1993; Walker and Streisinger, 1983), which have provided models for understanding their main developmental and pathological mechanisms, as it happened for MITF and TP53 (Berghmans et al., 2005). Additionally, Zebrafish genome is well characterized and present on the internet in websites like Ensembl (http://www.ensembl.org/index.html). Furthermore, a public database (http://www.zfin.org) provides information on genetic expression, phenotype and many protocols for the manipulation and husbandry of this model organism.

In the oncology field, many models have been developed that allow the use of zebrafish from the embryonic to the adult stage. Indeed, the embryonic and larval stage represents an effective and statistically strong platform to conduct pharmacological screenings, with multiple potential applications. Furthermore, in transgenic models, one can investigate the impact of specific alterations on how cancer cells interact with the environment and on the acquisition of harmful phenotypes, such as stemness programs, when challenged with treatment pressure. Of note, some models have been developed that can anticipate in earlier stages the phenotype normally found in adults, such as *kita*:RAS (Santoriello et al., 2010). Also, xenograft and allograft procedures for cell lines or patient-derived cells are possible, to monitor their responses to treatment in a physiologically relevant way. Otherwise, the adult stage lends itself to the study of tumor onset and progression, as well as pharmacological response, allowing the study of the interaction between the tumor and the environment.

Zebrafish is widely used for studying melanoma in vivo, as it provides a translational model for melanoma initiation and progression. Development of melanocytes is shared between humans and Zebrafish, which however has two additional pigment cells: the yellow xantophores and the silver iridophores that together with melanocytes form the typical zebra-like pattern of the fish (Rooijen et al., 2017). In melanoma many models have been developed that have highlighted multiple factors involved in the generation or progression of the tumor (i.e., SETDB1 (Ablain et al., 2018; Coel et al., 2011), Jmjd6 (Anelli et al., 2018), FATP1 (Zhang et al., 2018)).

2 Aims

In melanoma, the involvement of *BRAF* oncogene in its overactive form V600E is well known. Many studies have been carried out on its kinase function and involvement in the various stages of melanoma, as well as in pharmacological responses. Its relevance is such that it led to the development of targeted therapies against the specific BRAFV600E mutated form. Selective inhibitors of BRAFV600E (BRAFi) are very effective, but their effect is short-lived due to the rapid onset of drug resistance. Many studies have been done and continue to be performed to try to overcome tumor plasticity by attacking it from different sides, from complete inhibition of the signaling pathway, to strengthening the immune system. But much still needs to be done, where the ultimate goal will be to identify individual tumors' variables to deliver personalized therapy.

To better understand which aspects can be therapeutic targets, many tools and models have been developed aimed at discovering new characteristics or exploiting the already known characteristics of cancer cells. Zebrafish melanoma models are widely employed, allowing studies at the genetic, cellular, and environmental interaction level, given the observation by phylogenetic analyses that the MAPK signaling pathway is highly conserved between zebrafish and mammals.

Considering the key role of BRAFV600E during the development of melanoma, we hypothesized that the different transcript and protein isoforms of BRAF, which we have previously discovered, deserve to be studied systematically in order to establish their individual contributions to melanoma genesis, progression and pharmacological responses. Our hypothesis is that the selective overexpression of the individual isoforms and the respective 3'UTRs may have a different weight in the genesis or progression of melanoma, resulting from a different kinase activity of regulatory interactions. Moreover, we hypothesize that different variants may respond differently to the pharmacological treatments already in use or under development.

In particular, after generating the constructs for the *mitfa*-driven expression of *BRAFV600E* ref and X1 variants (cds only or cds + 3'UTR), our study focused on three main lines of research: analysis of the effects of each variant on the pigmentation phenotype in the different stages of development, up to the generation of tumors in mosaic conditions (I); generation of a stable transgenic line for each variant (II); generation and validation of a new reporter line based on *crestin* marker, capable of recording melanoma onset and progression at the cellular level, as well as of measuring the efficacy of new pharmacological combinations (III).

The generation of the mosaic and stable models was carried out using the Tol2 strategy, which allowed to follow along with development stages, the effect of the overexpression of each variant of the *BRAFV600E* gene. The overexpression was also validated by means of transcription

and histological analyses of the tumors. The genotyping of the new lines was carried out using Real Time techniques and Nanopore technology, favoring the sequencing of the insertion site by CRISPR-Cas9-mediated genome editing. The generation of a new drug screening tool focused on the quantification of *crestin*, which is reactivated in the melanoma-prone genetic context.

3. Materials and methods

3.1. Zebrafish husbandry

According to standard protocols, zebrafish (*Danio rerio*) were raised and maintained on a 14h/10h light/dark cycle at 28.5°C, in a zebrafish housing system (Tecniplast). Embryos were obtained from our animal colony by natural spawning and were maintained in E3 medium (5mM NaCl, 0.17mM KCl, 0.33mM $CaCl_2$, 0.33mM $MgSO_4$, 10^{-5} % methylene blue).

3.2. Ethics approval and consent to participate

The zebrafish facility has been authorized by the Italian Ministry of Health (authorization #297/2012-A, issued on December 21st, 2012). All the experimental procedures were carried out in accordance with the European Union guidelines for animal welfare [European Communities Council Directive of September 22, 2010 (2010/63/ UE)]. All experimental protocols were approved by the Italian Ministry of Health (authorizations #1222/2015-PR and #383/2020-PR).

3.3. Generation of transgenic lines

To generate all transgenic lines, the constructs were obtained using the Tol2kit, a gateway-based cloning kit for generating Tol2 transgenesis plasmids (http://tol2kit.genetics.utah.edu/index.php/Main_Page). Final pDEST plasmids were obtained through the action of LR clonase™ by combining four plasmids: 5' entry clone (p5E-XX) containing the promoter element flanked by attL4-attR1 sites; the central entry clone (pME-XX) with attL1-attL2 sites flanking an insert representing the coding sequence of a gene of interest or reporter; 3' input clone (p3E-XX) which contains the polyA transcription termination signal flanked by attR2-attL3 sites; pDestTol2pA providing the backbone flanked by attR4-attR3 (Fig. 13).

All combinations of plasmids and the final products are listed in Table 3, while Table 4 collects the sources from which the sequences of interest were extracted.

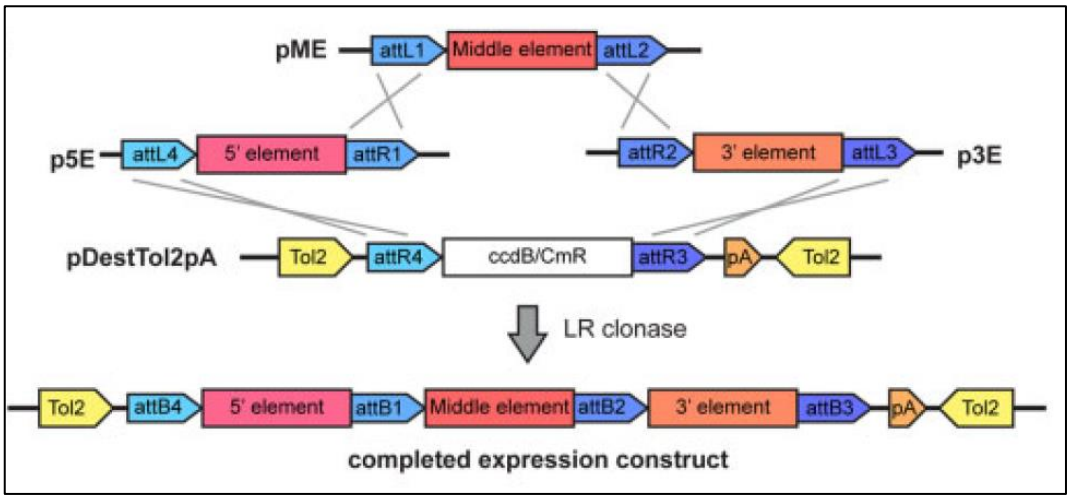

Figure 13 – Schematic representation of the LR cloning reaction between a 5'Entry Clone (p5E), a Middle Entry Clone (pME), a 3' Entry Clone (p3E) and a Destination Vector (pDestTol2pA) (Kwan et al., 2007).

Elements	Origin	Final plasmid
p5E-*mitfa* promoter	kind gift from Dr. Charles Kaufman, Washington University School of Medicine, St. Louis, USA	pDEST(*mitfa:-2.3Hsa.BRAF_V600E-220,myl7:eGFP*)
pME-(-*2.3)Hsa.BRAF_V600E-220*	SalI and SpeI restriction enzyme-mediated cloning in pME-MCS (Tol2kit)	
p3E-polyA	Tol2kit	
pDestTol2CG* backbone	pDestTol2pA with myl7:eGFP transgenesis marker, Tol2kit	
p5E-*mitfa* promoter		pDEST(*mitfa:-2.3Hsa.BRAF_V600E-204,myl7:eGFP*)
pME-(-*2.3)Hsa.BRAF_V600E-204*	SalI and SpeI restriction enzyme-mediated cloning in pME-MCS	
p3E-polyA		
pDestTol2CG* backbone		
p5E-*mitfa* promoter		pDEST(*mitfa:-2.3Hsa.BRAF_V600E-X2,myl7:eGFP*)
pME-(-*2.2)Hsa.BRAF_V600E-X2*	SalI and SpeI restriction enzyme-mediated cloning in pME-MCS	
p3E-polyA		
pDestTol2CG* backbone		
p5E-*mitfa* promoter		pDEST(*mitfa:-2.4Hsa.BRAF_V600E-220,myl7:eGFP*)
pME-(-*2.4)Hsa.BRAF_V600E-220*	SalI-SpeI and SpeI-NotI restriction enzyme-	

	mediated cloning in pME-MCS	
p3E-polyA		
pDestTol2CG* backbone		
p5E-*mitfa* promoter		pDEST(*mitfa:-9.4Hsa.BRAF_V600E-204,myl7:eGFP*)
pME-(-*9.4)Hsa.BRAF_V600E-204*	SalI-SpeI and SpeI-NotI restriction enzyme-mediated cloning in pME-MCS	
p3E-polyA		
pDestTol2CG* backbone		
p5E-*crestin* promoter	EcoRI restriction enzyme-mediated cloning in p5E-MCS (Tol2 kit)	pDEST*(-4.5-crestin:Luc2-P2A-mCherry,URAprom:URA)*
pME-*Luc2-P2A-mCherry;*	SpeI and NotI restriction enzyme-mediated cloning in pME-MCS	
p3E-polyA-*URA*	HindIII restriction enzyme-mediated p3E-polyA-MCS (Poliseno lab)	
pDestTol2pA		
p5E-*crestin* promoter		pDEST*(-4.5crestin:Luc2-P2A-mCherry,γcrist:VenusGFP)*
pME-*Luc2-P2A-mCherry*		
p3E-polyA		
pDestTol2pA-*γcryst:VenusGFP*	kind gift from Dr. Nadia Mercader-Huber, PhD, CNIC-ISCII, Madrid	
p5E-*crestin* promoter		pDEST*(-4.5crestin:Luc2-P2A-mCherry*
pME-*Luc2-P2A-mCherry*		
p3E-polyA		
pDestTol2pA		

Table 3. pDEST plasmids generation

Source plasmids	Methods	Final plasmid
pYES2-*BRAFV600E*-ref	Termed SalI and SpeI restriction site polymerase chain reaction (RS-PCR)	pME-(-*2.3)Hsa.BRAF_V600E-220*
pYES2-*BRAFV600E*-X1	Termed SalI and SpeI RS-PCR	pME-(-*2.3)Hsa.BRAF_V600E-204*
pYES2-*BRAFV600E*-X2	Termed SalI and SpeI RS-PCR	pME-(-*2.2)Hsa.BRAF_V600E-X2*
pYES2-*BRAFV600E*-ref and pGEM-UTR121nt	Termed SalI-SpeI and SpeI-NotI RS-PCRs	pME-(-*2.4)Hsa.BRAF_V600E-220*

pYES2-BRAFV600E-X1 and pMARRA-UTR7kb	Termed SalI-SpeI and SpeI-NotI RS-PCRs	pME-(-*9.4)Hsa.BRAF_V600E-204*
pGEM-*(-4.5)crestin*	SalI and SacII subcloning	p5E-*crestin* promoter
pDEST*(-4.5crestin:mCherry)*	EcoRI subcloning	pGEM-*(-4.5)crestin*
pMIR-ref-3'UTR (for Luc2) and pDEST*(-4.5crestin:mCherry)* (for mCherry)	Recombinant PCR with SpeI-NotI restriction sites	pME-*Luc2-P2A-mCherry*
pMA-150	HindIII subcloning	p3E-polyA-*URA*
p3E-polyA	MfeI linearization and oligo annealing	p3E-MCS
pDEST*(-4.5crestin:mCherry)*	kind gift from Dr. Charles Kaufman, Washington University School of Medicine, St. Louis, USA	
pMA-150	kind gift from Dr. Tiziana Cervelli, CNR-IFC, Pisa, Italy	

Table 4. Intermediate plasmids and their sources

All PCR reactions involved in cloning were performed using Phusion Flash High-Fidelity PCR Master Mix (Thermo-Fisher Scientific, Waltham, MA, USA) using primers listed in Table 5. The PCR amplicons were then run on a 0.8-2% agarose gel, extracted using QIAquick Gel Extraction Kit (Qiagen, Hilden, Germany). Successful cloning was confirmed subjecting plasmids to Sanger sequencing (Eurofins Genomics, Ebersberg Germany).

Primer	Sequence 5' → 3'	Application
hBRAF-cds common-SalI - Kozak sequence -Fw	ATAGTCGACGCCACCATGGCGGCGCTGAGCGGT	HsaBRAF cds cloning
hBRAF-ref cds SpeI stop codon Rev	ATAACTAGTTCAGTGGACAGGAAACG	HsaBRAF-ref cds cloning
hBRAF-ref X1SpeI stop codon Rev	ATAACTAGTCTACTTGAAGGCTGCAAATTCTC	HsaBRAF-X1 cds cloning
hBRAF-ref X2 SpeI stop codon Rev	ATAACTAGTTCAGCTTATGCATTGGAAATT	HsaBRAF-X2 cds cloning
hBRAF-ref 3'UTR SpeI Fw	ATAACTAGTTGAAACAAATGAGTGAGAGAG	HsaBRAF-ref 3'UTR cloning
hBRAF-ref 3'UTR NotI Rev	ATAGCGGCCGCTTCTTTGGTTCACCTTAA	
hBRAF-X1 3'UTR SpeI_Fw	ATAACTAGTTAGCCACCATCATGGCAGCATC	

hBRAF-X1 3'UTR NotI Rev	ATAGCGGCCGCTTCTCCATGCAGTCAATCT	HsaBRAF-X1 3'UTR cloning
Luc2 kozak sequence- SpeI Fw	ATAACTAGTGCAAACATGGAAGACGCCAAAAACATAAAG	Luc2-P2A-mCherry cloning
Luc2-P2A Rev	TCTCCAGCCTGCTTCAGCAGGCTGAAGTTGGTAGCTCCGCTTCCCAATTTGGACTTTCCGCCCT	
mCherry-P2A Fw	GCCTGCTGAAGCAGGCTGGAGACGTGGAGGAGAACCCTGGACCTATGGTGAGCAAGGGCGAGGA	
mCherry- NotI stop codon Rev	ATAGCGGCCGCTTACTTGTACAGCTCGTCCAT	
MCS top frame – MfeI-HindIII-SmaI-XmaI-NruI	AATTGAAGCTTCCCGGGCCCGGGTCGCGAt	MCS generation
MCS bottom frame – MfeI-HindIII-SmaI-XmaI-NruI	AATTaTCGCGACCCGGGCCCGGGAAGCTTC	

Table 5. Primer sequences in cloning

3.4. Microinjection

Zebrafish of the p53(lf) strain (ZDB-ALT-050428-2) (kind gift from Dr. Francesco Argenton, Università di Padova) were bred and embryos were collected for microinjection. 20-30pg of plasmidic DNA and 20-30 pg of Transposase mRNA were coinjected into 1-cell stage embryos for the largest plasmid pDEST(*mitfa:-9.4Hsa.BRAF_V600E-204,myl7:eGFP*). Following the calculation of molar concentrations, equimolar amounts of the other Hsa.BRAFV600E plasmids were microinjected. After microinjection, embryos were maintained in E3 medium at 28.5°C and at 24-48hpf they were selected on the basis of heart-specific green fluorescence (Leica MZ10F Stereomicroscope).

3.5. RNA extraction, retrotranscription and PCR amplification

Embryos and larvae were staged following standard parameters (Kimmel et al., 1995) and homogenized by insulin needle. Total RNA was extracted using QIAzol (Qiagen), following the manufacturer's instructions, quantified using Nanodrop Lite (Thermo Scientific), verified on 2% agarose gel and reverse transcribed with the SuperScript III RT reaction kit (Thermo Fisher Scientific) according to manufacturer instructions. The successful retrotranscription and the absence of contaminating genomic DNA were routinely checked through a control PCR (PCR Master Mix, Thermo-Fisher

Scientific) in which the exon-spanning primers for *actb1* mRNA are used. Of starting RNA, 10 ng was used for end point PCR analysis to characterize the expression of the *Hsa.BRAFV600E* gene in all its components depending on the line under examination. Following manufacturer's instructions, GoTaq® G2 Green Master Mix (PROMEGA) was used with 0.5µM primers concentration and annealing temperature of 58°C. The primers used are listed in the Table 6.

Primer	Sequence 5' → 3'	Application
hBRAFcds_377 Fw	CTAGCCTTTCAGTGCTACCTTCATCT	common coding
hBRAFcds_1001_Rw	GGACTGGTGAGAATTTGGGGC	
Ex14_1705 Fw	GCCAAGTCAATCATCCACAG	ref coding specific
hBRAFcdsRef_2300_Rev	CAGTGGACAGGAAACGCACCATAT	
Ex15_1841 Fw	CTGGATCCATTTTGTGGATG	X1-X2 coding specific (ex19)
hBRAFcdsX1_2300_Rev	CTTGAAGGCTGCAAATTCT	
Ex17_2075 Fw	TAATGGCAGAGTGCCTCAAA	ref cds-3'UTR junction specific
hBRAFutrRef_38 Rev	TGTTGCTACTCTCCTGAACTC	
X1 only qRT_2179 Fw	AGTGCATCAGAACCCTCCTT	X1 cds-3'UTR junction specific
hBRAFutrX1_387 Rev	TTGATCTGGTGGTTAGAAGGG	
hBRAFutrX1_6041Fw	TGTTAATGACCAACGTAAGTGGC	X1 3'UTR end specific
hBRAFutrX1_7155 Rev	GCAGTCAATCTTTATTATAGCAG	
Actb1_Intr311_Fw	TCAGGGAGTGATGGTTGGC	RNA control, exon spanning
Actb1_ Rev	CAACGGAAACGCTCATTGC	

Table 6. Primer sequences in end point PCR

3.6. qRT-PCR

Quantitative PCR analysis (qRT-PCR) was performed in triplicate with SSOADV Universal SYBR Green (Bio-Rad) in 15 µL final reaction volume on a CFX96 Real-Time System (Bio-Rad). 37.5 ng of of cDNA, 0.5uM primers and annealing temperature of 60°C were used for primers listed in Table 7. PCR efficiency calculation and data were analyzed using CFX Manager Software (Bio-Rad). Relative expression of targets was determined using the $2^{-\Delta\Delta Ct}$ method and data were normalized using housekeeping genes (*ef1a, actb1*).

Primer	Sequence 5' → 3'
Ef1a _Fw	GTACTTCTCAGGCTGACTGTG
Ef1a _Rw	ACGATCAGCTGTTTCACTCC
Actb1_ Fw	TGAGCAGGAGATGGGAACC
Actb1_ Rw	CAACGGAAACGCTCATTGC
crestin_qRT1 Fw	ACATGCTGACGTCGCTAACA
crestin_qRT1 Rev	CAGGTGAGTTTCGAGGGCTT
dre-Sox10 Fw	AGGGAGGAAAATCAGGCGAG
dre-Sox10 Rev	TTCGCCAATGTCCACGTTAC
hBRAFcds_377 Fw	CTAGCCTTTCAGTGCTACCTTCATCT
hBRAF-qRT1 Rev	TCCGTGCCACATCTGTGGGAT

Table 7. Primer sequences in qRT-PCR

3.7. Zebrafish image acquisition

To acquire the animals' images, they were anesthetized with tricaine 0.17 mg/mL MS-222 (Sigma, A5040). Specifically, 24hpf embryos and 5dpf larvae were immersed in methylcellulose, and the images were acquired using Leica M80 stereomicroscope equipped with a Nikon DS-Fi1 camera. The juvenile and adult stage specimens were instead anesthetized, and the images acquired in water by stereomicroscope for juvenile and adults with a ASUS Zenfone X00TD. Quantification of nevus area was performed in Image J software (http://rsb.info.nih.gov).

3.8. Whole mount in situ hybridization

24hpf zebrafish embryos, were anaesthetized, fixed in 4% paraformaldehyde (PFA) overnight (ON) at 4°C. The day after embryos were washed in PBS and dehydrated in a MeOH series for storage in 100% MeOH for at least 12h. Embryos were rehydrated stepwise in methanol /PBS, washed in PBT (PBS, Tween 0,1%). pre-hybridized for 3 h at 63°C in hybridization buffer and, incubated ON with 1ng/µL of riboprobe (kind gift from Dr. Letizia Pitto, CNR-IFC, Pisa, Italy) in hybridization solution at 63 °C (probe was denatured for 10 min at 95 °C). The probes were removed by 30 min stepwise washes with increasing 2X SSC (Saline-sodium citrate) ratio. Following 0.2X SSC for 30 min, maleic buffer tween-20 (MBT), 2% Roche Blocking Reagent (Roche, code 11096176001) for 2 h and, Ab incubation (Anti-Digoxigenin-AP, Fab fragments, Roche Applied Science, code 11093274910) at a 1:5'000 dilution in MAB ON at 4 °C. After several washes in MBT (MAB with Tween (0,1%), embryos were incubated in a staining buffer (NTMT) then, in BM Purple chromogenic substrate (Roche Applied Science, code 11 442 074 001) until staining was sufficiently developed. After stopping the reaction, embryos were post fixed in 4% PFA in 1X PBS for 20 min and, finally, stored in 95% glycerol at 4° C.

3.9. Fluorescence imaging

20-30hpf embryos *crestin* lines were dechorionated manually by forceps (Dumont No. 5; Sigma-Aldrich F6521-1EA), anesthetized and fluorescence imaging was carried out using the Nikon Eclipse E600 microscope equipped with CoolSnap-CF camera and NIS-Elements software version 4.0. *crestin* fluorescence signal was analyzed using ImageJ software.

3.10. Kaplan-Meyer analysis and analysis of tumor specimens

In tumors incidence monitoring, animals were observed weekly up to 50 weeks.

Three weeks after tumor onset, fish were euthanized by exposure to excess of tricaine. They were then fixed in 4% PFA for 48 h at 4°C, dehydrated through a series of graded ethanol baths and finally embedded in paraffin. Transverse paraffin-embedded tissue sections (5µm) were used. Hematoxylin and Eosin (H&E) staining was carried out using standard methods. For immunohistochemistry (IHC), tissue sections were stained using standard whole-mount immunostaining protocol with Vectastain elite ABC kit (Vector Laboratories) and 1:50 mouse anti-BRAFV600E VE1 primary antibody (ab228461, Abcam).

3.11. Drug treatment

6-8hpf embryos were treated with VEM 1/2µM, COB 1µM (Li et al., 2019), Leflu 6,5µM (White et al., 2011) and PTU (0,2mM) (Westerfield et al., 2000) alone or in combination using the vehicle (DMSO) at 1% dilution, in E3 medium.

3.12. Luciferase assay

Luciferase signal was quantified, in mosaic and transgenic lines, with Luminometer, using the Steady-Glo® Luciferase Assay System (Promega). Embryos were screened for mCherry signal in mosaic lines or eGFP signal in stable lines respectively at 24hpf or 48hpf and transferred into a 96-well with 50µL of E3 medium and 25µL of Steady-Glo®. Luciferase assay was left for 30-45 minutes of dark; quantification of Luciferase signal was evaluated with LUMIstar® Omega (BMG LABTECH) luminescence microplate reader.

3.13. Cytofluorimetric analysis

mCherry signal in embryos was recorded using CytoFlex® (Beckman Coulter) cytofluorimeter (excitation 488 nm, emission 610 nm). Embryos were dissociated using the following protocol: Phosphate Buffered Saline (PBS) washes, deyolking (55 mM NaCl, 3.6 mM KCl, and 1.25 mM $NaHCO_3$, 1 mM EDTA, (Purushothaman et al., 2019)), centrifuge at 500g for 10 minutes, 1mg/mL collagenase type I (Sigma-Aldrich, C0130) in Leibovitz's L-15 medium (Thermo Fisher Scientific) for 30 minutes into thermostatic bath at 28°C with a

pounder for continuing dissociation, centrifuge at 500g for 10 minutes, complete culture medium (add to L-15: Glutamine 1%, Penicillin- Streptomycin 1% and FBS 20 %) replacing, DAPI (ThermoFisher, D1306) addition. DAPI will allow the distinguish of dead cells from viable cells. For each experiment we have used 50-100 embryos per condition.

As described in the study of Weiss et al., 2022 (Fig. 14), gating strategy for cytofluorimeter analysis was performed in order to isolate cells positive for mCherry signal and negative for DAPI signal. Initially, debris and doublets were removed, dead cells positive for DAPI were removed and finally positive cells for mCherry signal were gated.

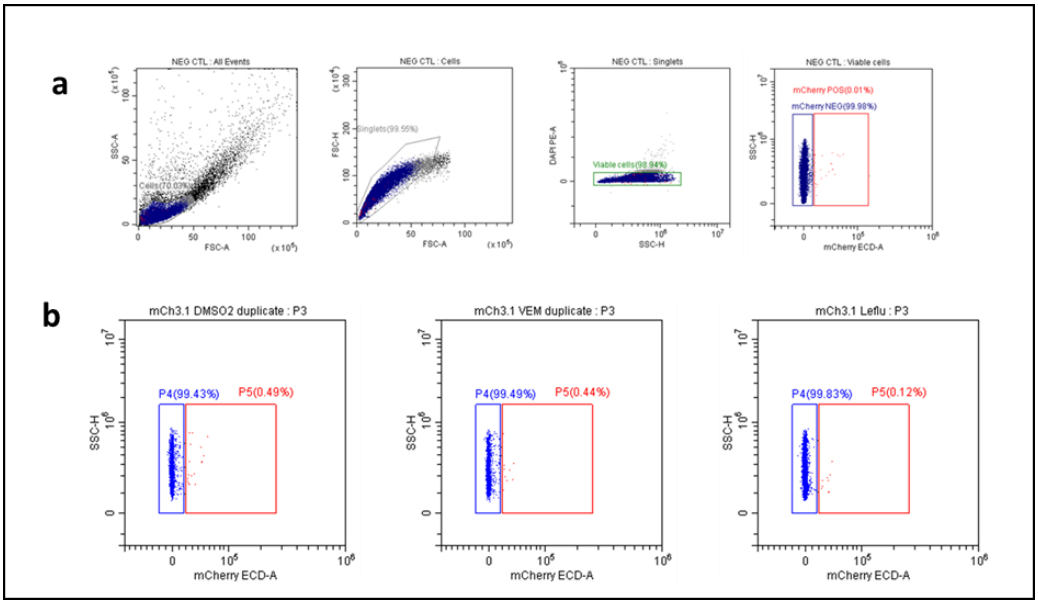

Figure 14 - Gating strategy. (a) percentage of cells positive for mCherry in *Tg(mitfa:BRAF_V600E); Tg(-4.5crestin:mCherry);p53(lf)*embryos at 24 hpf. (b) Representative results after drug treatment.

3.14. Statistical analyses

Data were analyzed according to their normality using parametric or non-parametric tests. Multiple comparisons for groups with a single variable (e.g. wt or *Hsa.BRAFV600E* line) were performed by one-way ANOVA analysis (Tukey, Dunnet), for groups with multiple variables (e.g. comparison wt and *Hsa.BRAFV600E* line) by two-way ANOVA analysis. To analyze the frequencies between two or more variables (e.g. tumor macro characteristics), we used the non-parametric Fisher test, while Mantel-Cox analysis was used for stratified data over time (Kaplan-Meyer curve). The significance of differences between two unpaired groups was determined by the non-parametric Mann-Whitney test. $P < 0.01$ or $P < 0.05$ was taken as a minimum level of

significance. Data are expressed as means ± SEM (standard error of the mean). In order to account for biological and technical variability, for each experiment at least 2 independent biological replicates were performed.

3.15. Fish genomic DNA extraction

Zebrafish genomic DNA (gDNA) extraction was performed by applying different protocols, depending on the ultimate application.

For Real Time PCR application, NTES buffer extraction was performed; for the locus identification site of transgenes, high-molecular-weight gDNA extraction was performed.

NTES buffer extraction of gDNA was performed from 5-10mg of tissue, adding 900µL of NTES buffer solution (Tris HCl pH8 50mM, EDTA pH8 50mM, NaCl 100mM, SDS 0.1%) with 6 µL of Proteinase K (20mg/mL) and incubating ON at 56°C rotate. The day after the digested material was centrifuged at 13’000 rpm for 5 min, to recovered supernatant were added saturated NaCl, vortexed aggressively for 10- 30 sec, centrifuged for 10 min at 13’000 rpm. The supernatant was transferred in absolute ethanol and inverted enough times to obtain maximum concentration of the precipitate DNA mass. The DNA was pulled out and washed in 70% ethanol, and finally dissolved in MilliQ water at 60°C for 10 min or ON at 37°C.

The extraction of high-molecular-weight gDNA from at least 100mg of adult fish tissue was performed according to the protocol described in The Zebrafish Book with only one modification: acetate ammonium salt was used instead of ammonium chloride in the DNA precipitation step.

3.16. Copy number identification by Real Time-PCR

In transgenic lines, to characterize the copy number of a transgene in the genome, Southern Blotting is largely used; however, this technique is time consuming and difficult to use when there are a lot of samples (Shepherd et al., 2009). Following the confirmation of one transgenic line (*Tg*(*mitfa:-2.3Hsa.BRAF_V600E-204,myl7:eGFP*) β) with the Southern technique (data not shown), we have shifted the search for our single insertion specimens using Real Time technique, a valid and much quicker alternative to Southern Blotting.

Real Time quantitative PCR (RT-qPCR) was used to identify the copy number of transgenes. This technique is called the “relative quantitation method”. Compared to Southern

Blotting is faster and suitable for large-scale analysis. Non-specific dsDNA binding dye was used (SYBR® green) to quantify the copy number: whenever specific primers bind a sequence and catalyse its amplification, the dye binds the double-strand. The threshold cycle (Ct) from the quantification with RT-qPCR of a transgene is compared with the Ct of a gene with known copy-number, like in our case actin beta 1 (ZDB-GENE-000329-1) on chromosome 1 (Fig.15).

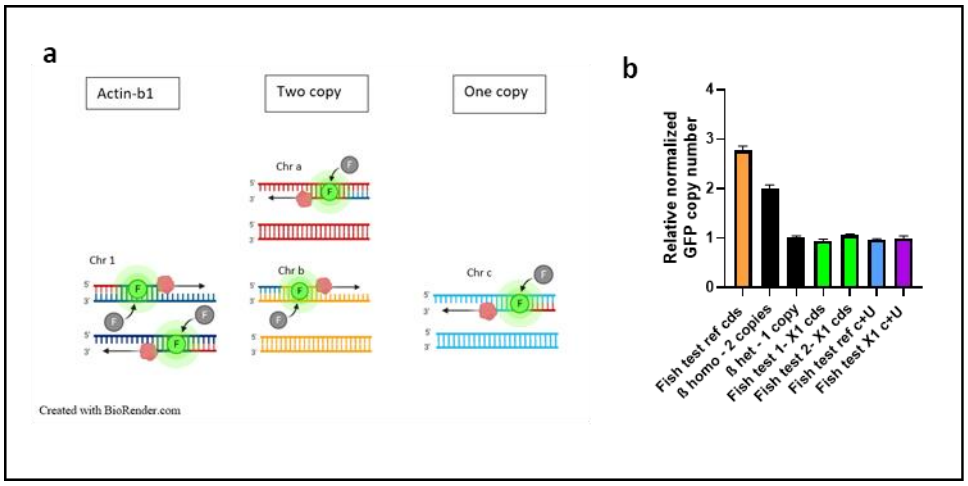

Figure 15. – Copy number identification strategy. (a) Schematic representation of transgenic lines genotyping with Real-Time qPCR. (b) Identification of transgene copy number in several specimens. *Tg*(*mitfa:-2.3Hsa.BRAF_V600E-204,myl7:eGFP*) β in homozygous (2 copies) and heterozygous (1 copy) conditions are used as control of the reaction (β homo and β het). The fishes (test) represent the specimens subjected to further analysis. A triple insertion fish was identified for -2.3Hsa.BRAF_V600E-220 (ref cds) line and at least one fish with single insertion for -2.3Hsa. BRAF_V600E-204 (X1 cds), -2.4Hsa.BRAF_V600E-220 (ref c+U), -9.4Hsa.BRAF_V600E-204 (X1 c+U).

To avoid interference, the copy number was determined by measuring the eGFP and mCherry genes belonging to the constructs, and using three dilutions for each genomic sample (5ng, 50ng, 200ng) (Table 8).

Primer	Sequence 5' → 3'
Actb1_ Fw	TGAGCAGGAGATGGGAACC
Actb1_ Rw	CAACGGAAACGCTCATTGC
GFP2_ qRT-Fw	CACATGAAGCAGCACGACTT
GFP2_ qRT-Rev	GGTCTTGTAGTTGCCGTCGT
mCherry3_qRT-Fw	GGACGGCGAGTTCATCTACA
mCherry3_qRT-Rev	AGCCCATGGTCTTCTTCTGC

Table 8. Primer sequences in qRT-PCR for copy number identification

3.17. Locus identification by CRISPR/Cas9-mediated editing and ONT-based sequencing

In a manuscript currently in preparation, we show the adaptation of CRISPR/Cas9 technique, with a precise DNA cut at the desired position, and long read sequencing (ONT) for the identification of transgene insertion site in *Hsa.BRAFV600E* transgenic lines.

Cas9-guided sequencing is based on the notion that a specific DNA cleavage enriches DNA ends in the region of interest, which are then ligated with the ONT sequencing adapters complexed with the motor proteins driving the DNA through the nanopore (Fig. 16). In published protocols, Cas9 is targeted to two sites flanking the region of interest. This grants the presence of phosphorylated 5' ends available for adapter ligation on both sides of the DNA fragments. However, this is not a viable option in our case, as the position of the transgene is not known. We therefore opted for two Cas9 targets within the eGFP coding sequence, even though that meant a possible decrease in the throughput due to the motor proteins being complexed only to one extremity of the fragment.

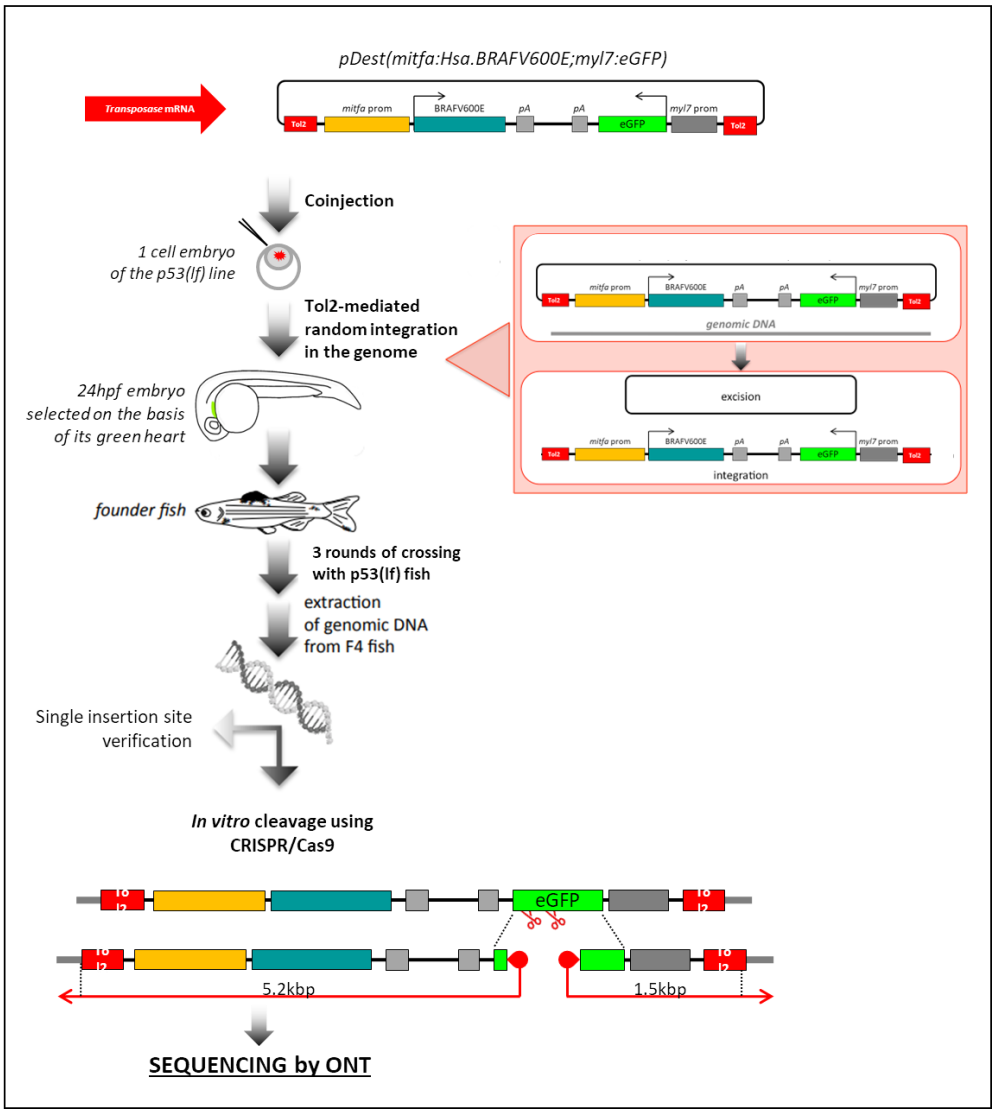

Figure 16 - Position identification strategy. Main experimental steps followed in order to obtain the *Hsa.BRAFV600E* transgenic fish that were used to extract genomic DNA and map the position of transgene insertion by Cas9/sgRNA-directed cut plus ONT sequencing of long hybrid reads. In the insert, schematic representation of the Tol2-mediated random insertion of the transgene within zebrafish genome.

After validating the guide RNAs (Fig. 17), we treated the genomic DNA with Cas9/guide RNA ribonucleoproteins and prepared the sequencing library from 3µg of cleaved genomic DNA. We then run it on several flow cell to understand which suits our purposes best (MinION, Flongue).

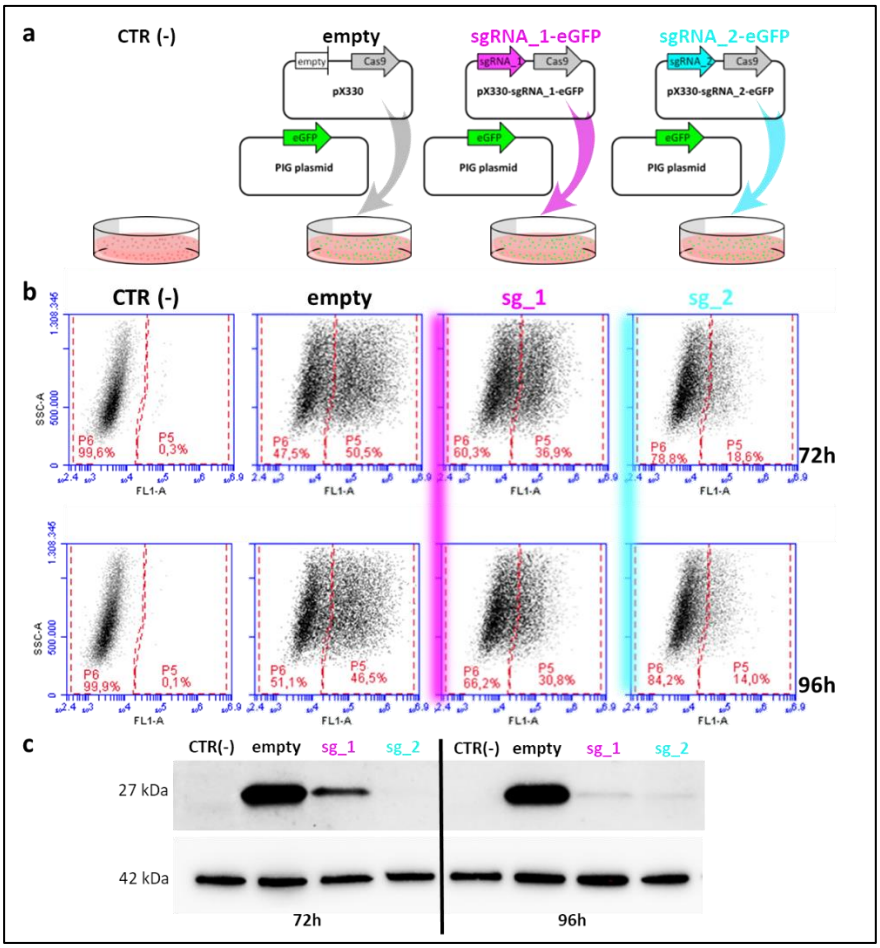

Figure 17 - Validation of the activity of sgRNA_1-eGFP and sgRNA_2-eGFP by cotransfection with a eGFP-expressing plasmid in HEK293 cells. (a) Schematic representation of the plasmids transfected in HEK293 cells. (b) Flow cytometry analysis of the decrease in eGFP fluorescence caused by the sgRNAs at 72 and 96h post transfection. (c) Western blot analysis of the decrease in eGFP protein caused by the sgRNAs at 72 and 96h post transfection.

To improve our chances, we worked on the factors that could affect the enrichment and the throughput of the sequencing run. Since genomic DNA is already fragmented, Cas9-mediated enriched fragments still account for a minimal fraction of the genome. Dephosphorylation of the 5' ends in the genomic fragments prior to Cas9 treatment represents a common workaround to limit untargeted reads, which still account for more than 90% of the throughput (Gilpatrick et al., 2022). To further decrease background noise, we decided to block the 3' end of the DNA fragments, by adding a dideoxynucleotide using Terminal deoxynucleotidyl Transferase.

An additional challenge in Cas9-based ONT-sequencing is that flow cells become exhausted relatively early, thus resulting in a low number of reads. This is probably due to

Cas9 protein remaining bound to DNA and interfering with the transfer of the DNA strand through the pore. We thus decided to treat the Cas9-cleaved gDNA with proteinase K to remove stuck Cas9.

In the first positive attempt, we identified 10 reads mapping to the transgene (not shown). Of these, 4 reads were hybrid and matched both on the chromosome (Chr.18) and the transgene sequences. PCR analysis of genomic DNA confirmed such location of the transgene (Fig. 18, left). In a second attempt, using all fresh reagents and repeating the analysis on an independent specimen of the same transgene, we identified 60 reads mapping to the transgene, with 30 of these allowing us to locate the genomic position (Chr.10, see PCR analysis in Fig. 18, right). This suggests how the state of the reagents is also fundamental.

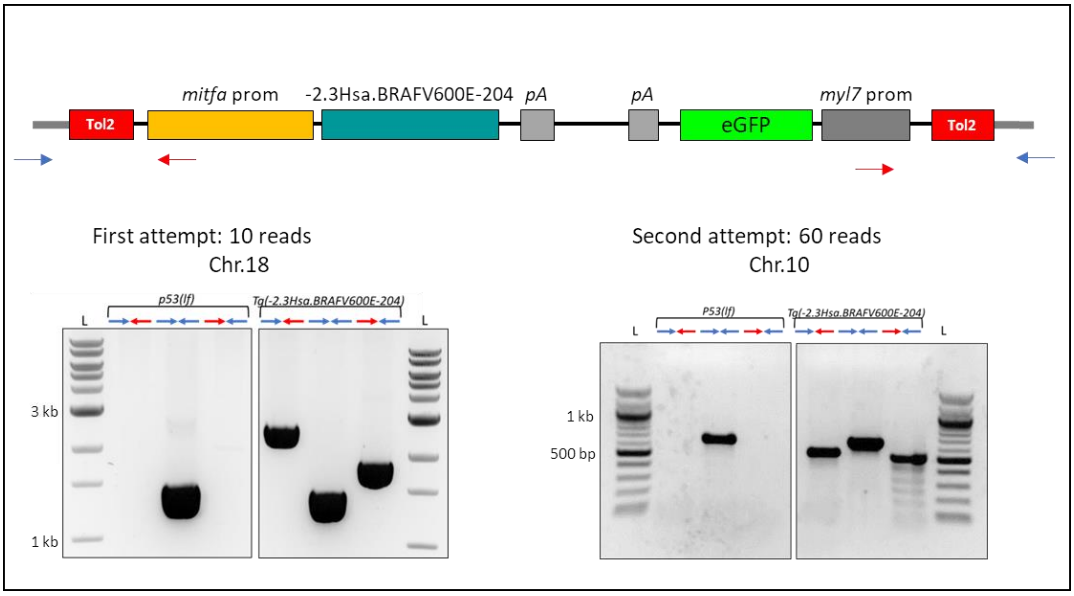

Figure 18 – Identification of transgene integration site in two fish of the *Tg(mitfa:-2.3Hsa.BRAF_V600E-204,myl7:eGFP)* line. In the first attempt we identified integration site on Chr.18 (left panel). In the second attempt, we identified integration site on Chr.10 (right panel). Specific genomic-transgene junctions (blue and red arrows) were amplified compared to the control (p53(lf) line). The amplicons for both positions (Chr.18 and 10) were used for Sanger sequencing, while Chr.10 amplicons were used for Sanger sequencing, as well as for the genotyping. L = Ladder 1kb (left) and 100bp (right)

To spur the technique and test its sensitivity, we also analyzed a specimen with 3 transgene copies, selected from the first generations with slightly altered phenotype. We

obtained 70 hybrid reads, which allowed us to univocally identify 2 out of 3 sites (chromosome 23 and 18), and to narrow down the localization of the third (a highly repeated point of chromosome 8 or 22). In turn, we used such information to expedite the generation of fish with single insertions, which will be used to establish the transgenic lines (Fig. 19)

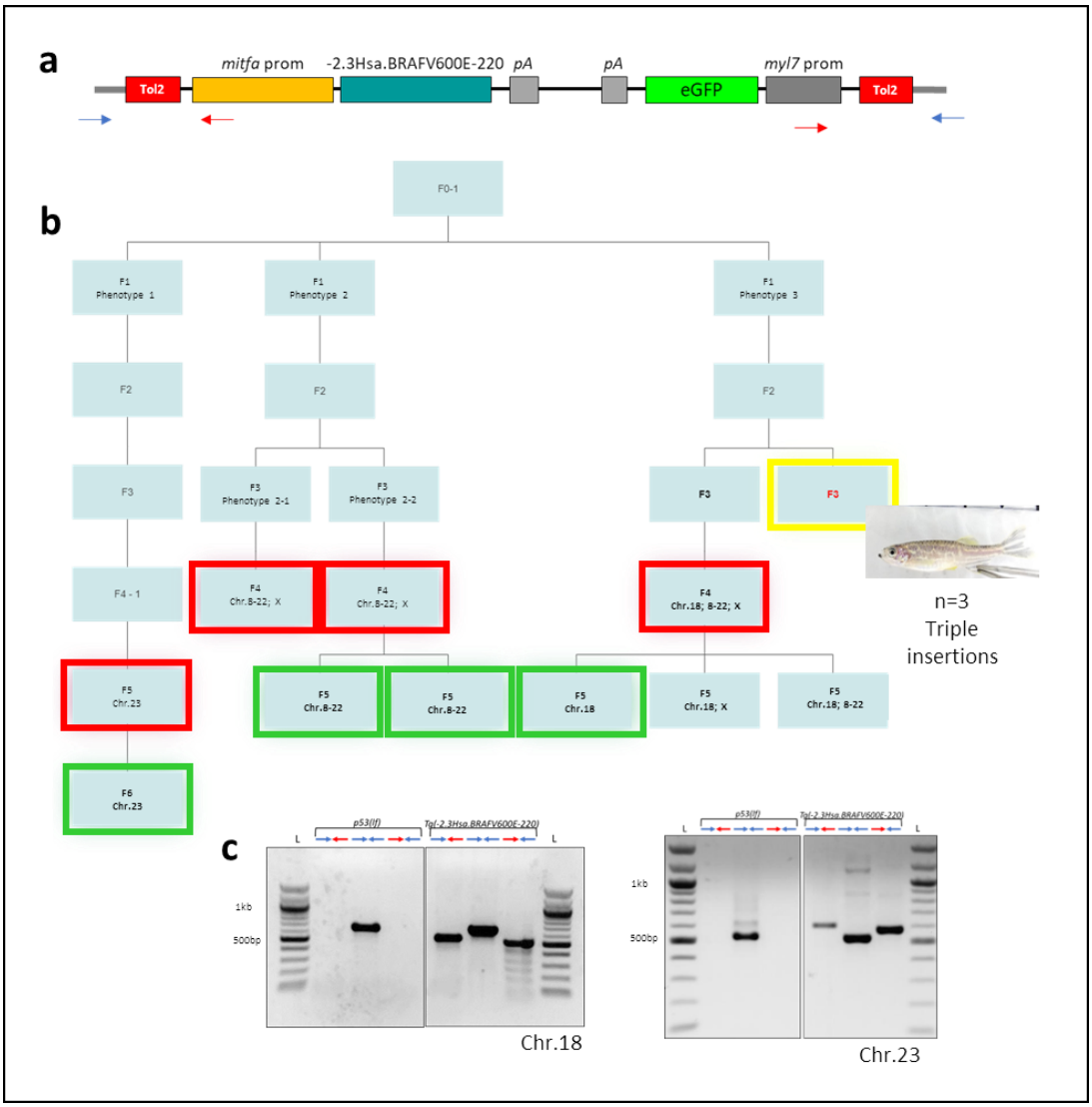

Figure 19 – Identification of multiple integration sites. For *Tg*(*mitfa:-2.3Hsa.BRAF_V600E-220,myl7:eGFP*) line (a), the number of 3 insertions was determined by performing RT-qPCR on an early generation specimen (F3) with a slightly irregular pigmentation pattern (yellow box in b). Using CRISPR/ONT sequencing strategy, 2 out of 3 integration sites were identified (chromosomes 23 and 18, see PCR analysis of genomic DNA reported in c). The third remains to be attributed to chromosome 8 or 22. Once integration sites were identified, the specimens in red boxes were analyzed to find out which insertions they carried. They were then crossed to generate fish with single insertions (green boxes).

We hypothesized that our methodology can be extensively used in the field of zebrafish as animal model, since the identification of transgene insertion sites remains a challenge. As well as it will be extended to other animal model and many fields of research. Of note, placing the sgRNA-mediated cut within a reporter gene (eGFP in our case) allows to use the same sgRNA(s) to determine the insertion sites of constructs expressing different transgenes, following a one-cut-fits-all approach. Finally, we can affirm that Cas9-guided sequencing allow to map multiple insertion sites within the genome, in turn allowing to follow allele segregation. In turn, this enables to bring the identification of animals with a single insertion site forward, i.e. earlier on in filial generations.

3.17.1. PCR on fish gDNA

The junctions between transgene sequence and flanking genomic regions were amplified by PCR, using Phusion Flash High-Fidelity PCR Master Mix (Thermo-Fisher Scientific) or GoTaq® G2 Green Master Mix (PROMEGA). 50 ng of gDNA were used as template and the primers are listed in Table 9. The PCR amplicons were then run on a 1% agarose gel, extracted using QIAquick Gel Extraction Kit (Qiagen, Hilden, Germany) and subjected to Sanger sequencing (Eurofins Genomics, Ebersberg Germany) using the same primers.

Primer	Sequence 5' → 3'	Application
beta chr.18 Fw	ACACTCCTTTGTGGTTGGCA	5' junction X1 β (Chr.18) for Sanger validation
beta eGFP Rv	CGCTTCTCGTTGGGGTCTT	
beta mitfa prom Fw	ACGTATGAACACTTTGGGG	3' junction X1 β (Chr.18) for Sanger validation
beta chr.18 Rv	TTCGCCATCGTCAGTGCAT	
GenX1 b 1Fw	GCGTGAAATTAATATGGGCTGGT	mutant allele for genotyping X1 β (Chr.18)
Tol5'-1	GGGAAAATAGAATGAAGTGATCTCC	
GenX1 b 2Fw	GGGCTGGTTTTTAACTCAATATCGC	wt allele for genotyping X1 β (Chr.18)
Gen-X1b_wt-2Rev	GTCAACACCACTGCCCACCTAAG	
Gen X1.1 Chr.10 wt Fw	CTGACCGATCCTTCACCCA	5' junction X1 Chr10 for genotyping (mutant allele) and Sanger validation
Tol2-3-3 Rev	CCTAAGTACTTGTACTTTCACTTG	
Gen-tol2-5 Fw1	CACTTCCAAAGGACCAATGAACA	3' junction X1 Chr10 for genotyping (mutant allele) and Sanger validation
Gen X1.1 Chr.10 wt Rev	GGCTGAAAATATTTAAATGTGCCAA	
Gen X1.1 Chr.10 wt Fw + Rev	See above	wt allele for genotyping X1 Chr10
Triple_chr.18 Fw1	CTGCTGTAGGTCACGAATCA	

beta mitfa prom Fw junctions	See above	5' junction ref (Chr.18) for Sanger validation
Triple_chr.23 Fw1	AGCTATTGGTGGAGTGGAG	5' junction ref (Chr.23) for Sanger validation
beta mitfa prom Fw junctions	See above	
Gen ref1 Chr.18 Fw1	CCTGAAGATGGAGGGCAGTC	5' junction ref (Chr.18) for genotyping
Gen-Tol2-3 Rev1	TGAGTAGCGTGTACTGGCATTAG	
Gen-tol2-5 Fw1	See above	3' junction ref (Chr.18) for genotyping
Gen ref1 Chr.18 Rev1	GAGCCAAACCCTCACGGATA	
Gen ref1 Chr.18 Fw1+ Rev1	See above	wt allele for genotyping ref (Chr18)
Gen ref1 Chr.23 Fw1	TCTGTGTGGAGCTTGCATGT	5' junction ref (Chr.23) for genotyping
Gen-Tol2-3 Rev1		
Gen-tol2-5 Fw1		3' junction ref (Chr.23) for genotyping
Gen ref1 Chr.23 Rev1	AGCAAATCCCTTCCAGCCAC	
Gen_ref1-Chr.23wt_Fw1	AGGATGATATGGCTGTGGTAGG	wt allele for genotyping ref (Chr23)
Gen_ref1-Chr.23wt_Rev1	ACCAACACATAACACGGGGA	

Table 9. Primer sequences for genotyping and locus integration validation

3.17.2. Cell culturing

Cells were grown at 37°C in a humidified atmosphere with 5% CO_2. HEK293 and A375-PIG cell lines were cultured in DMEM, low and high glucose respectively, supplemented with 10% fetal bovine serum, 1% glutamine (Sigma-Aldrich) and 1% penicillin/streptomycin (Euroclone). sgRNA_1-eGFP and sgRNA_2-eGFP sequence The crRNA portion was taken from the literature: crRNA_1-eGFP (5'-ggtgaaccgcatcgagctga-3' (Shalem et al., 2014)), crRNA_2-eGFP (5'-ggcgagggcgatgccaccta-3' (Auer et al., 2014)). Potential off-targets were analyzed using CRISPOR web tool (http://crispor.org). Cloning of pX330 plasmids pX330-U6-Chimeric_BB-CBh-hSpCas9 (pX330, kind gift from Feng Zhang, Addgene plasmid #42230) was used as negative control for transfection experiments and as backbone for the cloning of sgRNA_1-eGFP and sgRNA_2-eGFP. In details, sense and antisense oligos (sgRNA_1-eGFP sense (5'-caccggtgaaccgcatcgagctga-3') and antisense (5'-aaactcagctcgatgcggttcacc-3'); sgRNA_2-eGFP sense (5'-caccggcgagggcgatgccaccta-3') and antisense (5'-aaactaggtggcatcgccctcgcc-3')) were annealed to make a double strand fragment with sticky ends (BbsI). The double strand was then phosphorylated using PNK enzyme (New England BioLabs, Ipswich, MA, USA), according to the manufacturer's instructions, and finally cloned into the pX330 plasmid previously digested with BbsI enzyme (New England BioLabs, Ipswich, MA, USA).

3.17.3. Plasmid transfection

3×10^5 A375-PIG cells, which were stably infected with PIG-NotI (PIG) plasmid (Marranci et al., 2017), hence stably express eGFP, were seeded in 6well plates and 24h later they were transfected with 4µg of pX330, pX330-sgGFP-1 or pX330-sgGFP-2 and 10µL of 1 mg/ml LIPOFECTAMINE 2000™ (Thermo-Fisher Scientific, Waltham, MA, USA), following the manufacturer's protocol. 3×10^5 HEK293 cells were seeded in 6well plates and 24h later they were co-trasfected with 2µg of PIG eGFP-expressing plasmid, 2µg of pX330, pX330-sgGFP-1 or pX330-sgGFP-2 plasmid and 10µL of 1 mg/ml LIPOFECTAMINE 2000, following the manufacturer's protocol. At 72h and 96h post transfection, A375-PIG cells were collected for genomic analysis, while HEK293 cells were collected for cytofluorimeter and western blot analysis. In order to account for biological and technical variability, 2 independent replicates of this experiment were performed.

3.17.4. Analysis in Cas9/sgRNA-caused alterations in eGFP DNA sequence

gDNA extraction from A375-PIG cells was performed as described in (Vitiello et al, 2017). To detect Cas9/sgRNA caused alterations, eGFP DNA sequence was amplified by PCR, using Phusion Flash High-Fidelity PCR Master Mix (Thermo-Fisher Scientific, Waltham, MA, USA). 40ng of gDNA were used as template and the primers were: eGFP#2 Fw 5'-CATGGTGAGCAAGGGCGAG-3', eGFP#2 Rv 5'- TCGTCCATGCCGAGAGTGAT-3'. The reaction conditions were: 98°C 10s, (98°C 1s, 60°C 5s, 72°C 15s)×35 cycles, 72°C 1min. A S1000 Thermal Cycler (Bio-Rad, Hercules, CA, USA) was used. The PCR amplicons were then run on a 1% agarose gel, extracted using QIAquick Gel Extraction Kit (Qiagen, Hilden, Germany) and subjected to Sanger sequencing (Eurofins Genomics, Ebersberg Germany) using the same primers. TIDE web tool (https://tide.nki.nl/) was used to analyze genome editing efficiency.

3.17.5. Cytofluorimetric analysis

Transiently transfected HEK293T cells were washed once with PBS and the mean fluorescence of eGFP was then measured by flow cytometry. For each sample, 10^4 events were analyzed using Accuri C6 (BD Biosciences, San Jose, CA, USA).

3.17.6. Protein extraction

10^6 HEK293 cells were resuspended in 50µl of lysis buffer (50mM Tris HCl, 1% TritonX100, 0.25% NaDeoxicholate, 1mM PMSF, 2mM orthovanadate, proteinase inhibitors cocktail). The mixture was incubated for 30 minutes on ice and then centrifuged at 14000rpm for 30 minutes at 4°C. The supernatant was then quantified using Bradford reagent at 590nm (Vitiello et al, 2017). Western blot 20µg of proteins were combined with 4X loading buffer (Bio-Rad, Hercules, CA, USA) and then heated at 95°C for 5min, separated on 4-15% SDS-polyacrylamide gels (Mini-PROTEAN Precast gel, BioRad, Hercules, CA, USA) along with a marker (Bio-Rad, Hercules, CA, USA) and electrotransferred to polyvinylidene difluoride (PVDF), membranes using Trans-Blot Turbo system (Bio-Rad, Hercules, CA, USA). Membranes were blocked at room temperature for 1h using 3% milk in TBST. They were then incubated overnight at 4°C with the following primary antibodies: anti-β-ACTIN mouse monoclonal antibody (dilution 1:10000 in 5% milk in TBST; #A5441, Merck, Darmstadt, Germany); anti-eGFP rabbit polyclonal antibody (dilution 1:1000 in 5% milk in TBST; #A111-22, Molecular Probes, Eugene, OR, USA). Blots were washed 4 x 5 minutes in TBST and incubated for 1h in 5% milk in TBST with the appropriate secondary antibody (1:5000). Blots were again washed 4 x 5 min in TBST and developed using Clarity Western ECL blotting substrate (Bio-Rad, Hercules, CA, USA). Finally, bands were detected using the ChemiDoc imaging system (Bio-Rad, Hercules, CA, USA).

3.17.7. Cas9/gRNA Ribonucleoprotein assembly

Synthetic guide RNAs (5'-ggtgaaccgcatcgagctga-3' and 5'-ggcgagggcgatgccaccta-3', Synthego, Redwood City, CA, USA) were pooled into a 100µM equimolar mix. The ribonucleoprotein complex were assembled by combining 30pmol of guide RNA duplexes with 10 pmol of Cas9-NLS Nuclease (New England Biolabs, Ipswich, MA, USA) in 1× CutSmart Buffer (New England Biolabs, Ipswich, MA, USA).

3.17.8. Library preparation

3µg of gDNA were treated with Terminal deoxynucleotidyl Transferase (TdT, New England Biolabs, Ipswich, MA, USA) to add a single dideoxynucleotide to the 3' hydroxyl terminus of DNA molecules, in presence of 1mM dithiothreitol and 250µM $CaCl_2$, at 37°C for 30min. This step was followed by dephosphorylation of 5' ends with 3µL of Quick Calf-Intestinal alkaline Phosphatase (CIP) enzyme (New England Biolabs, Ipswich, MA, USA), for 15 min at

37°C. CIP enzyme was then heat-inactivated for 2min at 80°C. The assembled Cas9-gRNA ribonucleoprotein complex was added to the treated gDNA, followed by monoadenylation using the dA-tailing kit module (New England Biolabs, Ipswich, MA, USA) for adapter ligation. The sample was cleaned up using 1× Ampure XP beads (Beckman Coulter, Brea, CA, USA). Sequencing adapters from the Oxford Nanopore Ligation Sequencing Kit (Oxford Nanopore Technologies, Oxford, UK, #LSK109) were ligated to DNA ends, using T4-Quick Ligase (New England Biolabs, Ipswich, MA, USA) for 10min at room temperature. The sample was then cleaned up again using long-fragment buffer (Oxford Nanopore Technologies, Oxford, UK, #LSK109) and the libraries were prepared according to the Manufacturer's protocol (Oxford Nanopore Technologies, SQKLSK109 kit)

3.17.9. Sequencing

Samples were run on MinION or Flongle flow cells (v.9.4.1 pore), using the MK1B sequencer. Sequencing runs were operated using the MinKNOW software (v.19.2.2).

3.17.10. Analysis

Base calling was performed using GUPPY (v.3.0.3) to generate FASTQ reads from the electrical data. Reads were then aligned to the reference genome and analysed using minimap2 (v.2.17) (Li, 2018). For IGV visualization, BAM files were sorted according to mapped chromosomal location using sort from SAM tools (Handsaker et al., 2009) to visualize the reads mapped on to the reference genome (Thorvaldsdóttir et al., 2013)

4. Results

4.1. *mitfa*-driven expression of oncogenic BRAFV600E variants in mosaic zebrafish

4.1.1. Expression of BRAFV600E variants in mosaic embryos of the p53(lf) line

The first zebrafish cutaneous melanoma model for the *BRAFV600E* oncogene under the guide of *mitfa* promoter was developed in 2005 by the Zon group (ZDB-ALT-050419-2) (Patton et al., 2005). The transgene was created with a linearized pNP-P plasmid, with the oncoprotein BRAF Myc-tag fused. Subsequently, *Tg(mitfa:BRAF_V600E)* models were generated with the MiniCoopR system, which allows the study of several genetic elements simultaneously, by downregulating or overexpressing them (Ablain et al., 2015; Iyengar et al., 2012). The MiniCoopR system, like the latest transgenic models in zebrafish, exploits the Tol2 transposon system, that permits a high efficiency of integration into the genome and a high likelihood of inheritance by the F1 offspring.

Since there are no in vivo models for the study of BRAF variants, as well as the study of their respective 3' UTR, we used the rapid transgenic Tol2 system to model three BRAF variants *in vivo*. Using the melanocyte-specific *mitfa* promoter, we created mosaic transgenic fish expressing the coding sequences for BRAF-ref/X1/X2 and the BRAF-ref/X1 coding sequences (cds) complete with their respective three prime untranslated region (3'UTR) (Fig.20a). The constructs injected were:

- pDEST(*mitfa:-2.3Hsa.BRAF_V600E-220,myl7:eGFP*), expressing the coding sequence of the BRAFV600E-ref variant (ref cds),
- pDEST(*mitfa:-2.3Hsa.BRAF_V600E-204,myl7:eGFP*), expressing the coding sequence of the BRAFV600E-X1 variant (X1 cds),
- pDEST(*mitfa:-2.2Hsa.BRAF_V600E-X2,myl7:eGFP*), expressing the coding sequence of the BRAFV600E-X2 variant (X2 cds),
- pDEST(*mitfa:-2.4Hsa.BRAF_V600E-220,myl7:eGFP*), expressing the coding sequence complete of 3'UTR for the BRAFV600E-ref variant,
- pDEST(*mitfa:-9.4Hsa.BRAF_V600E-204,myl7:eGFP*), expressing the coding sequence complete of 3'UTR for the BRAFV600E-X1 variant.

The transgenic constructs for BRAFV600E variants were microinjected at one-cell stage in a genetic tumor prone background, the p53 mutant zebrafish line (ZDB-ALT-050428-2), which thus allows the generation of melanoma. To ensure that subsequent analysis was carried out on successfully microinjected samples, embryos were selected starting from 24 hours post

fertilization based on a cardiac fluorescent signal, *myl7*:eGFP. To validate the expression of *BRAFV600E* variant transgenes, we analyzed the transcripts using Reverse Transcriptase PCR (Fig.20b). Using human-specific *BRAF* primers, we confirmed the expression of the coding sequence for the common part (ex1-17) (black bar), as well as for the specific region in the last exons: Ex18.2/18b for ref variant (red bar), Ex18.2 + Ex19 for X1 variant (blue bar), Ex 19 only for X2 variant (blue bar) which appears with a lower amplification product (see Introduction for details). Furthermore, we observed the expression of the 3'UTR sequences for both the ref and X1 variants. Since the 3'UTR ref sequence is 121nt long, we can ensure its complete expression with a single amplification product (ochre bar). While for the 3'UTR X1, being 7163nt long, we have verified its complete expression by amplifying upstream and downstream portions (green and pink bars).

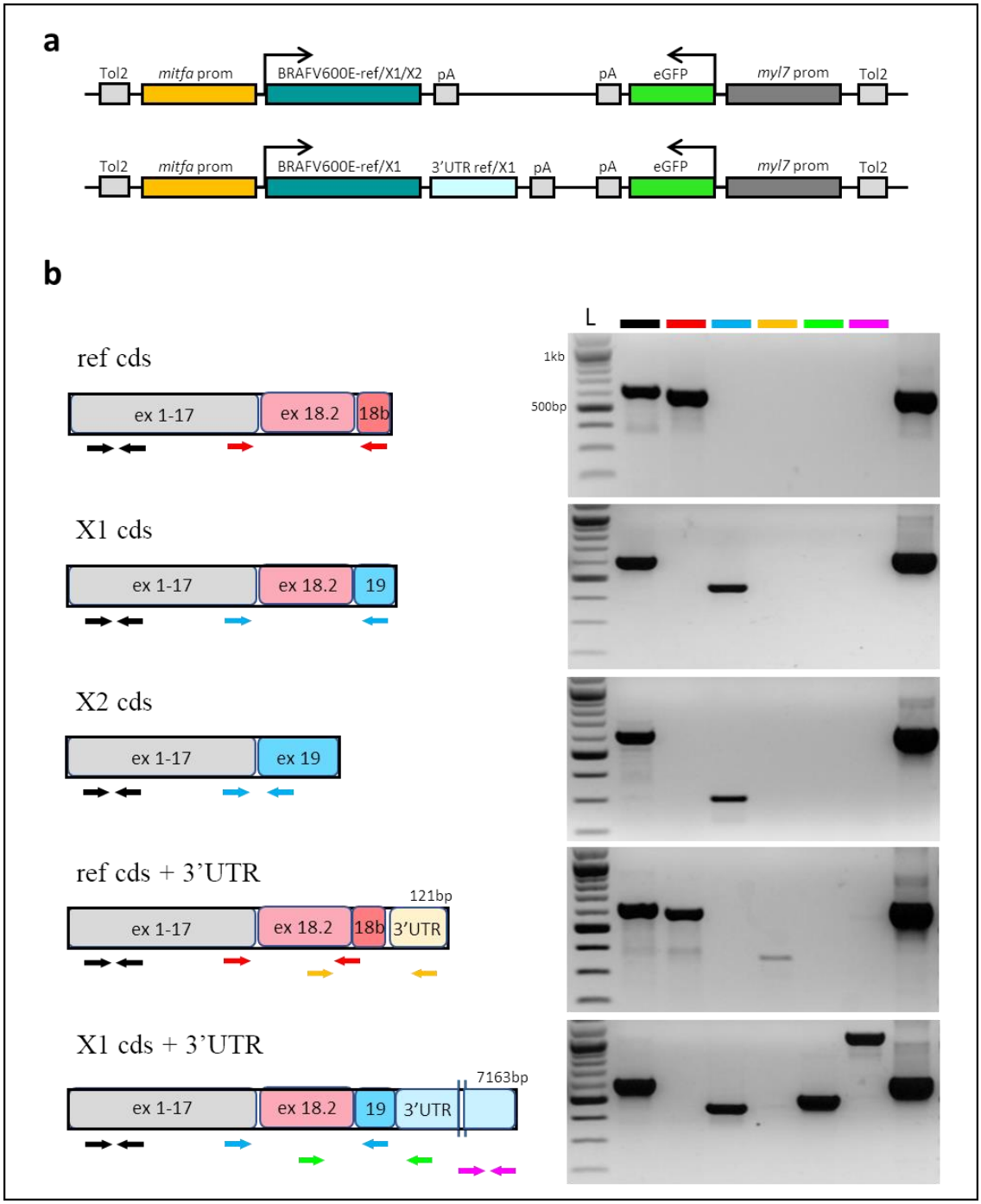

Figure 20 – Expression analysis of *Hsa.BRAFV600E* variants in embryos. (a) Schematic representation of the constructs (only coding top, coding and 3'UTR bottom) that express human *BRAFV600E* variants' coding sequence (oil green) and 3'UTR sequence (light blue) under the control of *mitfa* promoter (ochre), and eGFP reporter (green) under the control cardiac *myl7* promoter (dark grey). (b) Cartoon summarizing the position of the primers used to determine the expression of cds and 3'UTR of *BRAFV600E* variants (left). PCR performed on 1-cell stage p53(lf) injected embryos at 24hpf (right). *actb1* intron flanking primers (600bp for cDNA and 900bp for genome) are used as positive control; L: 100bp DNA Ladder.

4.1.2. *BRAFV600E* variant expression is increased

Since our constructs are of different sizes, particularly for X1 cds +3'UTR, 14220nt long, compared to cds, 7050nt long, we microinjected the same molarity for all the transgenic constructs. Nevertheless, we analysed the relative quantity of all variants. Using the relative quantification Real Time PCR technique, we observed similar expression levels for the ref/X1/X2 coding constructs and coding with ref 3'UTR, while the coding with X1 3'UTR construct showed a 4-5 times higher level of expression (Fig.21). The analysis was carried out at the 24hpf stage to observe the direct contribution of the injection and exclude possible technical errors and physiological effects, and at 5 days post fertilization, when the expression of *mitfa* is limited to the melanocyte-restricted line.

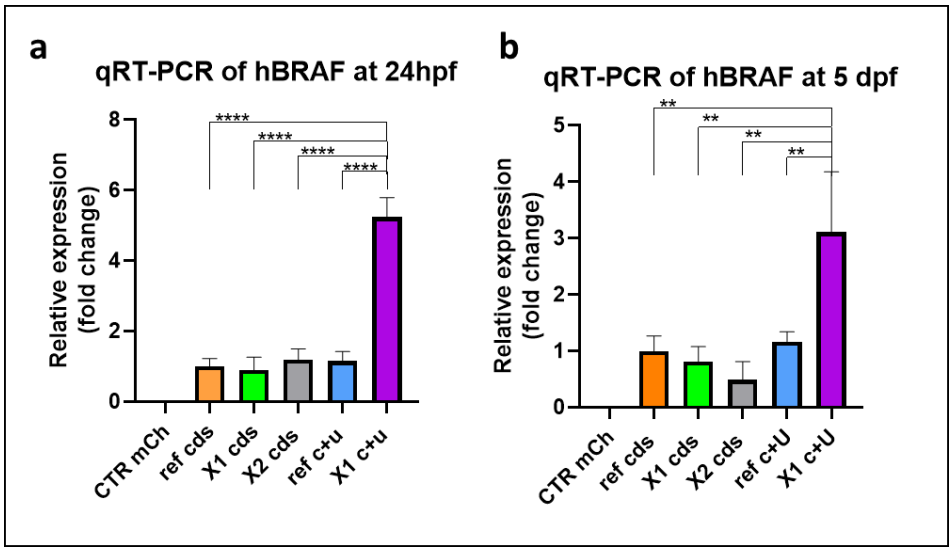

Figure 21 – *Hsa.BRAFV600E* variants expression level in development. qRT-PCR at 24 hpf (a) and 5dpf (b) of 1-cell stage p53(lf) injected embryos. *Tg(mitfa:mCherry,myl7:eGFP)* is used as negative control. Statistically significant differences are indicated with asterisks: **P<0.01, ****P<0.0001 (Dunnett's multiple comparisons test). (qRT-PCR: quantitative Real Time Polimerase Chain Reaction, hpf: hours post fertilization, dpf: days post fertilization)

4.1.3.*BRAFV600E* variants impact on pigmentation

The effect of increased pigmentation for the historical *BRAFV600E* model is recorded from 8 weeks of age. Pigmented clusters appear in the mosaic and become more widespread in the stable line (Patton et al., 2005). Here, we have monitored pigmentation in larvae, juvenile and adult stages.

In the historical model no changes in pigmentation at the embryonic or larval level were highlighted, while in our work we identify an increase compared to the control larvae. The different integration system used could be a possible explanation of the phenotype anticipation, confirming the higher efficacy of the Tol2 system compared to other methods previously used to generate transgenic constructs.

At 5dpf, injected larvae show an increase in pigmentation that appears as multiple pigmented spots homogeneously distributed across the body. Such an increase is highest for ref cds, then X1 cds, ref cds + 3'UTR and finally X1 cds + 3'UTR follow. Conversely, no pigmentation alterations are observed upon injection of X2 cds, which is consistent with a rapid degradation of BRAFV600E-X2 protein via proteasome, as previously described by our group (Marranci et al., 2017) (Fig. 22a).

These data on larvae are confirmed by the observations recorded later at the juvenile stage, defined when the animals acquire the fins and adult-pigmentation phenotype, although they are not sexually mature. At this stage (around 5 weeks of age), we recorded the percentage of animals that already showed pigmentation alterations and exhibited the formation of nevi. These are defined as flat, strongly pigmented clusters of melanocytes that disrupt the distinctive striping (Dovey et al., 2009; Patton e al, 2005). The data claim a higher effect of ref/X1 only coding transgenes, an intermediate effect for the ref cds + 3'UTR transgene and an extremely low effect for the X1 cds + 3'UTR transgene. Also, at this stage of development, no pigmentation alterations or nevi are observed for the X2 transgene (Fig. 22b).

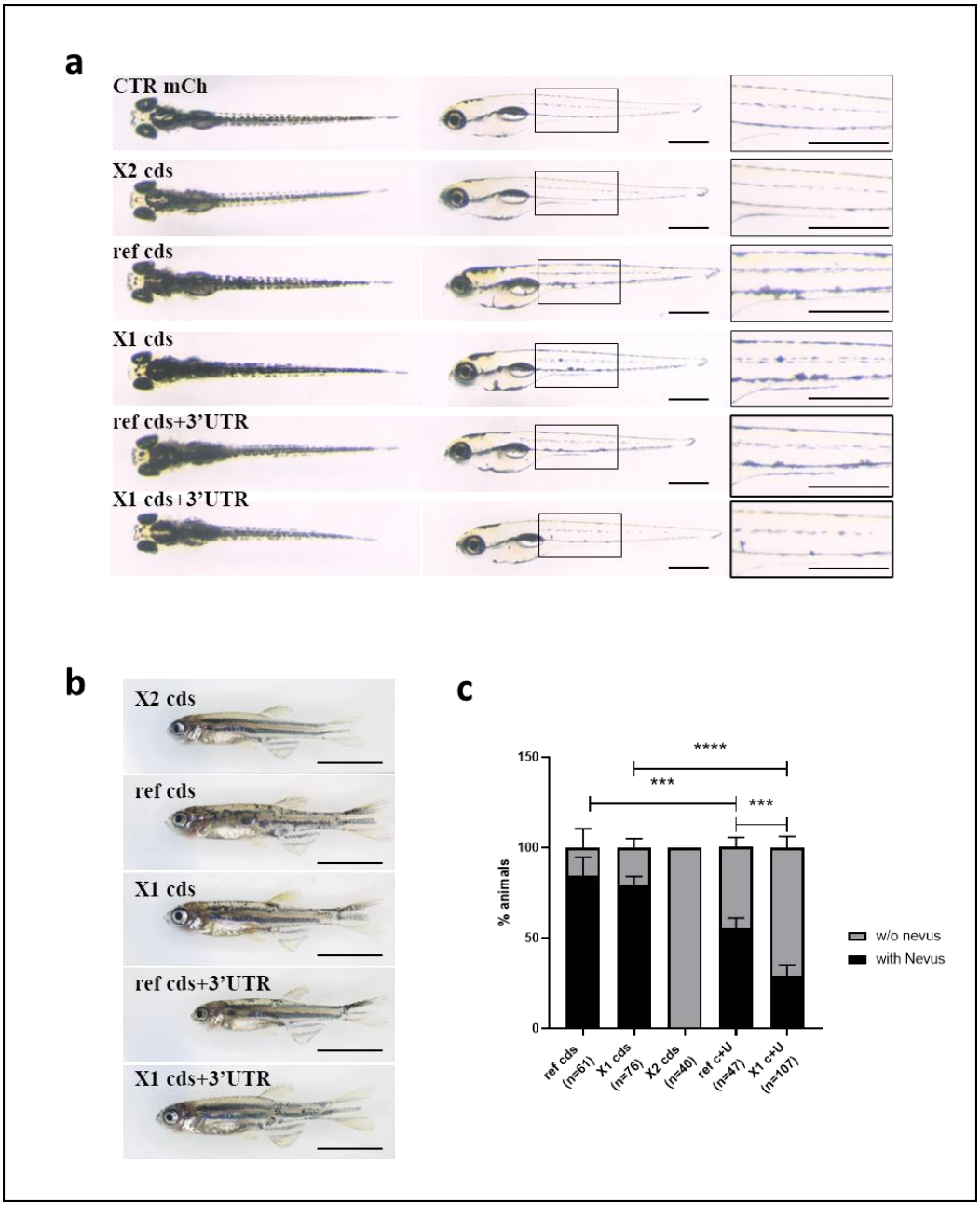

Figure 22 - Pigmentation pattern analysis in larvae and juveniles. (a) Pigmentation pattern in larvae at 5dpf. Dorsal view (left), lateral view (middle), lateral zoom view (right). *Tg(mitfa:mCherry,myl7:eGFP)*,p53(lf) is used as negative control (CTR mCh). Scale bar 500µm. (b) Representative nevi in juvenile fish. A fish injected with X2 cds construct is used as negative control. Scale bar 0.5cm. (c) Nevus percentage in juvenile fish. Statistically significant differences are indicated with asterisks: ***P<0.001, ****P<0.0001 (Fisher's exact test). In order to account for biological and technical variability, at least 2 independent biological replicates were performed, and the total number of fish studied for each condition is reported in the graph.

4.1.4.*BRAFV600E* variants impact on nevus progression

Reflecting the fact that nevi number, size and characterization are important clinical prognostic factors in human, we recorded nevi size and tumor incidence at the adult stage of zebrafish over a one-year observation period.

After three months of age, despite initial differences, the percentage of animals showing a nevus is similar regardless of the transgene they received, except for X2, which from this point on will no longer be included in the analyses as they do not develop pigmentation alterations nor nevi. (Fig. 23a). Although the percentage of animals with the presence of moles is very similar for all conditions (Fig. 23b), we evaluated whether the time to nevus onset could affect the area of hyperpigmented skin. Measuring the size of adult nevi at 3 months of age, the data show higher values for only-coding transgenes, while similar and smaller values for cds + 3'UTR transgenes (Fig. 23c).

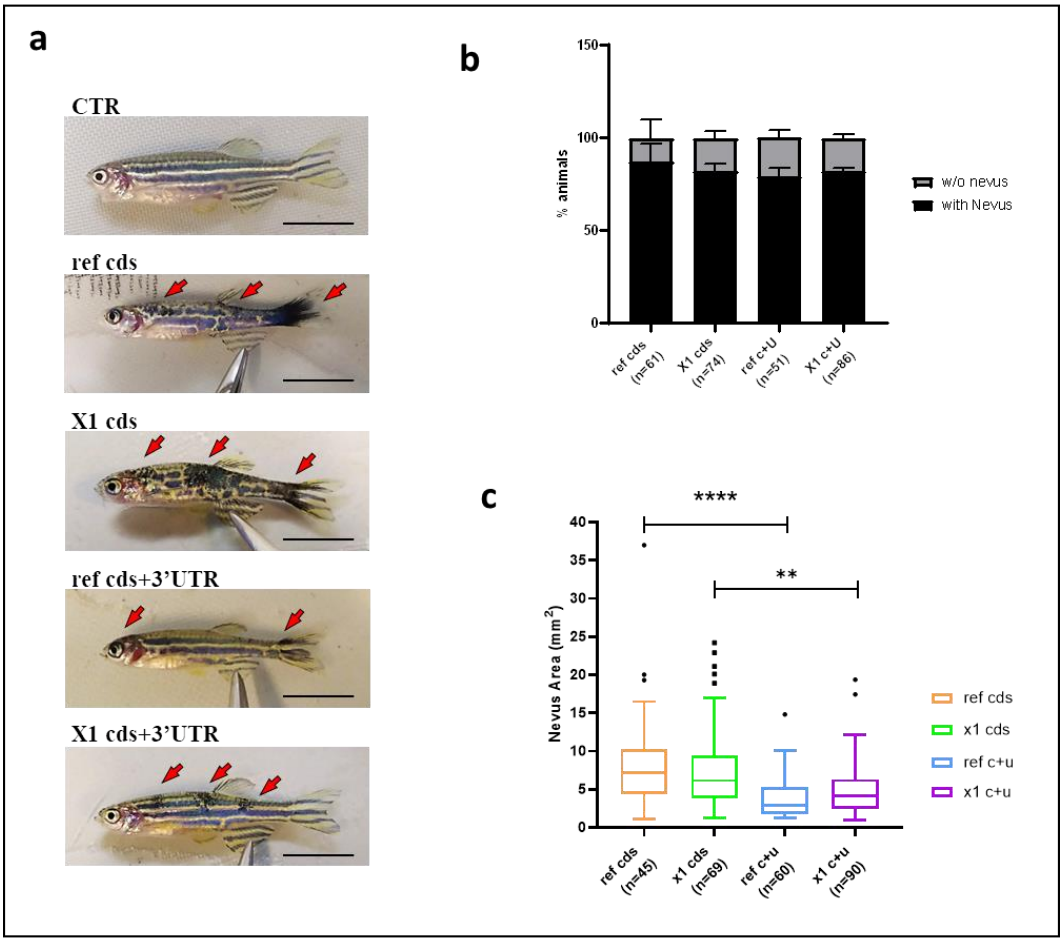

Figure 23 – Nevus analysis in adults. (a) Representative nevus (arrows) in tg adult fish (3 months of age). Scale bar 1cm. (b) Nevus percentage in adults (3 months of age). (b) Size of nevus in adults (3 months of age). Statistically significant differences are indicated with asterisks: ***P<0.001, ****P<0.0001 (Dunn's

multiple comparisons test). In order to account for biological and technical variability, at least 2 independent biological replicates were performed, and the total number of fish studied for each condition is reported in the graph.

4.1.5.*BRAFV600E*-ref variant has the highest transforming capacity

Finally, following the animals during a year of life, the incidence of tumors onset was recorded, which is once again greater for the coding-only transgenic lines compared to the respective cds + 3'UTR lines (Fig. 24a-b). The transition from nevus to melanoma was detected as pigmentation intensification, which turns into skin thickening, accompanied by an outward growth (Patton et al., 2011). The data also show a significant difference in tumor onset for the BRAF ref isoform, which is quicker compared to the X1 isoform (Fig. 24a-b). Even in one-year observation period, no pigmentation alteration or tumor onset was recorded for the BRAFV600E-X2 transgene, confirming the absence of the protein or at least of its function *in vivo*.

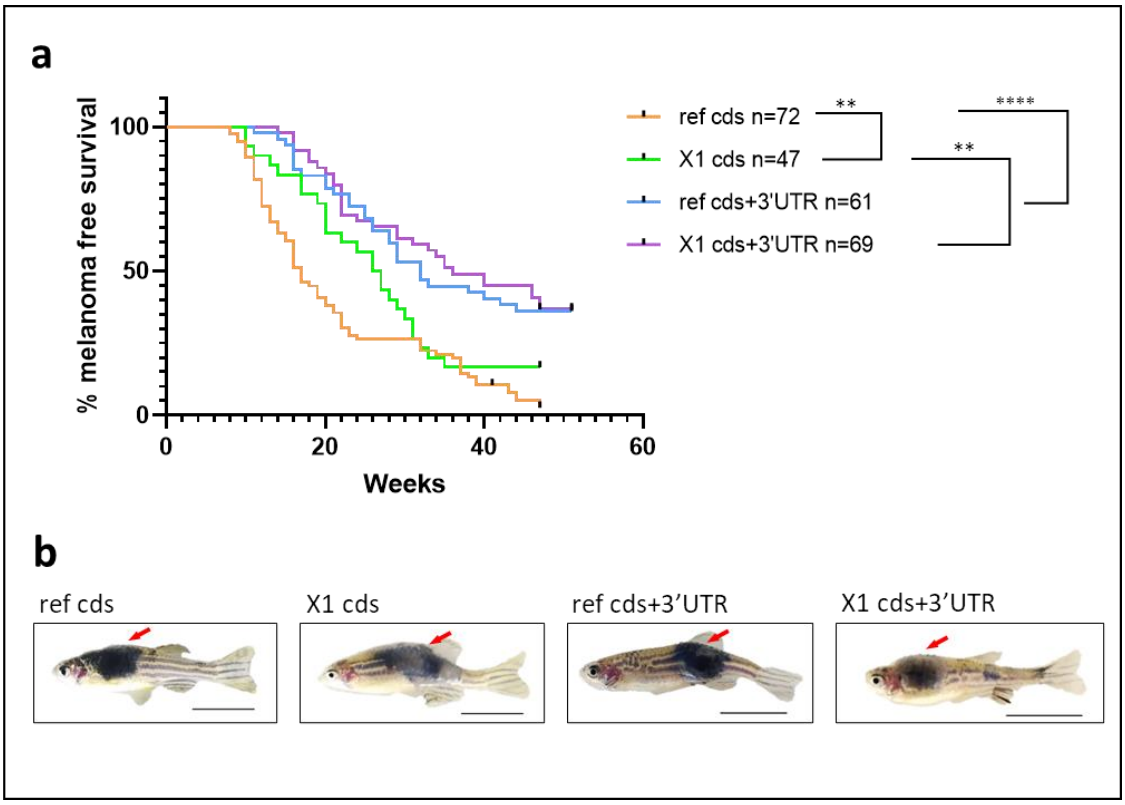

Figure 24 – Melanoma incidence analysis in adults. (a) One-year long melanoma free-survival curve. (b) Representative zebrafish with melanoma tumors (red arrows). ref cds: *Tg(mitfa:-2.3Hsa.BRAF_V600E-220,myl7:eGFP)*; X1 cds: *Tg(mitfa:-2.3Hsa.BRAF_V600E-204,myl7:eGFP)*; ref cds+3'UTR: *Tg(mitfa:-2.4Hsa.BRAF_V600E-220,myl7:eGFP)*; X1 cds+3'UTR: *Tg(mitfa:-9.4Hsa.BRAF_V600E-204,myl7:eGFP)*. Scale bar 1 cm. Statistically significant differences are indicated with asterisks:

**P<0.01, ****P<0.0001 (log-rank (Mantel–Cox) test). In order to account for biological and technical variability, at least 3 independent biological replicates were performed, and the total number of fish studied for each condition is reported in the graph.

To understand if the differences are caused by large cellular rearrangements, we recorded the body localization of tumors and their pigmentation phenotype, given the involvement of both aspects in tumor development. On one hand, the tumors' position may be indicative of a different genetic context, since the cell of origin is characterized by a unique transcriptional state determined by its differentiation status and environment interaction. This renders it susceptible only to certain oncogenic insults, as reported in literature (Weiss et al., 2022). On the other, the degree of pigmentation has been associated with different mutational signatures: Wnt signaling was associated with a higher pigmentation phenotype, PTEN alteration with a lower pigmentation phenotype and p53 with variable sectors of dark pigmentation (Hodis et al., 2022). Of note, pigmentation phenotype has been correlated with targeted therapy response too.

Therefore, we recorded the onset of tumors on the head, body and fins. The data show no difference among the different conditions (Fig. 25a). Next, the objective pigmentation appearance was recorded by defining pigmented (melanotic) or non-pigmented (amelanotic) melanomas. The data display a statistically significant difference between the ref and X1 coding variants, and a trend between the counterparts cds + 3'UTR variants, but this observation needs to be further confirmed; indeed, although some tumors may result amelanotic in the physical examination, the pigmentation is instead observed when processing the samples for histological examinations (Fig. 25b).

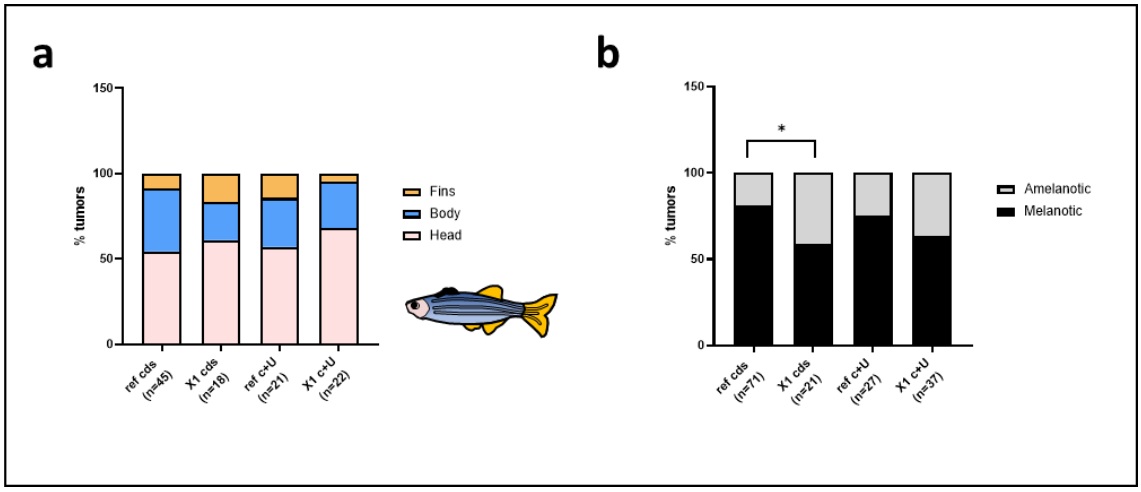

Figure 25– Melanoma macro features analysis in adults. (a) Tumors localization. (b) Melanotic pattern. Statistically significant differences are indicated with asterisks: *P<0.05 (Fisher's exact test).

To confirm the histological tumor characteristics of melanoma, we collected and analyzed tissue sections with multiple staining procedures. As per melanoma characteristics, tumors show hyperplasia, architectural disturbance, cytological atypia (by Hematoxylin and Eosin staining) (Fig.26a) and BRAFV600E presence (by immunochemistry) (Fig. 26b).

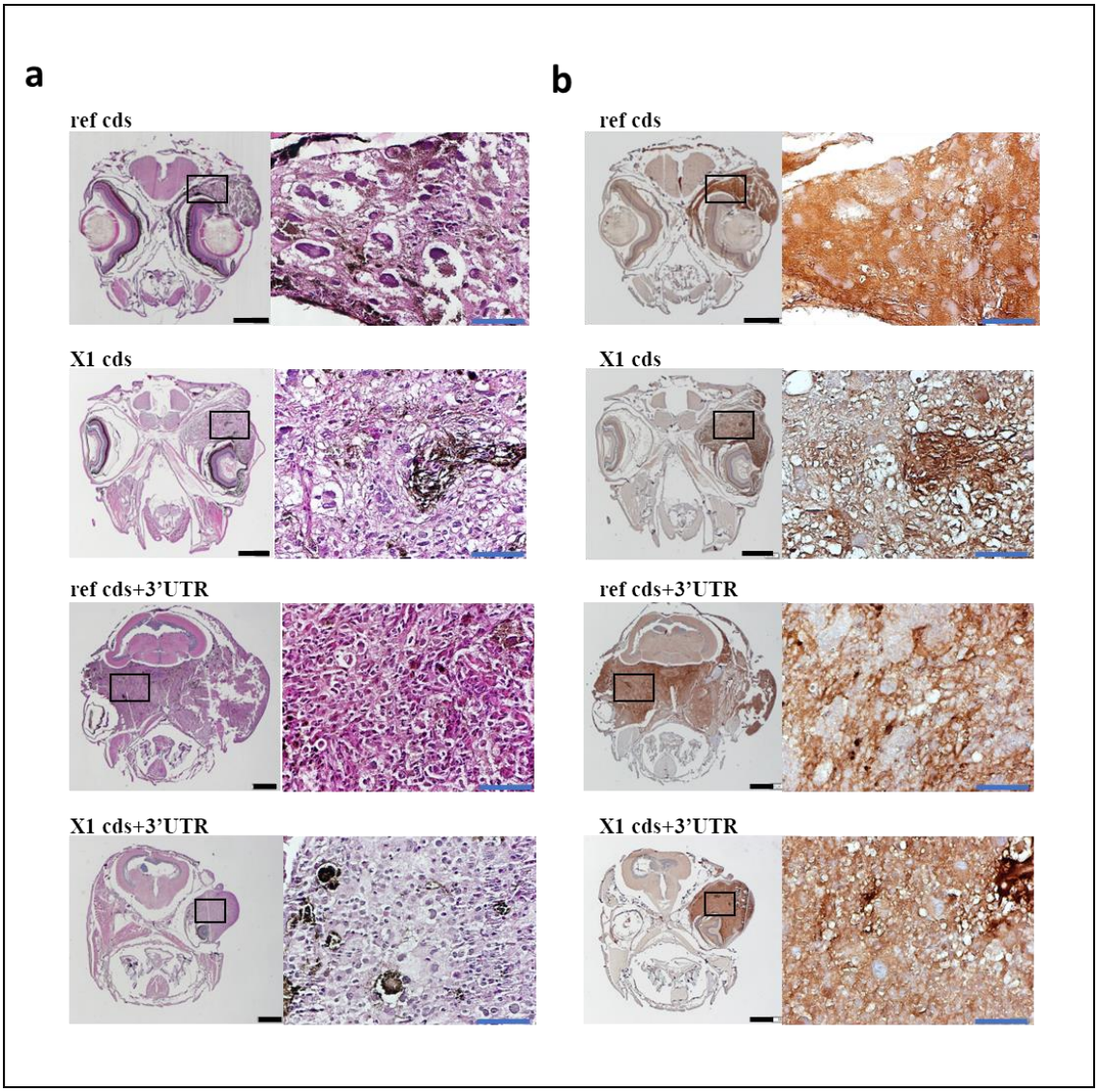

Figure 26 – Histological analysis of BRAFV600E variants tumors. Representative Hematoxylin and Eosin (H&E) stain (a) and BRAFV600E IHC (b) on a tumor sample. Black scale bar 500 µm, blue scale bar 90 µm.

4.2. *BRAFV600E* variants in stable zebrafish transgenic lines

4.2.1. Strategy for the generation of zebrafish transgenic lines expressing *BRAFV600E* variants

In the mosaic condition (F0), all *BRAFV600E* variant transgenes (except X2) generate the classic nevus as reported in the literature (Patton et al., 2005) (compare Fig.27a and b). In stable lines, instead, in the early generations (F1-F2) a high percentage of specimens show a strongly altered pigmentation, which no longer appears zebra-like (Fig. 27c-d). However, in the advanced

generations (F3-F4, Fig. 27e), a more regular pigmentation appears again, in accordance with literature data.

The irregularity of the pigmentation pattern is likely due to the high number of copies of the transgene, as well as to the repeated outcross with the p53(lf) line, which results in the accumulation of mutations. In addition, the repeated outcross with the p53(lf) line likely anticipate the spontaneous onset of tumors and increase their percentage, explaining the different data reported in the literature (Patton et al., 2005; Berghmans et al., 2005). In turn, this means that the same transgenic *BRAFV600E* line, with the same integration site, will have a different phenotype if kept in conditions of p53 mutant homozygosity or heterozygosity.

For these reasons, we first microinjected the *BRAFV600E* variants construct in p53(lf) embryos to ensure the selection of founders that generated moles and tumors. Then, after observing a strong pigmentation alteration in the early filial generations (Fig. 27c-d), we bred the selected animals to return to a p53 heterozygosity condition. In this way, we could establish that any altered pigmentation depended only on the integrated transgene number, removing the p53 variable. In turn, this allowed us to more accurately identify specimens carrying a low number of integration sites.

Accordingly, we have not yet recorded the tumors' percentages and localization sites pertaining to the *BRAFV600E* variants stable lines. To investigate this topic, we aim to first cross these fish with wild types to generate stable lines with a traceable homozygous single insertion at the genomic level and with a heterozygous p53 mutation. These fish, which we will define as experimental F0, will then be incrossed and the experimental F1 individuals with homozygous p53 mutation will be subjected to data record. This way, we will identify tumors' features that are specifically induced by the different *BRAFV600E* variants.

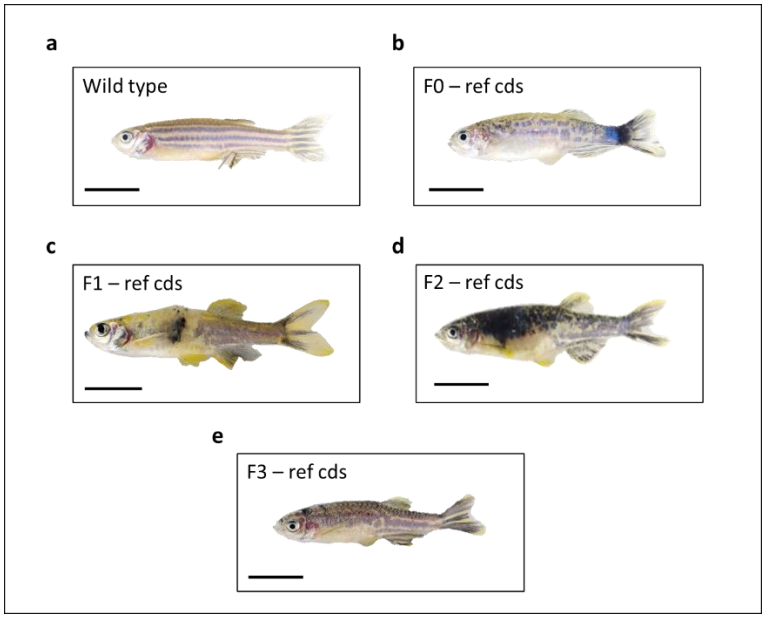

Figure 27 - Pigmentation pattern in mosaic and stable lines over generations. Lateral views of wild type (a), and *Tg(mitfa:-2.3Hsa.BRAF_V600E-220,myl7:eGFP)* fish expressing BRAFV600E ref cds in F0 (b), in F1 (c), in F2 (d) and in F3 (e). F: filial, scale bar 1cm.

4.2.2. Identification of transgenic lines expressing *BRAFV600E* transcript variants

Several branches for each transgenic line were studied to find at least two specimens with a single insertion, hence, to exclude possible genome position-dependent effects. Here, insertion number was measured using quantitative Real Time PCR, while genome integration site was identified using Nanopore technology (details in material and methods).

The lines identified so far are:

- *Tg(mitfa:-2.3Hsa.BRAF_V600E-204,myl7:eGFP)* for X1 cds, Chr.10 integration site
- *Tg(mitfa:-2.3Hsa.BRAF_V600E-204,myl7:eGFP)* for X1 cds, Chr.18 integration site
- *Tg(mitfa:-2.3Hsa.BRAF_V600E-220,myl7:eGFP)* for ref cds, Chr.18 integration site
- *Tg(mitfa:-2.3Hsa.BRAF_V600E-220,myl7:eGFP)* for ref cds, Chr. 23 integration site
- *Tg(mitfa:-2.4Hsa.BRAF_V600E-220,myl7:eGFP)* for ref cds and 3'UTR, in progress
- *Tg(mitfa:-9.4Hsa.BRAF_V600E-204,myl7:eGFP)*, for X1 cds and 3'UTR, in progress.

The work of generating the lines will continue until at least another founder for the line ref cds + 3'UTR and X1 cds + 3'UTR is found.

The generation of stable transgenic lines for BRAF variants will lead us to confirm and further study the phenotype obtained in the mosaic, as well as to perform drug screenings in a better-defined genetic context. Allowing to study BRAFV600E isoforms one by one, our model system can in turn contribute to identify new molecular factors involved in BRAFV600E-driven malignant transformation. This could also be expanded to tumor response and resistance to BRAF inhibitors, paving the way to design more informed combinatorial therapeutic strategies.

4.3. Transgenic *BRAFV600E* variants in drug screenings

4.3.1. Neural crest program in transgenic *BRAFV600E* variants

To quantify the efficacy of pharmacological treatments, the stable transgenic lines for the *BRAFV600E* variants will be crossed with a *crestin* reporter line.

crestin and *sox10* are genes expressed during embryonic development in the NCC, and they are reactivated in melanoma cells, when they reacquire the neural crest phenotype.

The choice of the *crestin* gene, compared to other genes better characterized in humans, lies in its high-level expression, which therefore allows a better resolution to observe the NCP (neural crest program) reactivation. Furthermore, literature data highlighted the role of *crestin* as drug or genetic treatments marker already at the embryonic stage. In the genetic condition of mutant homozygosity for p53 and overexpression of *BRAFV600E*, it has in fact been shown that *crestin* increases its expression levels at the embryonic and larvae stages (White et al., 2011).

We validated the same effect with the BRAF variants by in situ hybridization technique, showing an increase of *crestin* expression signal in all *BRAFV600E* variants transgenes (Fig. 28a).

Although a qualitative increase in the crestin signal is visualized, we did not observe the same results analyzing the expression of both *sox10* and *crestin* genes by quantitative Real Time -PCR technique (Fig. 28b). These data coincide with the strictly qualitative analyses for *crestin* expression in embryos found in the literature, where it is never reported using quantitative methods. Instead, quantitative approaches have been used to evaluate its re-expression in adult tumors and scales (McConnell et al., 2019; Kaufman et al., 2016).

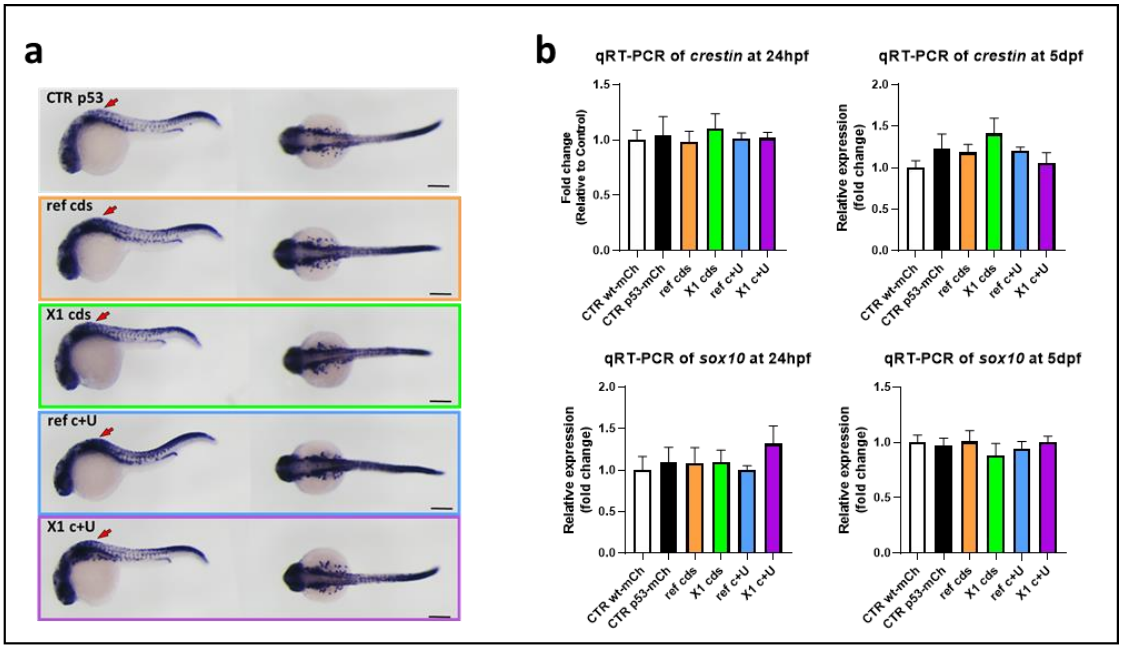

Figure 28 - Neural crest genes expression in embryos. (a) WISH for *crestin* at 24hpf, in 1-cell stage p53(lf) injected embryos. Lateral views (left) and dorsal views (right). A stronger signal is observed in all transgenics (red arrows). (b) qRT-PCR of *crestin* (top) and *sox10* (bottom) genes at 24hpf and 5dpf. (No statistically significant differences were obtained with ANOVA analysis). WISH: Whole mount in situ hybridization, qRT-PCR: quantitative Real Time Polymerase Chain Reaction, hpf: hours post fertilization, scale bar 250 µm. In order to account for biological and technical variability, at least 2 independent biological replicates were performed.

A possible explanation is in the composition of the *crestin* gene, which is limited to a single exon and whose promoter includes retroelement LTR sequences. This results in its repetition in the genome >40 times, which could saturate the quantification of the *crestin* transcript (Kaufman et al., 2016). Also, the strength of the *sox10* promoter could affect quantitative analysis (Kwak et al., 2013).

To overcome this problem, we decided to replicate the *Tg(-4.5crestin:mCherry)*,p53(lf) (ZDB-TGCONSTRCT-160208-3) line in our facility. Here, the *crestin* promoter directs the expression of mCherry, to use red fluorescence as an approximation of *crestin* expression. This line is an ideal model to investigate potential changes resulting from the injection of our constructs, as well as the efficacy of drug treatment regimens.

In parallel, we also decided to generate a transgenic line with two reporters under the guidance of the *crestin* promoter: *Tg(-4.5crestin:Luc2-P2A-mCherry)*. The purpose of this line is to use the mCherry reporter for qualitative analysis, and the Luciferase (Luc2) reporter for quantitative analysis. Indeed, the possibility to use the *crestin* signal in a quantitative way in embryos by means of Luciferase will expedite pharmacological screenings.

4.3.2. Responsiveness of *crestin* reporters to targeted therapy

However, before venturing into the generation of stable lines, we first investigated whether the approach was feasible. To this purpose, we verified *crestin* as readout of drug treatments. We tested single drugs and drug combinations, such as BRAFi plus MEKi, and BRAFi plus a pigmentation inhibitor (PIGMi).

To start, we analyzed the fluorescent signal of *crestin* in wild type (wt) and *Tg(mitfa:BRAF_V600E)*,p53(lf) embryos (ZDB-ALT-050419-2) microinjected with the construct pDEST(-*4.5crestin:*mCherry) and therefore in mosaic condition (Fig. 29a).

In line with data reported in the literature, we can highlight an increase in the basal signal of mCherry in the *Tg(mitfa:BRAFV_600E)*,p53(lf) line compared to wild type embryos and a reduction in the signal following treatment with leflunomide (leflu) (White et al., 2011), but also vemurafenib (vem) (BRAFi), oligomycin (OMY, mitochondrial ATP synthetase inhibitor), and 2,4-dinitrophenol (DNP, uncoupler of oxidative phosphorylation) treatment. The data show how non-targeted drugs (leflu, OMY, DNP) act indistinctly on WT and BRAFV600E embryos, while, in the vem treatment condition, we observe a significant effect only on BRAF embryos (Fig. 29b).

We further highlighted a dose-dependent reduction of the fluorescent signal upon treatment with vem, a combinatorial effect of BRAF and MEK inhibitors at individually suboptimal concentrations (vem and cob (cobimetinib), 1µM for both), as well as a combinatorial effect between vem and a PIGMi, represented by PTU (Fig. 29c).

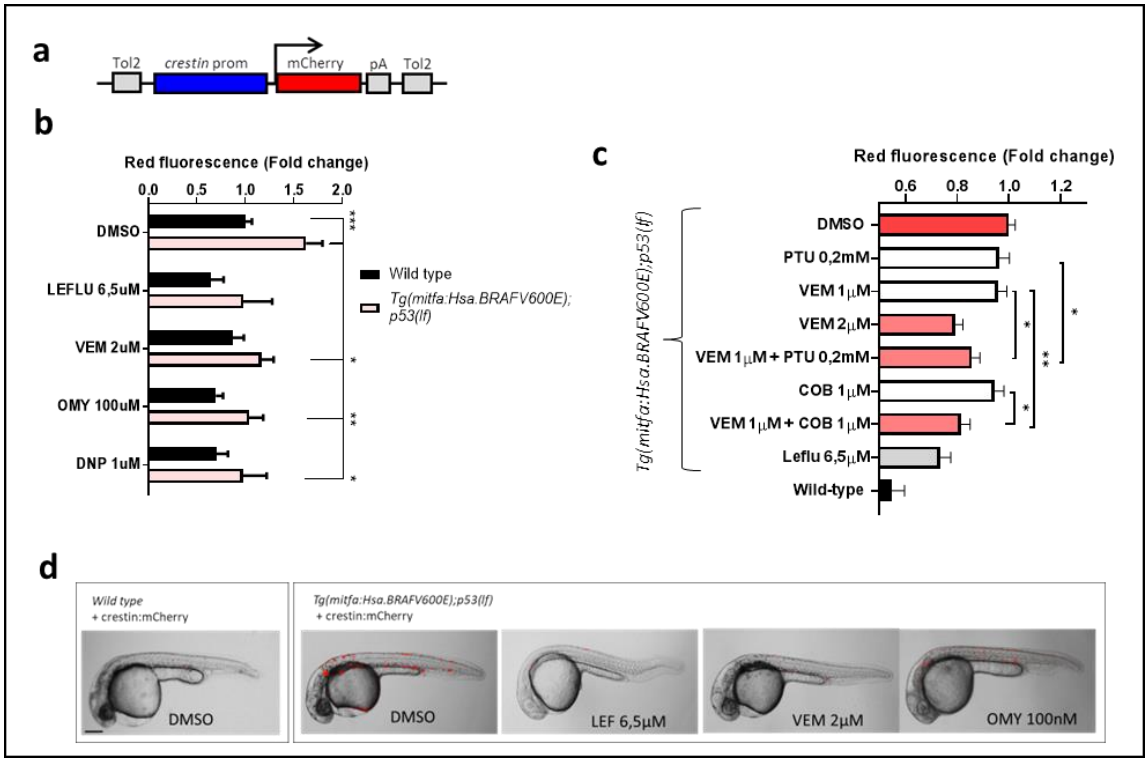

Figure 29 - Decrease in red fluorescence in Crestin single reporter mosaic line upon drug treatments. (a) Schematic representation of the *pDEST(-4.5-crestin:mCherry)* construct that expresses mCherry reporter (red) under the control of *crestin* promoter (blue). (b-c) Red fluorescence levels detected in 30hpf *Tg(mitfa:BRAF_V600E)*,p53(lf) and wild type zebrafish embryos that were injected with the mCherry construct at 1-cell stage and were treated with the indicated drugs (b) or drug combinations (c) at 6hpf. Vemurafenib (vem): BRAF inhibitor. Olygomicin (omy): ATP synthetase inhibitor. 2,4-dinitrophenol (dnp): uncoupler of oxidative phosphorylation. Cobimetinib (cob): MEK inhibitor. PTU: thyroid peroxidase inhibitor (pigmentation inhibitor – PIGMi). Leflunomide (leflu): mitochondrial dihydroorotate dehydrogenase inhibitor, is an inhibitor of the neural crest lineage and is used as positive control. (d) Representative decreased red fluorescent signal in treated embryos merged in bright field. Scale bar 200um. Statistically significant differences are indicated with asterisks: *P<0.01, **P<0.01, ***P<0.001 (Dunnett's multiple comparisons test (b) and Mann-Whitney test (c)).

To evaluate *crestin* expression as a quantitative tool, we then tested its use with the *pDEST(-4.5crestin:Luc2-P2A-mCherry)* construct (Fig. 30a).

After observing the same fluorescence signal between the single reporter and the dual reporter (Fig. 30b), we moved on and verified the trends associated with the Luciferase quantitative reporter. Following the same experimental design used above (Fig. 30), we evaluated a possible reduction of the Luciferase signal by microinjecting the dual reporter construct in

BRAFV600E; p53(lf) embryos. The data show us a strong reduction of Luciferase signal in *BRAFV600E* embryos treated with vem and leflu and the absence of Luciferase signal in the control embryos (*Tg(-4.5-crestin:mCherry)*) (Fig. 30c).

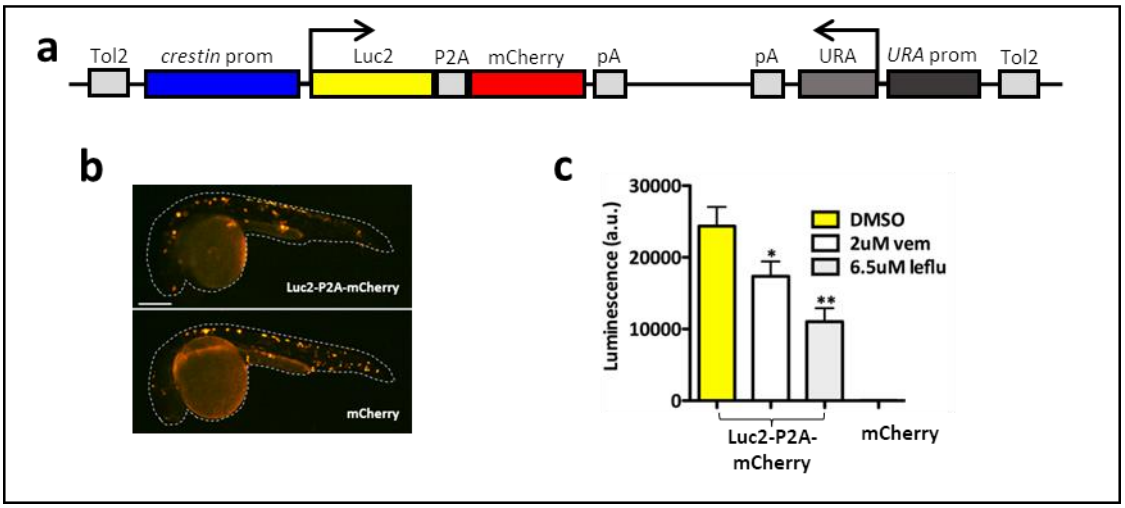

Figure 30 – Decrease in Luciferase signal in *crestin* double reporter mosaic line upon drug treatments. (a) Schematic representation of the pDEST*(-4.5-crestin:Luc2-P2A-mCherry,URAprom:URA)* construct that expresses Luciferase (Luc2, yellow) and mCherry (red) reporters, separated by P2A sequence, under the control of *crestin* promoter (blue). The URA gene with its promoter is inserted in the construct for a possible genotyping strategy, identifying the genome insertion site using yeast. (b) 30hpf *Tg(mitfa:BRAF_V600E)*, p53(lf) zebrafish embryos injected at 1-cell stage with the Luc2-P2A-mCherry construct show the same pattern of red fluorescence as embryos injected with the mCherry construct. (c) They also show a luminescence signal that responds to a 24h long treatment with vem and leflu. Statistically significant differences are indicated with asterisks: *P<0.05, **P<0.01 (Mann-Whitney test).

4.3.3. Generation of *crestin* reporter transgenic lines

While the results obtained on mosaic fish proved the feasibility of our approach, the generation of the corresponding stable lines was not free from stumbles. Although the mCherry fluorescent signal is similar in single and double reporter constructs in the mosaic condition (F0), in subsequent generations the results diverge.

The single reporter transgenic line (mCherry only) presents a complete neural crest expression pattern, as published, with a very strong signal visible with the stereo microscope and with epifluorescence (Fig. 31a). Following the pharmacological treatment with vem and leflu drugs, fluorescence analysis of the acquired images shows a reduced deviation and a greater effect compared to the mosaic condition (Fig. 31b-c). It is possible to quantify the effect of drug treatment on fluorescence also using the flow cytometer, although this is still in the optimization phase (Fig. 31d). Crucially, in adults it is possible to observe red signal from the earliest stages of tumor development in a very clear way (Fig. 31e).

The double reporter transgenic line (mCherry and Luciferase), on the other hand, has a much weaker signal, such that it is not detectable via epifluorescence in F1 and following generations (data not shown).

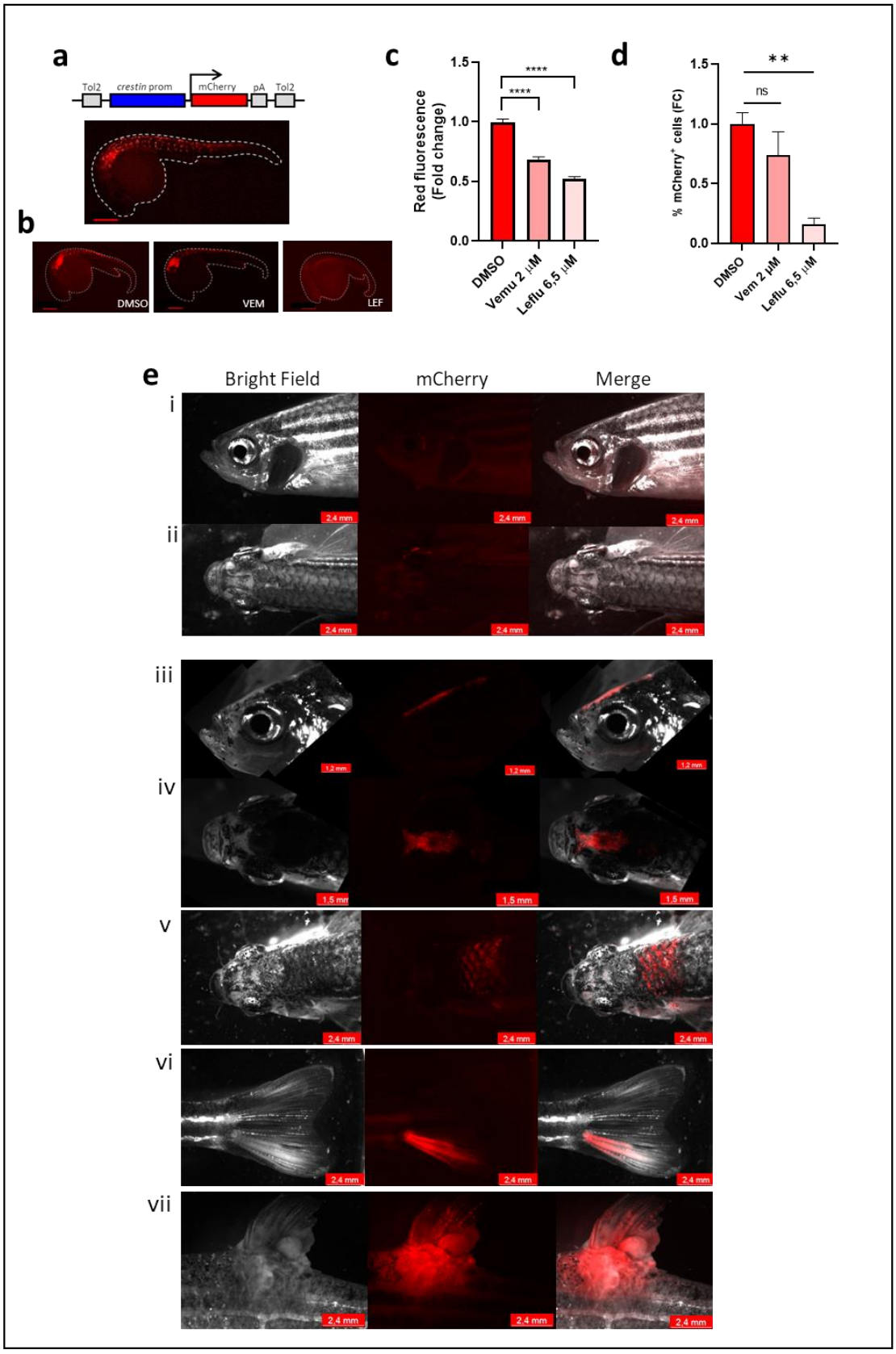

Figure 31 – Fluorescence signal in *crestin* single reporter stable line. (a) Neural crest expression pattern in stable *Tg(mitfa:BRAF_V600E),Tg(-4.5crestin:mCherry)* embryos at 24hpf. (b) Red fluorescence

reduction in 22hpf representative embryos after treatment with indicated drugs. (c) Fluorescence level by photo analysis. (d) Percentage of mCherry-positive cells measured via flow cytometry, shown as fold-change compared to DMSO. (e) Reactivation of mCherry signal in melanoma in adult zebrafish of *Tg(mitfa:BRAF_V600E),Tg(-4.5crestin:mCherry)*,p53(lf) line. i. control adult in lateral view; ii control adult in dorsal view; iii,vi first stage melanoma in lateral view; iv-v first stage melanoma in dorsal view; vii advanced melanoma in lateral view. Brightfield (left), fluorescence (middle) and merge (right). Statistically significant differences are indicated with asterisks: **P<0.01, ****P<0.01 (Dunnett's multiple comparisons test).

4.3.4. Alternative strategies to generate a transgenic line that expresses mCherry and Luciferase

To determine whether the double reporter construct was silenced, another construct was generated by adding a second fluorescent marker in the same expression cassette (Fig. 32a). Unfortunately in *Tg(-4.5crestin:Luc2-P2A-mCherry,γcrist:VenusGFP)*, although both the mCherry signal and VenusGFP expression in the lens were visible in the F0, in the stable generation (F1) the mCherry and Luciferase signals were both drastically reduced, while the VenusGFP signal in the lens was still visible (Fig. 32b-c).

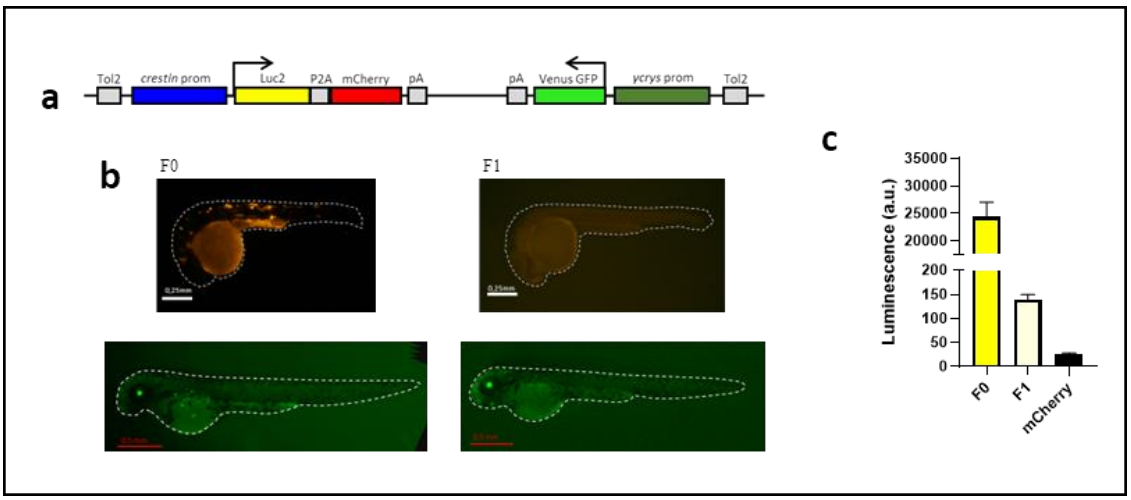

Figure 32- ***Tg(-4.5crestin:Luc2-P2A-mCherry,γcrist:VenusGFP).*** (a) Schematic representation of the pDEST*(-4.5crestin:Luc2-P2A-mCherry,γcrist:VenusGFP)* construct that expresses Luciferase (Luc2, yellow) and mCherry (red) reporters, joined by P2A sequence, under the control of *crestin* promoter (blue). The Venus GFP reporter (light green) under crystallin promoter (dark green) is inserted in the construct to verify the transgenic vector expression. (b) 30hpf *Tg(mitfa:BRAF_V600E)*.p53(lf) zebrafish embryos injected at 1-cell stage with the Luc2-P2A-mCherry construct show red fluorescence signal (F0, upper left panel) as well as GFP signal in the lens at 48hpf (lower left panel). In the following generation (F1), 30hpf embryos lost mCherry signal (upper right panel) but retained GFP signal in the lens at 48hpf (lower right

panel). (c) Signal reduction in F1 is noticeable also in terms of Luciferase signal, which decreases by more than 200 times.

Excluding a silencing of the construct, we evaluated the number of insertions that the lines possess. This way, we highlighted a very high number (> 30 copies) of genome insertions in the *Tg(-4.5crestin:mCherry)* line, while in dual reporter *Tg(-4.5crestin:Luc2-P2A-mCherry;γcrist:VenusGFP)* line the number of genome insertions was less than five copies (Fig. 33).

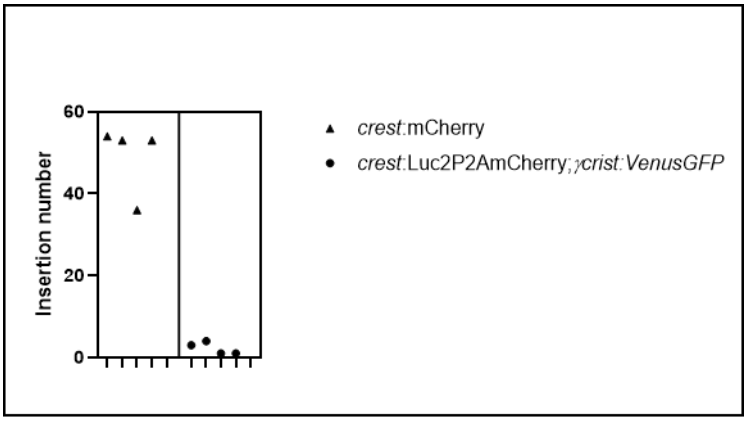

Figure 33– Number of insertions evaluation. The transgene copy-number changes in the different transgenic lines. In the *Tg(-4.5crestin:mCherry)* line the transgene copies number exceeds 30, while in the *Tg(-4.5crestin:Luc2-P2A-mCherry,γcrist:VenusGFP)* line it is less than 5.

This difference in the copies' number could explain the different signal level between the different lines. Considering the retroelement sequences present within *crestin* promoter, we hypothesize that the transgene is taking advantage of the *crestin* promoter by amplifying itself, but with a limited luggage capacity.

To understand if our hypothesis is correct, and considering that the *crestin* gene's coding sequence is 1782nt long while the mRNA is 4437nt long, we generated another short construct with nothing but the *crestin* promoter and reporter genes (pDEST:-*4.5crestin:Luc2P2AmCherry*). If the new construct amplifies itself in the genome like the mCherry single reporter, we will be able to obtain high expression of both our qualitative marker (red fluorescence) and our quantitative marker (Luciferase signal). This vector would take the *crestin* gene's advantages and match its high expression level in both drug screenings and characterization studies. But, on the other hand, having to follow over generations such a large insertions site number could make it difficult to reach a statistical power that minimizes errors and maximizes results across experimental replicates.

5. Discussion and future perspectives

5.1. Mosaic fish overexpressing *BRAFV600E* variants

Zebrafish is characterized by distinct pigmentation patterns in embryos/larvae and adults. Pigmented cells of adults are generated de novo during metamorphosis, by means of precursor cells, in contrast to a portion of adult xanthophores that result from an embryonic dedifferentiation-proliferation-differentiation derived process. The source of the de novo pigmented cells is hypothesized to be a stem/progenitor cell, equivalent to MSC. These cells derive from the neural crest, although their identity, number and location remain unclear. They reside in a quiescent state, maintained by the local niche, but retain their multipotency and reactivate upon stimuli such as in metamorphosis, regeneration, or tissue maintenance (Dawes et al., 2021). For example, a role for MAPK pathway has been highlighted in the control of melanocytes expansion during fin regeneration (Richardson et al., 2011).

The formation of moles may be precisely the result of the action of the oncogenic BRAFV600E on MSCs, while in presence of other genetic stimuli, such as the absence of wild type p53, neoplastic transformation occurs.

On mosaic fish, we consistently observed an effect on pigmentation in all development stages, from the larval stage to the juvenile and adult stage. Such effect is stronger for BRAFV600E coding-only lines compared to coding plus 3'UTR lines.

In addition, the melanoma onset data are of particular interest. Here, we observed differences in malignant transformation between the reference and X1 isoforms: despite the same starting point in terms of pigmentation, they seem to have a different neoplastic capacity. This phenotype is evident especially in the first months of animal life, probably when the accumulation effect of mutations induced by loss of p53 functions has not yet reached a certain threshold. The lack of differences in tumor macro features confirms that there are no major genetic rearrangements when comparing the two isoforms; therefore, the difference in the transforming capacity could reside in different allosteric conformations caused by the different C-term portions or by the distinct interactors they could be associated with. The isoform-specific features of BRAFV600E-ref vs BRAFV600E-X1 are a totally new field of investigation that we are spearheading. Specifically, our still unpublished studies in yeast show a stronger involvement of X1 variant in fatty acid metabolism compared to ref variant, supporting emerging evidence regarding the importance of lipid processing in melanoma progression (Lumaquin et al., 2021). Therefore, it would be interesting to observe in our *BRAFV600E* lines the lipid amounts in and around tumors in order to assess whether X1-driven melanoma relies more on lipids than ref-driven ones.

We have of course to exclude a possible effect due only to a minor presence of the protein. To address this point, it will be necessary to quantify protein levels of the two BRAFV600E isoforms by mass spectrometry. BRAFV600E protein levels in embryos are not sufficient to be detected by semi-quantitative techniques such as western blot, therefore we will perform the immunoprecipitation of BRAF protein, followed by mass spectrometry analysis in collaboration with Dr. Arrigoni group (University of Padova).

If a different protein-protein interaction network and/or a reduced expression could explain the difference between ref and X1 protein variants, it does not explain why this difference is not evident also in presence of the 3'UTR. Actually, it is interesting to note that, despite the different size of the 3'UTRs (121nt for ref and 7163nt for X1), they both cause a comparable delay in nevi appearance and tumor onset. This piece of experimental evidence certainly deserves to be studied further.

In general terms, we can hypothesize that 3'UTRs cause the transcripts to be subjected to post-transcriptional regulation. Specifically, we have already identified a set of microRNAs that act as positive or negative regulators of X1 mRNA transcription and translation in melanoma cells (Marranci et al., 2019), while miRNAs that regulate ref expression have been reported by others (Fattore et al., 2016). These data give us a glimpse on how tight the regulation of BRAF expression must be. It is also important to mention that, like in human cells (Marranci et al., 2017), also in zebrafish X1 mRNA is expressed at higher levels than ref mRNA, which suggests the presence of evolutionarily conserved regulatory regions between humans and fish. These regions could be revealed by aligning the *BRAF* gene between different vertebrate and invertebrate organisms. Once identified, they could be subjected to prediction studies for microRNA binding and tested by introducing appropriate deletions.

We also have to consider that the 3'UTR confers to *BRAFV600E* transcripts the ability to perform functions other than those related to their translation (Anelli et al., 2017), and such functions need to be taken into account as well.

For a comprehensive identification of the pathways that are impacted by *BRAFV600E*-ref/X1, with or without their 3'UTR, we will carry out transcriptomic (i.e, RNA-seq) and proteomic analyses. Before doing so, however, we still have to define whether it is better to analyze embryos, adult skin or tumors.

5.2. Transgenic zebrafish lines overexpressing *BRAFV600E* variants

The altered pigmentation observed in early generations likely arises from the sum of the high copy number of the *BRAFV600E* transgene and the damage and mutations accumulation induced by the loss of canonical p53 functions. This phenotype, not mentioned in the work in which the historical model of *BRAFV600E* in zebrafish is described (Patton et al., 2005), can be considered as evidence in favor of the higher efficiency of Tol2 system as strategy for transgene integration in the genome (Kawakami, 2007). Conversely, the regularization of the phenotype observed in advanced generations is consistent with a progressive segregation of *BRAFV600E* transgene copies.

After the identification of single insertion, each transgenic line will be once again crossed into the protumor genetic background (p53(lf)). Only then transgenic lines will be compared in melanoma-free survival curves and pharmacological treatments.

The identification of the exact location of the insertion site is crucial for many reasons: allele number needs to be established and correlated with phenotype severity, and position effects need to be considered so that transgene-unrelated phenotypes can be discerned. To this aim, quite a few techniques have been developed to obtain hybrid DNA fragments in which the transgene sequence is juxtaposed to the flanking genomic DNA (gDNA), which is unknown. Such techniques can be grouped into PCR-based vs. high-throughput sequencing-based. Although less laborious and time consuming than PCR-based methods, high-throughput methods usually produce reads that are too short to ensure the simultaneous coverage of the known transgene sequence and the flanking unknown genomic sequence. However, among the latest developments in sequencing approaches, ONT is intrinsically able to overcome the limitation represented by short reads, as it is endowed with the capacity to produce long reads (up to 2.3 Mb (Payne et al., 2019)). Adapting nCATs (nanopore Cas9-targeted sequencing) to the identification of the insertion site of a transgene, we targeted the transgene sequence and managed to obtain long hybrid reads, oriented towards the unknown flanking genomic regions. Using this approach, we have already identified quite a few insertion sites and we will go on until at least two insertion sites per construct are available. Also, our approach allows to map multiple insertion sites within the same genome, so that allele segregation can be tracked and fish carrying only one insertion can be identified sooner.

5.3. Single and double *crestin* reporter lines

Reports in literature indicate an increase of NCP in the *BRAFV600E*,p53(lf) melanoma-prone background, already at the embryonic level.

Our ISH data confirm this increase for both ref and X1 variants, also in presence of 3'UTRs. However, such data are only qualitative, not quantitative. Since we do not find data in the literature that define a method to quantitatively evaluate NCP by analyzing *crestin* signal in embryos, we decided to overcome this limitation using a reporter line for crestin. In particular, our aim is to create a dual reporter line that allows a qualitative analysis using the mCherry signal and a quantitative analysis using the Luciferase signal, so that both genetic analyses and pharmacological screenings can be accurately performed.

To ensure the validity of our approach, we performed preliminary drug treatments on the single reporter line *crestin:mCherry* using leflu, both of which have already been characterized in the literature (Kaufman et al., 2016; White et al., 2011). In the mosaic condition, we observed an increase in the fluorescent signal in the *BRAFV600E*,p53(lf) melanoma-prone background compared to wt embryos, and a reduction of it following pharmacological treatments. Specifically, the data show a reduction of red fluorescence following treatment with leflu, vem, omy and dnp, with vem specifically reducing *crestin* signal only in *BRAFV600E*,p53(lf) embryos, as expected. A *crestin* signal reduction was observed also upon combinatorial treatments between BRAFi and MEKi, as currently used in the clinic, and between vem and PTU. The combination of a BRAFi with a PIGMi is an approach we are pursuing in our lab. Prompted by the observation that pigmented metastatic melanoma tumors are more refractory to targeted therapy that non-pigmented ones, we found in vitro that metastatic melanoma cell lines that can get pigmented upon vem treatment are more resistant to the drug compared to those that can not. We also found that the sensitivity of pigmentable cells can be increased by combining vem with a pigmentation inhibitor such PTU, or with an inhibitor of oxidative phosphorylation, such as omy. This in turn reflects the link between mitochondria and melanosomes, as the former are necessary for the correct function of melanosomes and for melanin production (Vitiello et al., 2017).

Next, we verified the Luciferase signal in embryos possessing the dual reporter line in mosaic condition. Indeed, we found that Luciferase signal as well is reduced following vem and leflu treatments.

Then, we moved forward with the analysis of stable lines. Here, we obtained very different results in single vs double reporter lines. While the signal for the mCherry single reporter line is strong and responds well to pharmacological treatments, in the dual reporter Luciferase-

mCherry line the signal decreases dramatically. The red fluorescence is so low that is not visible using the epifluorescence microscope, and the Luciferase signal is reduced to a level so low that is not suitable for pharmacological screenings.

By adding a second fluorescent reporter into the same transgene, i.e. by expressing eGFP in the lens, we excluded that the reason for low signal is transgene silencing. We then tested the integration sites number owned by stable lines. This highlighted a strong discrepancy between the single mCherry reporter line and the dual reporter Luciferase-mCherry line. The high number of transgene insertions in the single mCherry line (>30) compared with very low number (<5) in the dual Luciferase2-mCherry reporter line suggests that the retro-element activity of the *crestin* promoter could be reactivated when driving small coding sequences or when inserted in a small expression cassette, leading to a strong signal (Kaufman et al., 2016). This hypothesis is currently under testing, by reducing the transgene size with a construct made up of *crestin* promoter and coding Luc2P2AmCherry only. The expected result is that the smaller transgene will in fact be retrotransposed, producing a strong signal for both mCherry and Luciferase. Of course, this approach has its drawbacks, as a line with many insertions is difficult to handle, when ideally the transgenic lines are made up of a single identifiable insertion. In other words, we are facing a trade-off between a strong signal at high copy number vs a weak signal at low copy number.

While we wait for the new dual reporter Luciferase2-mCherry line to be ready, we are assessing whether we can adapt the single reporter mCherry line, which is already available to us, to drug screenings. On one side, filial generations of the single reporter mCherry line are currently studied to evaluate whether there are variations in the integrated transgene number from one filial to the next, i.e. to understand the stability of crestin promoter as retrotrasposon. On the other side, we are optimizing mCherry quantification by measuring the percentage of fluorescence positive cells by flow cytometry. In this way, we have the option to use mCherry fluorescence as both qualitative and quantitative marker.

Once we identify the reporter transgenic line that meets all the requirements, it will be crossed with our fish carrying the single oncogenic variants of *BRAFV600E*, thus obtaining the fish:

- *Tg(mitfa:-2.3Hsa.BRAF_V600E-220,myl7:eGFP),Tg(-4.5crestin:(Luc2-P2A-)mCherry)*p53(lf)
- *Tg(mitfa:-2.3Hsa.BRAF_V600E-204,myl7:eGFP),Tg(-4.5crestin:(Luc2-P2A-)mCherry)*p53(lf)
- *Tg(mitfa:-2.4Hsa.BRAF_V600E-220,myl7:eGFP),Tg(-4.5crestin:(Luc2-P2A-)mCherry)*p53(lf)
- *Tg(mitfa:-9.4Hsa.BRAF_V600E-204,myl7:eGFP),Tg(-4.5crestin:(Luc2-P2A-)mCherry)*p53(lf)

At the embryonic stage, these lines will be used for drug screenings. Ideally, using Luciferase signal it will be possible to screen simultaneously 32 compounds or combinations in a 96 multiwell plate. These lines will also be useful to identify and track the single cells in which the NCP gets activated upon BRAFV600E expression.

At the adult stage, these transgenic lines will be characterized for tumor generation and progression. In particular, nevi will be monitored over time and the gain of red fluorescence will be taken as a more accurate marker of melanoma onset compared to visual inspection for pigmentation intensification, skin thickening and outward growth (Patton et al., 2011). On the other hand, pharmacological treatments will be performed using the soaking method and tumor reduction will be evaluated not only in terms of tumor mass area, but also in terms of *crestin* signal. However, we will consider the possibility to perform different pharmacological treatments on the same tumor, by homogenizing it, dividing it into several wells and treating it *in vitro*.

6. References

1. Ablain J, Durand EM, Yang S, Zhou Y, Zon LI. A CRISPR/Cas9 vector system for tissue-specific gene disruption in zebrafish. Dev Cell. 2015 Mar 23;32(6):756-64. doi: 10.1016/j.devcel.2015.01.032. Epub 2015 Mar 5. PMID: 25752963; PMCID: PMC4379706.
2. Ablain J, Xu M, Rothschild H, Jordan RC, Mito JK, Daniels BH, Bell CF, Joseph NM, Wu H, Bastian BC, Zon LI, Yeh I. Human tumor genomics and zebrafish modeling identify SPRED1 loss as a driver of mucosal melanoma. Science. 2018 Nov 30;362(6418):1055-1060. doi: 10.1126/science.aau6509. Epub 2018 Nov 1. PMID: 30385465; PMCID: PMC6475924.
3. Akasu R. Diagnosis and differential diagnosis of malignant melanoma by dermatoscope and videomicroscope. J Dermatol. 1994 Nov;21(11):891-3. doi: 10.1111/j.1346-8138.1994.tb03308.x. PMID: 7852653.
4. Ampe C, Van Troys M. Mammalian Actins: Isoform-Specific Functions and Diseases. Handb Exp Pharmacol. 2017;235:1-37. doi: 10.1007/164_2016_43. PMID: 27757757.
5. Anelli V, Mione M. Melanoma niche formation: it is all about melanosomes making CAFs. Pigment Cell Melanoma Res. 2017 Jan;30(1):8-10. doi: 10.1111/pcmr.12545. PMID: 27774768.
6. Anelli V, Ordas A, Kneitz S, Sagredo LM, Gourain V, Schartl M, Meijer AH, Mione M. Ras-Induced miR-146a and 193a Target Jmjd6 to Regulate Melanoma Progression. Front Genet. 2018 Dec 18;9:675. doi: 10.3389/fgene.2018.00675. PMID: 30619488; PMCID: PMC6305343.
7. Aramini JM, Vorobiev SM, Tuberty LM, Janjua H, Campbell ET, Seetharaman J, Su M, Huang YJ, Acton TB, Xiao R, Tong L, Montelione GT. The RAS-Binding Domain of Human BRAF Protein Serine/Threonine Kinase Exhibits Allosteric Conformational Changes upon Binding HRAS. Structure. 2015 Aug 4;23(8):1382-1393. doi: 10.1016/j.str.2015.06.003. Epub 2015 Jul 9. PMID: 26165597; PMCID: PMC4963008.
8. Arrington JH 3rd, Reed RJ, Ichinose H, Krementz ET. Plantar lentiginous melanoma: a distinctive variant of human cutaneous malignant melanoma. Am J Surg Pathol. 1977 Jun;1(2):131-43. PMID: 602975.
9. Auer TO, Duroure K, De Cian A, Concordet JP, Del Bene F. Highly efficient CRISPR/Cas9-mediated knock-in in zebrafish by homology-independent DNA repair. Genome Res. 2014 Jan;24(1):142-53. doi: 10.1101/gr.161638.113. Epub 2013 Oct 31. PMID: 24179142; PMCID: PMC3875856.
10. Banky JP, Kelly JW, English DR, Yeatman JM, Dowling JP. Incidence of new and changed nevi and melanomas detected using baseline images and dermoscopy in patients at high risk for melanoma. Arch Dermatol. 2005 Aug;141(8):998-1006. doi: 10.1001/archderm.141.8.998. PMID: 16103329.
11. Bauer J, Büttner P, Murali R, Okamoto I, Kolaitis NA, Landi MT, Scolyer RA, Bastian BC. BRAF mutations in cutaneous melanoma are independently associated with age, anatomic site of the primary tumor, and the degree of solar elastosis at the primary tumor site. Pigment Cell Melanoma Res. 2011 Apr;24(2):345-51. doi: 10.1111/j.1755-148X.2011.00837.x. PMID: 21324100; PMCID: PMC3107974.
12. Berghmans S, Murphey RD, Wienholds E, Neuberg D, Kutok JL, Fletcher CD, Morris JP, Liu TX, Schulte-Merker S, Kanki JP, Plasterk R, Zon LI, Look AT. tp53 mutant zebrafish develop malignant peripheral nerve sheath tumors. Proc Natl Acad Sci U S A. 2005 Jan 11;102(2):407-12. doi: 10.1073/pnas.0406252102. Epub 2005 Jan 3. PMID: 15630097; PMCID: PMC544293.

13. Bootorabi F, Manouchehri H, Changizi R, Barker H, Palazzo E, Saltari A, Parikka M, Pincelli C, Aspatwar A. Zebrafish as a Model Organism for the Development of Drugs for Skin Cancer. Int J Mol Sci. 2017 Jul 18;18(7):1550. doi: 10.3390/ijms18071550. PMID: 28718799; PMCID: PMC5536038.
14. Bowyer S, Lee R, Fusi A, Lorigan P. Dabrafenib and its use in the treatment of metastatic melanoma. Melanoma Manag. 2015 Aug;2(3):199-208. doi: 10.2217/mmt.15.21. Epub 2015 Aug 10. PMID: 30190849; PMCID: PMC6094610.
15. Box NF, Terzian T. The role of p53 in pigmentation, tanning and melanoma. Pigment Cell Melanoma Res. 2008 Oct;21(5):525-33. doi: 10.1111/j.1755-148X.2008.00495.x. Epub 2007 Aug 6. PMID: 18761658.
16. Braicu C, Buse M, Busuioc C, Drula R, Gulei D, Raduly L, Rusu A, Irimie A, Atanasov AG, Slaby O, Ionescu C, Berindan-Neagoe I. A Comprehensive Review on MAPK: A Promising Therapeutic Target in Cancer. Cancers (Basel). 2019 Oct 22;11(10):1618. doi: 10.3390/cancers11101618. PMID: 31652660; PMCID: PMC6827047.
17. Breslow A. Melanoma thickness and elective node dissection. Arch Dermatol. 1978 Sep;114(9):1399. doi: 10.1001/archderm.1978.01640210078029. PMID: 686759.
18. Breslow A. Thickness, cross-sectional areas and depth of invasion in the prognosis of cutaneous melanoma. Ann Surg. 1970 Nov;172(5):902-8. doi: 10.1097/00000658-197011000-00017. PMID: 5477666; PMCID: PMC1397358.
19. Bronner-Fraser M. Segregation of cell lineage in the neural crest. Curr Opin Genet Dev. 1993 Aug;3(4):641-7. doi: 10.1016/0959-437x(93)90101-t. PMID: 7902150.
20. Brosseau, JP. Splicing isoform-specific functional genomic in cancer cells. Appl Cancer Res 38, 18 (2018). https://doi.org/10.1186/s41241-018-0068-6
21. Burotto M, Chiou VL, Lee JM, Kohn EC. The MAPK pathway across different malignancies: a new perspective. Cancer. 2014 Nov 15;120(22):3446-56. doi: 10.1002/cncr.28864. Epub 2014 Jun 19. PMID: 24948110; PMCID: PMC4221543.
22. Cancer Genome Atlas Network. Genomic Classification of Cutaneous Melanoma. Cell. 2015 Jun 18;161(7):1681-96. doi: 10.1016/j.cell.2015.05.044. PMID: 26091043; PMCID: PMC4580370.
23. Cebollero A, Puértolas T, Pajares I, Calera L, Antón A. Comparative safety of BRAF and MEK inhibitors (vemurafenib, dabrafenib and trametinib) in first-line therapy for BRAF-mutated metastatic melanoma. Mol Clin Oncol. 2016 Oct;5(4):458-462. doi: 10.3892/mco.2016.978. Epub 2016 Aug 4. PMID: 27699043; PMCID: PMC5038159.
24. Ceol CJ, Houvras Y, Jane-Valbuena J, Bilodeau S, Orlando DA, Battisti V, Fritsch L, Lin WM, Hollmann TJ, Ferré F, Bourque C, Burke CJ, Turner L, Uong A, Johnson LA, Beroukhim R, Mermel CH, Loda M, Ait-Si-Ali S, Garraway LA, Young RA, Zon LI. The histone methyltransferase SETDB1 is recurrently amplified in melanoma and accelerates its onset. Nature. 2011 Mar 24;471(7339):513-7. doi: 10.1038/nature09806. PMID: 21430779; PMCID: PMC3348545.
25. Chapman PB, Hauschild A, Robert C, Haanen JB, Ascierto P, Larkin J, Dummer R, Garbe C, Testori A, Maio M, Hogg D, Lorigan P, Lebbe C, Jouary T, Schadendorf D, Ribas A, O'Day SJ, Sosman JA, Kirkwood JM, Eggermont AM, Dreno B, Nolop K, Li J, Nelson B, Hou J, Lee RJ, Flaherty KT, McArthur GA; BRIM-3 Study Group. Improved survival with vemurafenib in melanoma with BRAF V600E mutation. N Engl J Med. 2011 Jun 30;364(26):2507-16. doi: 10.1056/NEJMoa1103782. Epub 2011 Jun 5. PMID: 21639808; PMCID: PMC3549296.

26. Chin L, Merlino G, DePinho RA. Malignant melanoma: modern black plague and genetic black box. Genes Dev. 1998 Nov 15;12(22):3467-81. doi: 10.1101/gad.12.22.3467. PMID: 9832500.
27. Cichorek M, Wachulska M, Stasiewicz A, Tymińska A. Skin melanocytes: biology and development. Postepy Dermatol Alergol. 2013 Feb;30(1):30-41. doi: 10.5114/pdia.2013.33376. Epub 2013 Feb 20. PMID: 24278043; PMCID: PMC3834696.
28. Clark Jr WH . A classification of malignant melanoma in man correlated with histogenesis and biological behaviour. In: Montagna W, Hu F (eds). Advances in the Biology of the Skin, Vol. VIII. Pergamon: New York, 1967, pp 621–647.
29. Clark WH Jr, From L, Bernardino EA, Mihm MC. The histogenesis and biologic behavior of primary human malignant melanomas of the skin. Cancer Res. 1969 Mar;29(3):705-27. PMID: 5773814.
30. Cotto-Rios XM, Agianian B, Gitego N, Zacharioudakis E, Giricz O, Wu Y, Zou Y, Verma A, Poulikakos PI, Gavathiotis E. Inhibitors of BRAF dimers using an allosteric site. Nat Commun. 2020 Sep 1;11(1):4370. doi: 10.1038/s41467-020-18123-2. PMID: 32873792; PMCID: PMC7462985.
31. Csányi I, Houshmand N, Szűcs M, Ócsai H, Kemény L, Oláh J, Baltás E. Acral lentiginous melanoma: a single-centre retrospective review of four decades in East-Central Europe. J Eur Acad Dermatol Venereol. 2020 Sep;34(9):2004-2010. doi: 10.1111/jdv.16227. Epub 2020 Mar 20. PMID: 31989672.
32. Cuevas BD, Abell AN, Johnson GL. Role of mitogen-activated protein kinase kinase kinases in signal integration. Oncogene. 2007 May 14;26(22):3159-71. doi: 10.1038/sj.onc.1210409. PMID: 17496913.
33. Cunningham RL, Kramer ET, DeGeorgia SK, Godoy PM, Zarov AP, Seneviratne S, Grigura V, Kaufman CK. Functional in vivo characterization of sox10 enhancers in neural crest and melanoma development. Commun Biol. 2021 Jun 7;4(1):695. doi: 10.1038/s42003-021-02211-0. PMID: 34099848; PMCID: PMC8184803.
34. Daniotti M, Oggionni M, Ranzani T, Vallacchi V, Campi V, Di Stasi D, Torre GD, Perrone F, Luoni C, Suardi S, Frattini M, Pilotti S, Anichini A, Tragni G, Parmiani G, Pierotti MA, Rodolfo M. BRAF alterations are associated with complex mutational profiles in malignant melanoma. Oncogene. 2004 Aug 5;23(35):5968-77. doi: 10.1038/sj.onc.1207780. PMID: 15195137.
35. Dawes JHP, Kelsh RN. Cell Fate Decisions in the Neural Crest, from Pigment Cell to Neural Development. Int J Mol Sci. 2021 Dec 16;22(24):13531. doi: 10.3390/ijms222413531. PMID: 34948326; PMCID: PMC8706606.
36. den Hertog J. Tumor Suppressors in Zebrafish: From TP53 to PTEN and Beyond. Adv Exp Med Biol. 2016;916:87-101. doi: 10.1007/978-3-319-30654-4_4. PMID: 27165350.
37. Dinehart MS, Dinehart SM, Sukpraprut-Braaten S, High WA. Immunohistochemistry utilization in the diagnosis of melanoma. J Cutan Pathol. 2020 May;47(5):446-450. doi: 10.1111/cup.13648. Epub 2020 Jan 27. PMID: 31955450.
38. Domingues B, Lopes JM, Soares P, Pópulo H. Melanoma treatment in review. Immunotargets Ther. 2018 Jun 7;7:35-49. doi: 10.2147/ITT.S134842. PMID: 29922629; PMCID: PMC5995433.
39. Donehower LA. The p53-deficient mouse: a model for basic and applied cancer studies. Semin Cancer Biol. 1996 Oct;7(5):269-78. doi: 10.1006/scbi.1996.0035. PMID: 9110404.

40. Dorsky RI, Raible DW, Moon RT. Direct regulation of nacre, a zebrafish MITF homolog required for pigment cell formation, by the Wnt pathway. Genes Dev. 2000 Jan 15;14(2):158-62. PMID: 10652270; PMCID: PMC316348.
41. Dovey M, White RM, Zon LI. Oncogenic NRAS cooperates with p53 loss to generate melanoma in zebrafish. Zebrafish. 2009 Dec;6(4):397-404. doi: 10.1089/zeb.2009.0606. PMID: 19954345; PMCID: PMC2943216.
42. Driever W, Solnica-Krezel L, Schier AF, Neuhauss SC, Malicki J, Stemple DL, Stainie DY, Zwartkruis F, Abdelilah S, Rangini Z, Belak J, Boggs C. A genetic screen for mutations affecting embryogenesis in zebrafish. Development. 1996 Dec;123:37-46. PubMed PMID: 9007227.
43. Ducreux M, Chamseddine A, Laurent-Puig P, Smolenschi C, Hollebecque A, Dartigues P, Samallin E, Boige V, Malka D, Gelli M. Molecular targeted therapy of BRAF-mutant colorectal cancer. Ther Adv Med Oncol. 2019 Jun 18;11:1758835919856494. doi: 10.1177/1758835919856494. PMID: 31244912; PMCID: PMC6582307.
44. Elder DE, Bastian BC, Cree IA, Massi D, Scolyer RA. The 2018 World Health Organization Classification of Cutaneous, Mucosal, and Uveal Melanoma: Detailed Analysis of 9 Distinct Subtypes Defined by Their Evolutionary Pathway. Arch Pathol Lab Med. 2020 Apr;144(4):500-522. doi: 10.5858/arpa.2019-0561-RA. Epub 2020 Feb 14. PMID: 32057276.
45. Estrada C, Mirabal-Ortega L, Méry L, Dingli F, Besse L, Messaoudi C, Loew D, Pouponnot C, Bertolotto C, Eychène A, Druillennec S. MITF activity is regulated by a direct interaction with RAF proteins in melanoma cells. Commun Biol. 2022 Jan 28;5(1):101. doi: 10.1038/s42003-022-03049-w. PMID: 35091687; PMCID: PMC8799692.
46. Fattore L, Mancini R, Acunzo M, Romano G, Laganà A, Pisanu ME, Malpicci D, Madonna G, Mallardo D, Capone M, Fulciniti F, Mazzucchelli L, Botti G, Croce CM, Ascierto PA, Ciliberto G. miR-579-3p controls melanoma progression and resistance to target therapy. Proc Natl Acad Sci U S A. 2016 Aug 23;113(34):E5005-13. doi: 10.1073/pnas.1607753113. Epub 2016 Aug 8. PMID: 27503895; PMCID: PMC5003278.
47. Fleming YM, Ferguson GJ, Spender LC, Larsson J, Karlsson S, Ozanne BW, Grosse R, Inman GJ. TGF-beta-mediated activation of RhoA signalling is required for efficient (V12)HaRas and (V600E)BRAF transformation. Oncogene. 2009 Feb 19;28(7):983-93. doi: 10.1038/onc.2008.449. Epub 2008 Dec 15. PMID: 19079344.
48. Fox RI, Herrmann ML, Frangou CG, Wahl GM, Morris RE, Strand V, Kirschbaum BJ. Mechanism of action for leflunomide in rheumatoid arthritis. Clin Immunol. 1999 Dec;93(3):198-208. doi: 10.1006/clim.1999.4777. PMID: 10600330.
49. Gambichler T, Petig AL, Stockfleth E, Stücker M. Expression of SOX10, ABCB5 and CD271 in melanocytic lesions and correlation with survival data of patients with melanoma. Clin Exp Dermatol. 2016 Oct;41(7):709-16. doi: 10.1111/ced.12928. PMID: 27663144.
50. Garbe C, Amaral T, Peris K, Hauschild A, Arenberger P, Basset-Seguin N, Bastholt L, Bataille V, Del Marmol V, Dréno B, Fargnoli MC, Forsea AM, Grob JJ, Höller C, Kaufmann R, Kelleners-Smeets N, Lallas A, Lebbé C, Lytvynenko B, Malvehy J, Moreno-Ramirez D, Nathan P, Pellacani G, Saiag P, Stratigos AJ, Van Akkooi ACJ, Vieira R, Zalaudek I, Lorigan P; European Dermatology Forum (EDF), the European Association of Dermato-Oncology (EADO), and the European Organization for Research and Treatment of Cancer (EORTC). European consensus-based interdisciplinary guideline for melanoma. Part 1: Diagnostics:

Update 2022. Eur J Cancer. 2022 Jul;170:236-255. doi: 10.1016/j.ejca.2022.03.008. Epub 2022 May 12. PMID: 35570085.

51. Garcia-Blanco MA, Baraniak AP, Lasda EL. Alternative splicing in disease and therapy. Nat Biotechnol. 2004 May;22(5):535-46. doi: 10.1038/nbt964. PMID: 15122293.
52. Gershenwald JE, Morton DL, Thompson JF, et al, Collaborators of the AJCC/UICC Melanoma Task Force. Staging and Prognostic Factors for Stage IV Melanoma: Initial Results of an American Joint Committee on Cancer (AJCC) International Evidence-Based Assessment of 4,895 Melanoma Patients. J Clin Oncol. 2008;26(May 20 suppl; abstr 9035). Abstract presented at American Society of Clinical Oncology (ASCO) 2008 Annual Meeting Balch CM, Buzaid AC, Soong S-J, et al. Final version of the American Joint Committee on Cancer Staging System for Cutaneous Melanoma. J Clin Oncol. 2001;19(16):3635-3648.
53. Gershenwald JE, Scolyer RA, Hess KR, et al. Melanoma of the skin. In: Amin MB, et al. (eds) AJCC cancer staging manual. Switzerland: Springer, 2017:563–85; 2. AIOM linee guida - 2018; 3. Morton DL. Et al. Validation of the accuracy of intraoperative lymphatic mapping and sentinel lympadenectomy for early- stage melanoma: a multicenter trial. Multicenter selective lymphadenectomy trial group. Ann. Surg. 1999; 4. Ives et al. Adjuvant interferon alpha for the treatment of high risk melanoma: an individual patient data meta-analysis. Eur. J. of Cancer 2017; 5. G.V. Long et al. Adjuvant Dabrafenib plus Trametinib in Stage IIIBRAF-Mutated MelanomaN Engl J Med 2017;377:1813-23; 6. Weber J et al. Adjuvant Nivolumab versus Ipilimumabin Resected Stage III or IV MelanomaN Engl J Med. 2017;377:1824-1835.
54. Gibney GT, Messina JL, Fedorenko IV, Sondak VK, Smalley KS. Paradoxical oncogenesis--the long-term effects of BRAF inhibition in melanoma. Nat Rev Clin Oncol. 2013 Jul;10(7):390-9. doi: 10.1038/nrclinonc.2013.83. Epub 2013 May 28. PMID: 23712190; PMCID: PMC3983565.
55. Gilpatrick T, Lee I, Graham JE, Raimondeau E, Bowen R, Heron A, Downs B, Sukumar S, Sedlazeck FJ, Timp W. Targeted nanopore sequencing with Cas9-guided adapter ligation. Nat Biotechnol. 2020 Apr;38(4):433-438. doi: 10.1038/s41587-020-0407-5. Epub 2020 Feb 10. PMID: 32042167; PMCID: PMC7145730.
56. Goel VK, Ibrahim N, Jiang G, Singhal M, Fee S, Flotte T, Westmoreland S, Haluska FS, Hinds PW, Haluska FG. Melanocytic nevus-like hyperplasia and melanoma in transgenic BRAFV600E mice. Oncogene. 2009 Jun 11;28(23):2289-98. doi: 10.1038/onc.2009.95. Epub 2009 Apr 27. PMID: 19398955; PMCID: PMC3125533.
57. Graf SA, Busch C, Bosserhoff AK, Besch R, Berking C. SOX10 promotes melanoma cell invasion by regulating melanoma inhibitory activity. J Invest Dermatol. 2014 Aug;134(8):2212-2220. doi: 10.1038/jid.2014.128. Epub 2014 Mar 7. PMID: 24608986.
58. Hardcastle IR, Ahmed SU, Atkins H, Farnie G, Golding BT, Griffin RJ, Guyenne S, Hutton C, Källblad P, Kemp SJ, Kitching MS, Newell DR, Norbedo S, Northen JS, Reid RJ, Saravanan K, Willems HM, Lunec J. Small-molecule inhibitors of the MDM2-p53 protein-protein interaction based on an isoindolinone scaffold. J Med Chem. 2006 Oct 19;49(21):6209-21. doi: 10.1021/jm0601194. PMID: 17034127.
59. Harte RA, Farrell CM, Loveland JE, Suner MM, Wilming L, Aken B, Barrell D, Frankish A, Wallin C, Searle S, Diekhans M, Harrow J, Pruitt KD. Tracking and coordinating an international curation effort for the CCDS Project. Database (Oxford). 2012 Mar 20;2012:bas008. doi: 10.1093/database/bas008. PMID: 22434842; PMCID: PMC3308164.

60. Hayward NK, Wilmott JS, Waddell N, Johansson PA, Field MA, Nones K, Patch AM, Kakavand H, Alexandrov LB, Burke H, Jakrot V, Kazakoff S, Holmes O, Leonard C, Sabarinathan R, Mularoni L, Wood S, Xu Q, Waddell N, Tembe V, Pupo GM, De Paoli-Iseppi R, Vilain RE, Shang P, Lau LMS, Dagg RA, Schramm SJ, Pritchard A, Dutton-Regester K, Newell F, Fitzgerald A, Shang CA, Grimmond SM, Pickett HA, Yang JY, Stretch JR, Behren A, Kefford RF, Hersey P, Long GV, Cebon J, Shackleton M, Spillane AJ, Saw RPM, López-Bigas N, Pearson JV, Thompson JF, Scolyer RA, Mann GJ. Whole-genome landscapes of major melanoma subtypes. Nature. 2017 May 11;545(7653):175-180. doi: 10.1038/nature22071. Epub 2017 May 3. PMID: 28467829.
61. Heppt MV, Wang JX, Hristova DM, Wei Z, Li L, Evans B, Beqiri M, Zaman S, Zhang J, Irmler M, Berking C, Besch R, Beckers J, Rauscher FJ 3rd, Sturm RA, Fisher DE, Herlyn M, Fukunaga-Kalabis M. MSX1-Induced Neural Crest-Like Reprogramming Promotes Melanoma Progression. J Invest Dermatol. 2018 Jan;138(1):141-149. doi: 10.1016/j.jid.2017.05.038. Epub 2017 Sep 18. PMID: 28927893; PMCID: PMC5902795.
62. Hess J, Angel P, Schorpp-Kistner M. AP-1 subunits: quarrel and harmony among siblings. J Cell Sci. 2004 Dec 1;117(Pt 25):5965-73. doi: 10.1242/jcs.01589. PMID: 15564374.
63. Hoath, S. B. & Leahy, D. G. The organization of human epidermis: functional epidermal units and phi proportionality. J. Invest. Dermatol. 121, 1440–1446 (2003)
64. Hodis E, Torlai Triglia E, Kwon JYH, Biancalani T, Zakka LR, Parkar S, Hütter JC, Buffoni L, Delorey TM, Phillips D, Dionne D, Nguyen LT, Schapiro D, Maliga Z, Jacobson CA, Hendel A, Rozenblatt-Rosen O, Mihm MC Jr, Garraway LA, Regev A. Stepwise-edited, human melanoma models reveal mutations' effect on tumor and microenvironment. Science. 2022 Apr 29;376(6592):eabi8175. doi: 10.1126/science.abi8175. Epub 2022 Apr 29. PMID: 35482859.
65. Holmila R, Fouquet C, Cadranel J, Zalcman G, Soussi T. Splice mutations in the p53 gene: case report and review of the literature. Hum Mutat. 2003 Jan;21(1):101-2. doi: 10.1002/humu.9104. PMID: 12497643.
66. Howe K, Clark MD, Torroja CF, Torrance J, Berthelot C, Muffato M, Collins JE, Humphray S, McLaren K, Matthews L, McLaren S, Sealy I, Caccamo M, Churcher C, Scott C, Barrett JC, Koch R, Rauch GJ, White S, Chow W, Kilian B, Quintais LT, Guerra-Assunção JA, Zhou Y, Gu Y, Yen J, Vogel JH, Eyre T, Redmond S, Banerjee R, Chi J, Fu B, Langley E, Maguire SF, Laird GK, Lloyd D, Kenyon E, Donaldson S, Sehra H, Almeida-King J, Loveland J, Trevanion S, Jones M, Quail M, Willey D, Hunt A, Burton J, Sims S, McLay K, Plumb B, Davis J, Clee C, Oliver K, Clark R, Riddle C, Elliot D, Threadgold G, Harden G, Ware D, Begum S, Mortimore B, Kerry G, Heath P, Phillimore B, Tracey A, Corby N, Dunn M, Johnson C, Wood J, Clark S, Pelan S, Griffiths G, Smith M, Glithero R, Howden P, Barker N, Lloyd C, Stevens C, Harley J, Holt K, Panagiotidis G, Lovell J, Beasley H, Henderson C, Gordon D, Auger K, Wright D, Collins J, Raisen C, Dyer L, Leung K, Robertson L, Ambridge K, Leongamornlert D, McGuire S, Gilderthorp R, Griffiths C, Manthravadi D, Nichol S, Barker G, Whitehead S, Kay M, Brown J, Murnane C, Gray E, Humphries M, Sycamore N, Barker D, Saunders D, Wallis J, Babbage A, Hammond S, Mashreghi-Mohammadi M, Barr L, Martin S, Wray P, Ellington A, Matthews N, Ellwood M, Woodmansey R, Clark G, Cooper J, Tromans A, Grafham D, Skuce C, Pandian R, Andrews R, Harrison E, Kimberley A, Garnett J, Fosker N, Hall R, Garner P, Kelly D, Bird C, Palmer S, Gehring I, Berger A, Dooley CM, Ersan-Ürün Z, Eser C, Geiger H, Geisler M, Karotki L, Kirn A, Konantz J, Konantz M, Oberländer M, Rudolph-Geiger S, Teucke M, Lanz C, Raddatz G, Osoegawa K, Zhu B, Rapp

A, Widaa S, Langford C, Yang F, Schuster SC, Carter NP, Harrow J, Ning Z, Herrero J, Searle SM, Enright A, Geisler R, Plasterk RH, Lee C, Westerfield M, de Jong PJ, Zon LI, Postlethwait JH, Nüsslein-Volhard C, Hubbard TJ, Roest Crollius H, Rogers J, Stemple DL. The zebrafish reference genome sequence and its relationship to the human genome. Nature. 2013 Apr 25;496(7446):498-503. doi: 10.1038/nature12111. Epub 2013 Apr 17. Erratum in: Nature. 2014 Jan 9;505(7482):248. Cooper, James [corrected to Cooper, James D]; Eliott, David [corrected to Elliot, David]; Mortimer, Beverly [corrected to Mortimore, Beverley]; Begum, Sharmin [added]; Lloyd, Christine [added]; Lanz, Christa [added]; Raddatz, Günter [added]; Schuster, Ste. PMID: 23594743; PMCID: PMC3703927.

67. Hu W, Jiang C, Kim M, Xiao Y, Richter HJ, Guan D, Zhu K, Krusen BM, Roberts AN, Miller J, Steger DJ, Lazar MA. Isoform-specific functions of PPARγ in gene regulation and metabolism. Genes Dev. 2022 Mar 1;36(5-6):300-312. doi: 10.1101/gad.349232.121. Epub 2022 Mar 10. PMID: 35273075; PMCID: PMC8973844.
68. Ilouz R, Lev-Ram V, Bushong EA, Stiles TL, Friedmann-Morvinski D, Douglas C, Goldberg JL, Ellisman MH, Taylor SS. Isoform-specific subcellular localization and function of protein kinase A identified by mosaic imaging of mouse brain. Elife. 2017 Jan 12;6:e17681. doi: 10.7554/eLife.17681. PMID: 28079521; PMCID: PMC5300705.
69. Imai S. The prognosis of skin carcinoma and malignant melanoma with special reference to their extents as represented in terms of T, N, and M of union internationale contre le cancer (UICC). J Dermatol. 1976 Aug;3(4):147-54. doi: 10.1111/j.1346-8138.1976.tb01835.x. PMID: 15633969.
70. Iyengar S, Houvras Y, Ceol CJ. Screening for melanoma modifiers using a zebrafish autochthonous tumor model. J Vis Exp. 2012 Nov 13;(69):e50086. doi: 10.3791/50086. PMID: 23183931; PMCID: PMC3520576.
71. Jemal A, Siegel R, Ward E, Hao Y, Xu J, Murray T, Thun MJ. Cancer statistics, 2008. CA Cancer J Clin. 2008 Mar-Apr;58(2):71-96. doi: 10.3322/CA.2007.0010. Epub 2008 Feb 20. PMID: 18287387.
72. Kahraman A, Karakulak T, Szklarczyk D, von Mering C. Pathogenic impact of transcript isoform switching in 1,209 cancer samples covering 27 cancer types using an isoform-specific interaction network. Sci Rep. 2020 Sep 2;10(1):14453. doi: 10.1038/s41598-020-71221-5. PMID: 32879328; PMCID: PMC7468103.
73. Kakumani PK. AGO-RBP crosstalk on target mRNAs: Implications in miRNA-guided gene silencing and cancer. Transl Oncol. 2022 Jul;21:101434. doi: 10.1016/j.tranon.2022.101434. Epub 2022 Apr 26. PMID: 35477066; PMCID: PMC9136600.
74. Kalkhoran S, Milne O, Zalaudek I, Puig S, Malvehy J, Kelly JW, Marghoob AA. Historical, clinical, and dermoscopic characteristics of thin nodular melanoma. Arch Dermatol. 2010 Mar;146(3):311-8. doi: 10.1001/archdermatol.2009.369. PMID: 20231503.
75. Kamran MZ, Patil P, Gude RP. Role of STAT3 in cancer metastasis and translational advances. Biomed Res Int. 2013;2013:421821. doi: 10.1155/2013/421821. Epub 2013 Oct 2. PMID: 24199193; PMCID: PMC3807846.
76. Karreth FA, Reschke M, Ruocco A, Ng C, Chapuy B, Léopold V, Sjoberg M, Keane TM, Verma A, Ala U, Tay Y, Wu D, Seitzer N, Velasco-Herrera Mdel C, Bothmer A, Fung J, Langellotto F, Rodig SJ, Elemento O, Shipp MA, Adams DJ, Chiarle R, Pandolfi PP. The BRAF pseudogene functions as a competitive endogenous RNA and induces lymphoma in vivo. Cell. 2015 Apr 9;161(2):319-32. doi: 10.1016/j.cell.2015.02.043. Epub 2015 Apr 2. PMID: 25843629; PMCID: PMC6922011.

77. Kaufman CK, Mosimann C, Fan ZP, Yang S, Thomas AJ, Ablain J, Tan JL, Fogley RD, van Rooijen E, Hagedorn EJ, Ciarlo C, White RM, Matos DA, Puller AC, Santoriello C, Liao EC, Young RA, Zon LI. A zebrafish melanoma model reveals emergence of neural crest identity during melanoma initiation. Science. 2016 Jan 29;351(6272):aad2197. doi: 10.1126/science.aad2197. Epub 2016 Jan 28. PMID: 26823433; PMCID: PMC4868069.
78. Kawakami A, Fisher DE. The master role of microphthalmia-associated transcription factor in melanocyte and melanoma biology. Lab Invest. 2017 Jun;97(6):649-656. doi: 10.1038/labinvest.2017.9. Epub 2017 Mar 6. PMID: 28263292.
79. Kawakami K. Tol2: a versatile gene transfer vector in vertebrates. Genome Biol. 2007;8 Suppl 1(Suppl 1):S7. doi: 10.1186/gb-2007-8-s1-s7. PMID: 18047699; PMCID: PMC2106836..
80. Keung EZ, Gershenwald JE. The eighth edition American Joint Committee on Cancer (AJCC) melanoma staging system: implications for melanoma treatment and care. Expert Rev Anticancer Ther. 2018 Aug;18(8):775-784. doi: 10.1080/14737140.2018.1489246. PMID: 29923435; PMCID: PMC7652033.
81. Kim S, Kim S, Chang HR, Kim D, Park J, Son N, Park J, Yoon M, Chae G, Kim YK, Kim VN, Kim YK, Nam JW, Shin C, Baek D. The regulatory impact of RNA-binding proteins on microRNA targeting. Nat Commun. 2021 Aug 20;12(1):5057. doi: 10.1038/s41467-021-25078-5. PMID: 34417449; PMCID: PMC8379221.
82. Kimmel CB, Ballard WW, Kimmel SR, Ullmann B, Schilling TF. Stages of embryonic development of the zebrafish. Dev Dyn. 1995 Jul;203(3):253-310. doi: 10.1002/aja.1002030302. PMID: 8589427.
83. Kimmel CB. Patterning the brain of the zebrafish embryo. Annu Rev Neurosci. 1993;16:707-32. doi: 10.1146/annurev.ne.16.030193.003423. PMID: 8460906.
84. Kreft S, Gesierich A, Eigentler T, Franklin C, Valpione S, Ugurel S, Utikal J, Haferkamp S, Blank C, Larkin J, Garbe C, Schadendorf D, Lorigan P, Schilling B. Efficacy of PD-1-based immunotherapy after radiologic progression on targeted therapy in stage IV melanoma. Eur J Cancer. 2019 Jul;116:207-215. doi: 10.1016/j.ejca.2019.05.015. Epub 2019 Jun 15. PMID: 31212163.
85. Kuske M, Westphal D, Wehner R, Schmitz M, Beissert S, Praetorius C, Meier F. Immunomodulatory effects of BRAF and MEK inhibitors: Implications for Melanoma therapy. Pharmacol Res. 2018 Oct;136:151-159. doi: 10.1016/j.phrs.2018.08.019. Epub 2018 Aug 23. PMID: 30145328.
86. Kwak J, Park OK, Jung YJ, Hwang BJ, Kwon SH, Kee Y. Live image profiling of neural crest lineages in zebrafish transgenic lines. Mol Cells. 2013 Mar;35(3):255-60. doi: 10.1007/s10059-013-0001-5. Epub 2013 Feb 26. PMID: 23456294; PMCID: PMC3887912.
87. Kwan KM, Fujimoto E, Grabher C, Mangum BD, Hardy ME, Campbell DS, Parant JM, Yost HJ, Kanki JP, Chien CB. The Tol2kit: a multisite gateway-based construction kit for Tol2 transposon transgenesis constructs. Dev Dyn. 2007 Nov;236(11):3088-99. doi: 10.1002/dvdy.21343. PMID: 17937395.
88. Lezcano C, Jungbluth AA, Busam KJ. Comparison of Immunohistochemistry for PRAME With Cytogenetic Test Results in the Evaluation of Challenging Melanocytic Tumors. Am J Surg Pathol. 2020 Jul;44(7):893-900. doi: 10.1097/PAS.0000000000001492. PMID: 32317605; PMCID: PMC7289661.
89. Li H, Handsaker B, Wysoker A, Fennell T, Ruan J, Homer N, Marth G, Abecasis G, Durbin R; 1000 Genome Project Data Processing Subgroup. The Sequence Alignment/Map format

and SAMtools. Bioinformatics. 2009 Aug 15;25(16):2078-9. doi: 10.1093/bioinformatics/btp352. Epub 2009 Jun 8. PMID: 19505943; PMCID: PMC2723002.
90. Li H. Minimap2: pairwise alignment for nucleotide sequences. Bioinformatics. 2018 Sep 15;34(18):3094-3100. doi: 10.1093/bioinformatics/bty191. PMID: 29750242; PMCID: PMC6137996.
91. Li S, Ma J, Si Y, Cheng S, Hu M, Zhi X, Li B, Yu H, Jiang WG. Differential expression and functions of Ehm2 transcript variants in lung adenocarcinoma. Int J Oncol. 2019 May;54(5):1747-1758. doi: 10.3892/ijo.2019.4732. Epub 2019 Feb 27. PMID: 30816447
92. Li T, Gu M, Deng A, Qian C. Increased expression of YTHDF1 and HNRNPA2B1 as potent biomarkers for melanoma: a systematic analysis. Cancer Cell Int. 2020 Jun 15;20:239. doi: 10.1186/s12935-020-01309-5. PMID: 32549786; PMCID: PMC7294677.
93. Lister JA, Robertson CP, Lepage T, Johnson SL, Raible DW. nacre encodes a zebrafish microphthalmia-related protein that regulates neural-crest-derived pigment cell fate. Development. 1999 Sep;126(17):3757-67. doi: 10.1242/dev.126.17.3757. PMID: 10433906.
94. Long GV, Eroglu Z, Infante J, Patel S, Daud A, Johnson DB, Gonzalez R, Kefford R, Hamid O, Schuchter L, Cebon J, Sharfman W, McWilliams R, Sznol M, Redhu S, Gasal E, Mookerjee B, Weber J, Flaherty KT. Long-Term Outcomes in Patients With BRAF V600-Mutant Metastatic Melanoma Who Received Dabrafenib Combined With Trametinib. J Clin Oncol. 2018 Mar 1;36(7):667-673. doi: 10.1200/JCO.2017.74.1025. Epub 2017 Oct 9. PMID: 28991513.
95. Luke JJ, Hodi FS. Vemurafenib and BRAF inhibition: a new class of treatment for metastatic melanoma. Clin Cancer Res. 2012 Jan 1;18(1):9-14. doi: 10.1158/1078-0432.CCR-11-2197. Epub 2011 Nov 14. PMID: 22083257.
96. Lumaquin D, Johns E, Montal E, Weiss JM, Ola D, Abuhashem A, White RM. An in vivo reporter for tracking lipid droplet dynamics in transparent zebrafish. Elife. 2021 Jun 11;10:e64744. doi: 10.7554/eLife.64744. PMID: 34114952; PMCID: PMC8195600.
97. Ma Y, Xia R, Ma X, Judson-Torres RL, Zeng H. Mucosal Melanoma: Pathological Evolution, Pathway Dependency and Targeted Therapy. Front Oncol. 2021 Jul 19;11:702287. doi: 10.3389/fonc.2021.702287. PMID: 34350118; PMCID: PMC8327265.
98. Marranci A, D'Aurizio R, Vencken S, Mero S, Guzzolino E, Rizzo M, Pitto L, Pellegrini M, Chiorino G, Greene CM, Poliseno L. Systematic evaluation of the microRNAome through miR-CATCHv2.0 identifies positive and negative regulators of BRAF-X1 mRNA. RNA Biol. 2019 Jul;16(7):865-878. doi: 10.1080/15476286.2019.1600934. Epub 2019 Apr 19. PMID: 30929607; PMCID: PMC6546394.
99. Marranci A, Jiang Z, Vitiello M, Guzzolino E, Comelli L, Sarti S, Lubrano S, Franchin C, Echevarría-Vargas I, Tuccoli A, Mercatanti A, Evangelista M, Sportoletti P, Cozza G, Luzi E, Capobianco E, Villanueva J, Arrigoni G, Signore G, Rocchiccioli S, Pitto L, Tsinoremas N, Poliseno L. The landscape of BRAF transcript and protein variants in human cancer. Mol Cancer. 2017 Apr 28;16(1):85. doi: 10.1186/s12943-017-0645-4. PMID: 28454577; PMCID: PMC5410044.
100. Marranci A, Tuccoli A, Vitiello M, Mercoledi E, Sarti S, Lubrano S, Evangelista M, Fogli A, Valdes C, Russo F, Monte MD, Caligo MA, Pellegrini M, Capobianco E, Tsinoremas N, Poliseno L. Identification of BRAF 3'UTR Isoforms in Melanoma. J Invest Dermatol. 2015 Jun;135(6):1694-1697. doi: 10.1038/jid.2015.47. Epub 2015 Feb 16. PMID: 25685929.

101. Mazar J, DeYoung K, Khaitan D, Meister E, Almodovar A, Goydos J, Ray A, Perera RJ. The regulation of miRNA-211 expression and its role in melanoma cell invasiveness. PLoS One. 2010 Nov 1;5(11):e13779. doi: 10.1371/journal.pone.0013779. PMID: 21072171; PMCID: PMC2967468.
102. McConnell AM, Mito JK, Ablain J, Dang M, Formichella L, Fisher DE, Zon LI. Neural crest state activation in NRAS driven melanoma, but not in NRAS-driven melanocyte expansion. Dev Biol. 2019 May 15;449(2):107-114. doi: 10.1016/j.ydbio.2018.05.026. Epub 2018 Jun 5. PMID: 29883661; PMCID: PMC6281797.
103. McGovern VJ, Mihm MC Jr, Bailly C, Booth JC, Clark WH Jr, Cochran AJ, Hardy EG, Hicks JD, Levene A, Lewis MG, Little JH, Milton GW. The classification of malignant melanoma and its histologic reporting. Cancer. 1973 Dec;32(6):1446-57. doi: 10.1002/1097-0142(197312)32:6<1446::aid-cncr2820320623>3.0.co;2-8. PMID: 4757934.
104. McKenna JK, Florell SR, Goldman GD, Bowen GM. Lentigo maligna/lentigo maligna melanoma: current state of diagnosis and treatment. Dermatol Surg. 2006 Apr;32(4):493-504. doi: 10.1111/j.1524-4725.2006.32102.x. PMID: 16681656.
105. Menzies AM, Haydu LE, Visintin L, Carlino MS, Howle JR, Thompson JF, Kefford RF, Scolyer RA, Long GV. Distinguishing clinicopathologic features of patients with V600E and V600K BRAF-mutant metastatic melanoma. Clin Cancer Res. 2012 Jun 15;18(12):3242-9. doi: 10.1158/1078-0432.CCR-12-0052. Epub 2012 Apr 24. PMID: 22535154.
106. Mirea MA, Eckensperger S, Hengstschläger M, Mikula M. Insights into Differentiation of Melanocytes from Human Stem Cells and Their Relevance for Melanoma Treatment. Cancers (Basel). 2020 Sep 3;12(9):2508. doi: 10.3390/cancers12092508. PMID: 32899370; PMCID: PMC7564443.
107. Moan J, Dahlback A, Setlow RB. Epidemiological Support for an Hypothesis for Melanoma Induction Indicating a Role for UVA Radiation. Photochem Photobiol (1999) 70:243–7. doi: 10.1111/j.1751-1097.1999.tb07995.x
108. Murugan AK, Liu R, Xing M. Identification and characterization of two novel oncogenic mTOR mutations. Oncogene. 2019 Jun;38(26):5211-5226. doi: 10.1038/s41388-019-0787-5. Epub 2019 Mar 27. PMID: 30918329; PMCID: PMC6597304.
109. Napolitano A, Panzella L, Monfrecola G, d'Ischia M. Pheomelanin-induced oxidative stress: bright and dark chemistry bridging red hair phenotype and melanoma. Pigment Cell Melanoma Res. 2014 Sep;27(5):721-33. doi: 10.1111/pcmr.12262. Epub 2014 Jun 6. PMID: 24814217.
110. Nasti TH, Timares L. MC1R, eumelanin and pheomelanin: their role in determining the susceptibility to skin cancer. Photochem Photobiol. 2015 Jan-Feb;91(1):188-200. doi: 10.1111/php.12335. Epub 2014 Nov 7. PMID: 25155575; PMCID: PMC4299862.
111. Oliveira Filho RS, Oliveira DA, Souza MC, Silva Md, Brandão MD. Suspected melanoma only when the lesion is greater than 6mm may harm patients. Einstein (Sao Paulo). 2015 Oct-Dec;13(4):506-9. doi: 10.1590/S1679-45082015AO3436. PMID: 26761547; PMCID: PMC4878622.
112. Park RK, Liu Y, Durden DL. A role for Shc, Grb2, and Raf-1 in FcgammaRI signal relay. J Biol Chem. 1996 Jun 7;271(23):13342-8. doi: 10.1074/jbc.271.23.13342. PMID: 8662746.

113. Patton EE, Mathers ME, Schartl M. Generating and analyzing fish models of melanoma. Methods Cell Biol. 2011;105:339-66. doi: 10.1016/B978-0-12-381320-6.00014-X. PMID: 21951537.
114. Patton EE, Mueller KL, Adams DJ, Anandasabapathy N, Aplin AE, Bertolotto C, Bosenberg M, Ceol CJ, Burd CE, Chi P, Herlyn M, Holmen SL, Karreth FA, Kaufman CK, Khan S, Kobold S, Leucci E, Levy C, Lombard DB, Lund AW, Marie KL, Marine JC, Marais R, McMahon M, Robles-Espinoza CD, Ronai ZA, Samuels Y, Soengas MS, Villanueva J, Weeraratna AT, White RM, Yeh I, Zhu J, Zon LI, Hurlbert MS, Merlino G. Melanoma models for the next generation of therapies. Cancer Cell. 2021 May 10;39(5):610-631. doi: 10.1016/j.ccell.2021.01.011. Epub 2021 Feb 4. PMID: 33545064; PMCID: PMC8378471.
115. Patton EE, Widlund HR, Kutok JL, Kopani KR, Amatruda JF, Murphey RD, Berghmans S, Mayhall EA, Traver D, Fletcher CD, Aster JC, Granter SR, Look AT, Lee C, Fisher DE, Zon LI. BRAF mutations are sufficient to promote nevi formation and cooperate with p53 in the genesis of melanoma. Curr Biol. 2005 Feb 8;15(3):249-54. doi: 10.1016/j.cub.2005.01.031. PMID: 15694309
116. Payne A, Holmes N, Rakyan V, Loose M. BulkVis: a graphical viewer for Oxford nanopore bulk FAST5 files. Bioinformatics. 2019 Jul 1;35(13):2193-2198. doi: 10.1093/bioinformatics/bty841. PMID: 30462145; PMCID: PMC6596899.
117. Poliseno L, Salmena L, Zhang J, Carver B, Haveman WJ, Pandolfi PP. A coding-independent function of gene and pseudogene mRNAs regulates tumour biology. Nature. 2010 Jun 24;465(7301):1033-8. doi: 10.1038/nature09144. PMID: 20577206; PMCID: PMC3206313.
118. Poulikakos PI, Persaud Y, Janakiraman M, Kong X, Ng C, Moriceau G, Shi H, Atefi M, Titz B, Gabay MT, Salton M, Dahlman KB, Tadi M, Wargo JA, Flaherty KT, Kelley MC, Misteli T, Chapman PB, Sosman JA, Graeber TG, Ribas A, Lo RS, Rosen N, Solit DB. RAF inhibitor resistance is mediated by dimerization of aberrantly spliced BRAF(V600E). Nature. 2011 Nov 23;480(7377):387-90. doi: 10.1038/nature10662. PMID: 22113612; PMCID: PMC3266695.
119. Pruitt KD, Harrow J, Harte RA, Wallin C, Diekhans M, Maglott DR, Searle S, Farrell CM, Loveland JE, Ruef BJ, Hart E, Suner MM, Landrum MJ, Aken B, Ayling S, Baertsch R, Fernandez-Banet J, Cherry JL, Curwen V, Dicuccio M, Kellis M, Lee J, Lin MF, Schuster M, Shkeda A, Amid C, Brown G, Dukhanina O, Frankish A, Hart J, Maidak BL, Mudge J, Murphy MR, Murphy T, Rajan J, Rajput B, Riddick LD, Snow C, Steward C, Webb D, Weber JA, Wilming L, Wu W, Birney E, Haussler D, Hubbard T, Ostell J, Durbin R, Lipman D. The consensus coding sequence (CCDS) project: Identifying a common protein-coding gene set for the human and mouse genomes. Genome Res. 2009 Jul;19(7):1316-23. doi: 10.1101/gr.080531.108. Epub 2009 Jun 4. Erratum in: Genome Res. 2009 Aug;19(8):1506. PMID: 19498102; PMCID: PMC2704439.
120. Pujar S, O'Leary NA, Farrell CM, Loveland JE, Mudge JM, Wallin C, Girón CG, Diekhans M, Barnes I, Bennett R, Berry AE, Cox E, Davidson C, Goldfarb T, Gonzalez JM, Hunt T, Jackson J, Joardar V, Kay MP, Kodali VK, Martin FJ, McAndrews M, McGarvey KM, Murphy M, Rajput B, Rangwala SH, Riddick LD, Seal RL, Suner MM, Webb D, Zhu S, Aken BL, Bruford EA, Bult CJ, Frankish A, Murphy T, Pruitt KD. Consensus coding sequence (CCDS) database: a standardized set of human and mouse protein-coding regions

supported by expert curation. Nucleic Acids Res. 2018 Jan 4;46(D1):D221-D228. doi: 10.1093/nar/gkx1031. PMID: 29126148; PMCID: PMC5753299.

121. Pupo GM, Boyd SC, Fung C, Carlino MS, Menzies AM, Pedersen B, Johansson P, Hayward NK, Kefford RF, Scolyer RA, Long GV, Rizos H. Clinical significance of intronic variants in BRAF inhibitor resistant melanomas with altered BRAF transcript splicing. Biomark Res. 2017 May 11;5:17. doi: 10.1186/s40364-017-0098-3. PMID: 28503307; PMCID: PMC5426037.

122. Purushothaman K, Das PP, Presslauer C, Lim TK, Johansen SD, Lin Q, Babiak I. Proteomics Analysis of Early Developmental Stages of Zebrafish Embryos. Int J Mol Sci. 2019 Dec 17;20(24):6359. doi: 10.3390/ijms20246359. PMID: 31861170; PMCID: PMC6940819.

123. Qin H, Ni H, Liu Y, Yuan Y, Xi T, Li X, Zheng L. RNA-binding proteins in tumor progression. J Hematol Oncol. 2020 Jul 11;13(1):90. doi: 10.1186/s13045-020-00927-w. PMID: 32653017; PMCID: PMC7353687.

124. Rásó E. Splice variants of RAS-translational significance. Cancer Metastasis Rev. 2020 Dec;39(4):1039-1049. doi: 10.1007/s10555-020-09920-8. Epub 2020 Aug 8. PMID: 32772213; PMCID: PMC7680328.

125. Rastrelli M, Tropea S, Rossi CR, Alaibac M. Melanoma: epidemiology, risk factors, pathogenesis, diagnosis and classification. In Vivo. 2014 Nov-Dec;28(6):1005-11. PMID: 25398793.

126. Richardson J, Zeng Z, Ceol C, Mione M, Jackson IJ, Patton EE. A zebrafish model for nevus regeneration. Pigment Cell Melanoma Res. 2011 Apr;24(2):378-81. doi: 10.1111/j.1755-148X.2011.00839.x. PMID: 21324102; PMCID: PMC3084990.

127. Samatar AA, Poulikakos PI. Targeting RAS-ERK signalling in cancer: promises and challenges. Nat Rev Drug Discov. 2014 Dec;13(12):928-42. doi: 10.1038/nrd4281. PMID: 25435214.

128. Sandru A, Voinea S, Panaitescu E, Blidaru A. Survival rates of patients with metastatic malignant melanoma. J Med Life. 2014 Oct-Dec;7(4):572-6. PMID: 25713625; PMCID: PMC4316142.

129. Sang N, Stiehl DP, Bohensky J, Leshchinsky I, Srinivas V, Caro J. MAPK signaling up-regulates the activity of hypoxia-inducible factors by its effects on p300. J Biol Chem. 2003 Apr 18;278(16):14013-9. doi: 10.1074/jbc.M209702200. Epub 2003 Feb 13. PMID: 12588875; PMCID: PMC4518846.

130. Santoriello C, Gennaro E, Anelli V, Distel M, Kelly A, Köster RW, Hurlstone A, Mione M. Kita driven expression of oncogenic HRAS leads to early onset and highly penetrant melanoma in zebrafish. PLoS One. 2010 Dec 10;5(12):e15170. doi: 10.1371/journal.pone.0015170. PMID: 21170325; PMCID: PMC3000817.

131. Sardana K, Chakravarty P, Goel K. Optimal management of common acquired melanocytic nevi (moles): current perspectives. Clin Cosmet Investig Dermatol. 2014 Mar 19;7:89-103. doi: 10.2147/CCID.S57782. PMID: 24672253; PMCID: PMC3965271.

132. Shalem O, Sanjana NE, Hartenian E, Shi X, Scott DA, Mikkelson T, Heckl D, Ebert BL, Root DE, Doench JG, Zhang F. Genome-scale CRISPR-Cas9 knockout screening in human cells. Science. 2014 Jan 3;343(6166):84-87. doi: 10.1126/science.1247005. Epub 2013 Dec 12. PMID: 24336571; PMCID: PMC4089965.

133. Shepherd CT, Moran Lauter AN, Scott MP. Determination of transgene copy number by real-time quantitative PCR. Methods Mol Biol. 2009;526:129-34. doi: 10.1007/978-1-59745-494-0_11. PMID: 19378009.
134. Shi H, Hugo W, Kong X, Hong A, Koya RC, Moriceau G, Chodon T, Guo R, Johnson DB, Dahlman KB, Kelley MC, Kefford RF, Chmielowski B, Glaspy JA, Sosman JA, van Baren N, Long GV, Ribas A, Lo RS. Acquired resistance and clonal evolution in melanoma during BRAF inhibitor therapy. Cancer Discov. 2014 Jan;4(1):80-93. doi: 10.1158/2159-8290.CD-13-0642. Epub 2013 Nov 21. PMID: 24265155; PMCID: PMC3936420.
135. Shibahara S, Takeda K, Yasumoto K, Udono T, Watanabe K, Saito H, Takahashi K. Microphthalmia-associated transcription factor (MITF): multiplicity in structure, function, and regulation. J Investig Dermatol Symp Proc. 2001 Nov;6(1):99-104. doi: 10.1046/j.0022-202x.2001.00010.x. PMID: 11764295.
136. Silva JM, Deuker MM, Baguley BC, McMahon M. PIK3CA-mutated melanoma cells rely on cooperative signaling through mTORC1/2 for sustained proliferation. Pigment Cell Melanoma Res. 2017 May;30(3):353-367. doi: 10.1111/pcmr.12586. Epub 2017 Apr 20. PMID: 28233937; PMCID: PMC5411292.
137. Singh M, Durairaj P, Yeung J. Uveal Melanoma: A Review of the Literature. Oncol Ther. 2018 Jun;6(1):87-104. doi: 10.1007/s40487-018-0056-8. Epub 2018 Feb 6. Erratum in: Oncol Ther. 2019 Jun;7(1):93. PMID: 32700136; PMCID: PMC7359963.
138. Slominski RM, Sarna T, Płonka PM, Raman C, Brożyna AA, Slominski AT. Melanoma, Melanin, and Melanogenesis: The Yin and Yang Relationship. Front Oncol. 2022 Mar 14;12:842496. doi: 10.3389/fonc.2022.842496. PMID: 35359389; PMCID: PMC8963986.
139. Sosman JA, Kim KB, Schuchter L, Gonzalez R, Pavlick AC, Weber JS, McArthur GA, Hutson TE, Moschos SJ, Flaherty KT, Hersey P, Kefford R, Lawrence D, Puzanov I, Lewis KD, Amaravadi RK, Chmielowski B, Lawrence HJ, Shyr Y, Ye F, Li J, Nolop KB, Lee RJ, Joe AK, Ribas A. Survival in BRAF V600-mutant advanced melanoma treated with vemurafenib. N Engl J Med. 2012 Feb 23;366(8):707-14. doi: 10.1056/NEJMoa1112302. PMID: 22356324; PMCID: PMC3724515.
140. Stamm S, Ben-Ari S, Rafalska I, Tang Y, Zhang Z, Toiber D, Thanaraj TA, Soreq H. Function of alternative splicing. Gene. 2005 Jan 3;344:1-20. doi: 10.1016/j.gene.2004.10.022. Epub 2004 Dec 10. PMID: 15656968.
141. Storer NY, Zon LI. Zebrafish models of p53 functions. Cold Spring Harb Perspect Biol. 2010 Aug;2(8):a001123. doi: 10.1101/cshperspect.a001123. Epub 2010 May 5. PMID: 20679337; PMCID: PMC2908773.
142. Strub T, Giuliano S, Ye T, Bonet C, Keime C, Kobi D, Le Gras S, Cormont M, Ballotti R, Bertolotto C, Davidson I. Essential role of microphthalmia transcription factor for DNA replication, mitosis and genomic stability in melanoma. Oncogene. 2011 May 19;30(20):2319-32. doi: 10.1038/onc.2010.612. Epub 2011 Jan 24. PMID: 21258399.
143. Thomas L, Tranchand P, Berard F, Secchi T, Colin C, Moulin G. Semiological value of ABCDE criteria in the diagnosis of cutaneous pigmented tumors. Dermatology. 1998;197(1):11-7. doi: 10.1159/000017969. PMID: 9693179.
144. Thorvaldsdóttir H, Robinson JT, Mesirov JP. Integrative Genomics Viewer (IGV): high-performance genomics data visualization and exploration. Brief Bioinform. 2013

Mar;14(2):178-92. doi: 10.1093/bib/bbs017. Epub 2012 Apr 19. PMID: 22517427; PMCID: PMC3603213.

145. Tribulo C, Aybar MJ, Nguyen VH, Mullins MC, Mayor R. Regulation of Msx genes by a Bmp gradient is essential for neural crest specification. Development. 2003 Dec;130(26):6441-52. doi: 10.1242/dev.00878. Epub 2003 Nov 19. PMID: 14627721.

146. Tropea S, Del Fiore P, Maurichi A, Patuzzo R, Santinami M, Ribero S, Quaglino P, Caliendo V, Borgognoni L, Sestini S, Giudice G, Nacchiero E, Caracò C, Cordova A, Solari N, Piazzalunga D, Tauceri F, Carcoforo P, Lombardo M, Cavallari S, Mocellin S; Italian Melanoma Intergroup (IMI). The role of sentinel node tumor burden in modeling the prognosis of melanoma patients with positive sentinel node biopsy: an Italian melanoma intergroup study (N = 2,086). BMC Cancer. 2022 Jun 3;22(1):610. doi: 10.1186/s12885-022-09705-y. PMID: 35659273; PMCID: PMC9166524.

147. Tudrej KB, Czepielewska E, Kozłowska-Wojciechowska M. SOX10-MITF pathway activity in melanoma cells. Arch Med Sci. 2017 Oct;13(6):1493-1503. doi: 10.5114/aoms.2016.60655. Epub 2016 Jun 17. PMID: 29181082; PMCID: PMC5701683.

148. van Rooijen E, Fazio M, Zon LI. From fish bowl to bedside: The power of zebrafish to unravel melanoma pathogenesis and discover new therapeutics. Pigment Cell Melanoma Res. 2017 Jul;30(4):402-412. doi: 10.1111/pcmr.12592. Epub 2017 Jun 8. PMID: 28379616; PMCID: PMC6038924.

149. Varga M, Berkesi O, Darula Z, May NV, Palágyi A. Structural characterization of allomelanin from black oat. Phytochemistry. 2016 Oct;130:313-20. doi: 10.1016/j.phytochem.2016.07.002. Epub 2016 Jul 14. PMID: 27427433.

150. Venables JP. Aberrant and alternative splicing in cancer. Cancer Res. 2004 Nov 1;64(21):7647-54. doi: 10.1158/0008-5472.CAN-04-1910. PMID: 15520162.

151. Vido MJ, Le K, Hartsough EJ, Aplin AE. BRAF Splice Variant Resistance to RAF Inhibitor Requires Enhanced MEK Association. Cell Rep. 2018 Nov 6;25(6):1501-1510.e3. doi: 10.1016/j.celrep.2018.10.049. PMID: 30404005; PMCID: PMC6261462.

152. Vitiello M, Tuccoli A, D'Aurizio R, Sarti S, Giannecchini L, Lubrano S, Marranci A, Evangelista M, Peppicelli S, Ippolito C, Barravecchia I, Guzzolino E, Montagnani V, Gowen M, Mercoledi E, Mercatanti A, Comelli L, Gurrieri S, Wu LW, Ope O, Flaherty K, Boland GM, Hammond MR, Kwong L, Chiariello M, Stecca B, Zhang G, Salvetti A, Angeloni D, Pitto L, Calorini L, Chiorino G, Pellegrini M, Herlyn M, Osman I, Poliseno L. Context-dependent miR-204 and miR-211 affect the biological properties of amelanotic and melanotic melanoma cells. Oncotarget. 2017 Apr 11;8(15):25395-25417. doi: 10.18632/oncotarget.15915. PMID: 28445987; PMCID: PMC5421939.

153. Walker C, Streisinger G. Induction of Mutations by gamma-Rays in Pregonial Germ Cells of Zebrafish Embryos. Genetics. 1983 Jan;103(1):125-36. doi: 10.1093/genetics/103.1.125. PMID: 17246099; PMCID: PMC1202017.

154. Weiss JM, Hunter MV, Cruz NM, Baggiolini A, Tagore M, Ma Y, Misale S, Marasco M, Simon-Vermot T, Campbell NR, Newell F, Wilmott JS, Johansson PA, Thompson JF, Long GV, Pearson JV, Mann GJ, Scolyer RA, Waddell N, Montal ED, Huang TH, Jonsson P, Donoghue MTA, Harris CC, Taylor BS, Xu T, Chaligné R, Shliaha PV, Hendrickson R, Jungbluth AA, Lezcano C, Koche R, Studer L, Ariyan CE, Solit DB, Wolchok JD, Merghoub T, Rosen N, Hayward NK, White RM. Anatomic position determines oncogenic specificity in melanoma. Nature. 2022 Apr;604(7905):354-361. doi: 10.1038/s41586-022-04584-6. Epub 2022 Mar 30. PMID: 35355015.

155. Wessely A, Steeb T, Berking C, Heppt MV. How Neural Crest Transcription Factors Contribute to Melanoma Heterogeneity, Cellular Plasticity, and Treatment Resistance. Int J Mol Sci. 2021 May 28;22(11):5761. doi: 10.3390/ijms22115761. PMID: 34071193; PMCID: PMC8198848.
156. Westerfield, M. (2000). The zebrafish book. A guide for the laboratory use of zebrafish (Danio rerio). 4th ed., Univ. of Oregon Press, Eugene.
157. White RM, Cech J, Ratanasirintrawoot S, Lin CY, Rahl PB, Burke CJ, Langdon E, Tomlinson ML, Mosher J, Kaufman C, Chen F, Long HK, Kramer M, Datta S, Neuberg D, Granter S, Young RA, Morrison S, Wheeler GN, Zon LI. DHODH modulates transcriptional elongation in the neural crest and melanoma. Nature. 2011 Mar 24;471(7339):518-22. doi: 10.1038/nature09882. PMID: 21430780; PMCID: PMC3759979.
158. White RM, Sessa A, Burke C, Bowman T, LeBlanc J, Ceol C, Bourque C, Dovey M, Goessling W, Burns CE, Zon LI. Transparent adult zebrafish as a tool for in vivo transplantation analysis. Cell Stem Cell. 2008 Feb 7;2(2):183-9. doi: 10.1016/j.stem.2007.11.002. PMID: 18371439; PMCID: PMC2292119.
159. Zeng H, Liu F, Zhou H, Zeng C. Individualized Treatment Strategy for Cutaneous Melanoma: Where Are We Now and Where Are We Going? Front Oncol. 2021 Nov 4;11:775100. doi: 10.3389/fonc.2021.775100. PMID: 34804979; PMCID: PMC8599821.
160. Zhang M, Di Martino JS, Bowman RL, Campbell NR, Baksh SC, Simon-Vermot T, Kim IS, Haldeman P, Mondal C, Yong-Gonzales V, Abu-Akeel M, Merghoub T, Jones DR, Zhu XG, Arora A, Ariyan CE, Birsoy K, Wolchok JD, Panageas KS, Hollmann T, Bravo-Cordero JJ, White RM. Adipocyte-Derived Lipids Mediate Melanoma Progression via FATP Proteins. Cancer Discov. 2018 Aug;8(8):1006-1025. doi: 10.1158/2159-8290.CD-17-1371. Epub 2018 Jun 14. PMID: 29903879; PMCID: PMC6192670.
161. Zubovits J, Buzney E, Yu L, Duncan LM. HMB-45, S-100, NK1/C3, and MART-1 in metastatic melanoma. Hum Pathol. 2004 Feb;35(2):217-23. doi: 10.1016/j.humpath.2003.09.019. PMID: 14991540.